TECHNICAL MEMORANDUM

X-236

HC $3.00
MP .75

STATIC LONGITUDINAL, DIRECTIONAL, AND LATERAL STABILITY AND CONTROL DATA AT A MACH NUMBER OF 6.83 OF THE FINAL CONFIGURATION OF THE X-15 RESEARCH AIRPLANE

By Jim A. Penland and David E. Fetterman, Jr.

Langley Research Center
Langley Field, Va.

NATIONAL AERONAUTICS AND SPACE ADMINISTRATION

WASHINGTON

April 1960

NATIONAL AERONAUTICS AND SPACE ADMINISTRATION

TECHNICAL MEMORANDUM X-236

STATIC LONGITUDINAL, DIRECTIONAL, AND LATERAL STABILITY AND CONTROL DATA AT A MACH NUMBER OF 6.83 OF THE FINAL CONFIGURATION OF THE X-15 RESEARCH AIRPLANE*

By Jim A. Penland and David E. Fetterman, Jr.

SUMMARY

An investigation to determine the static longitudinal, directional, and lateral stability and control characteristics of the final configuration of the X-15 research airplane, configuration 3, has been carried out in the Langley 11-inch hypersonic tunnel. The tests were made at an average Mach number of 6.83 and a Reynolds number of 640,000 based on the wing mean aerodynamic chord. Data were obtained for an angle-of-attack range from -20° to 24° at angles of sideslip of 0° and -4.5°. The horizontal-tail deflection was varied from -35° to 15°, the vertical-tail deflection from 0° to -7.5°, and the speed-brake deflection from 0° to 50°. The longitudinal stability data are referred to the stability-axis system whereas the directional and lateral stability data are referred to the body-axis system.

INTRODUCTION

Since the initiation of the hypersonic research airplane project by the NACA in early 1954 that resulted in the X-15 airplane project, a vast amount of information concering hypersonic airplane stability has been accumulated. Several modifications of an airplane configuration having a cylindrical fuselage and a trapezoidal wing were tested at Mach numbers of 4.06 and 6.86 and reported in references 1 to 7. From the data of these references and other available data, North American Aviation, Inc., in collaboration with the NACA, U.S. Air Force, and U.S. Navy established a preliminary developmental X-15 configuration, designated configuration 1. This original configuration has

*Title, Unclassified.

undergone two major changes since its conception and as many as nine alterations on components such as the vertical tail or side fairings. Data obtained over a wide Mach number range from investigations of the original configuration 1 and the intermediate configuration 2 are reported in references 8 to 17. The present investigation is confined to an investigation of the final configuration 3 and some of the minor modifications of this configuration. The static longitudinal, directional, and lateral stability and control characteristics of the model are presented at a Mach number of 6.83, a Reynolds number of 640,000 based on the model wing mean aerodynamic chord, an angle-of-attack range from -20° to 24°, and angles of sideslip of 0° and -4.5°. Analysis of these data has been omitted in order to expedite release of this information.

L
7
3
9

SYMBOLS

C_A	axial-force coefficient, F_A/qS
C_L	lift coefficient, F_L/qS
C_D	drag coefficient, F'_D/qS
C_m	pitching-moment coefficient, $M_Y/qS\bar{c}$
C_l	rolling-moment coefficient, M_X/qSb
C_n	yawing-moment coefficient, M_Z/qSb
C_N	normal-force coefficient, F_N/qS
C_Y	side-force coefficient, F_Y/qS
F_A	force along -X-axis
F'_D	force along $-X_s$-axis
F_Y	force along Y-axis
F_L	force along $-Z_s$-axis
F_N	force along -Z-axis

M_X moment about X-axis

M_Y moment about Y-axis

M_Z moment about Z-axis

C_{Y_β} rate of change of side-force coefficient with angle of sideslip at zero sideslip angle, $\left(\frac{\partial C_Y}{\partial \beta}\right)_{\beta=0^\circ}$

C_{l_β} rate of change of rolling-moment coefficient with angle of sideslip at zero sideslip angle, $\left(\frac{\partial C_l}{\partial \beta}\right)_{\beta=0^\circ}$

C_{n_β} rate of change of yawing-moment coefficient with angle of sideslip at zero sideslip angle, $\left(\frac{\partial C_n}{\partial \beta}\right)_{\beta=0^\circ}$

$C_{Y_{\delta v}}$ rate of change of side-force coefficient with vertical-tail deflection, $\frac{\partial C_Y}{\partial \delta_V}$

$C_{l_{\delta v}}$ rate of change of rolling-moment coefficient with vertical-tail deflection, $\frac{\partial C_l}{\partial \delta_V}$

$C_{n_{\delta v}}$ rate of change of yawing-moment coefficient with vertical-tail deflection, $\frac{\partial C_n}{\partial \delta_V}$

$C_{Y_{\delta h'}}$ rate of change of side-force coefficient with differential horizontal-tail deflection, $\frac{\partial C_Y}{\partial \delta_{h'}}$

$C_{l_{\delta h'}}$ rate of change of rolling-moment coefficient with differential horizontal-tail deflection, $\frac{\partial C_l}{\partial \delta_{h'}}$

$C_{n_{\delta h'}}$ rate of change of yawing-moment coefficient with differential horizontal-tail deflection, $\frac{\partial C_n}{\partial \delta_{h'}}$

b	wing span
$\bar{c}$	mean aerodynamic chord of total wing
M	free-stream Mach number
q	free-stream dynamic pressure
R	free-stream Reynolds numbers, based on $\bar{c}$
S	total wing area including area within body and fairings
X,Y,Z	longitudinal, lateral, and vertical axes
x	distance along chord from leading edge
y	distance perpendicular to chord
α	angle of attack, deg
β	angle of sideslip, deg
δ_H	horizontal-tail deflection, positive to produce positive lift coefficient, deg
δ_{H_e}	equivalent pitch deflection of differentially deflected horizontal tails, positive to produce positive lift coefficient, $\frac{\delta_{H_L} + \delta_{H_R}}{2}$, deg
$\delta_{h'}$	differential horizontal-tail deflection, positive to produce positive rolling moment about X-axis, $\delta_{H_L} - \delta_{H_R}$, deg
δ_J	speed-brake deflection, deg
δ_V	vertical-tail deflection, positive to produce positive side-force coefficient, deg
δ_{V_e}	equivalent vertical-tail deflection of differentially deflected speed brakes, positive to produce positive side-force coefficient, $\frac{\delta_{J_{L3}} - \delta_{J_{R3}}}{2}$, deg

Model component designations:

The following designations of various components of the configurations were used throughout most of the wind-tunnel program as carried out in various research facilities and is therefore retained for the present investigation. Where applicable, these component designations are also used as subscripts.

B_2	fuselage including canopy of configurations 2 and 3
B_4	fuselage B_2 with wing moved forward 0.0734 inch on model
H_3	horizontal tail of configurations 2 and 3 with hinge line at 31.4 percent of horizontal-tail mean aerodynamic chord
H_9	horizontal tail H_3 moved 0.108 inch rearward on model such that the hinge line was located at 25 percent of horizontal-tail mean aerodynamic chord
J_{U2}	upper speed brakes used with V_{U5}
J_{L2}	lower speed brakes used with V_{L7}
J_{U3}	upper speed brakes used with V_{U8} as directional control
J_{L3}	lower speed brakes used with V_{L9} as directional control
V_{U5}	upper 10° wedge vertical tail of configuration 3
V_{L7}	lower 10° wedge vertical tail of configuration 3
V_{U8}	upper vertical tail used with differentially deflected speed brakes J_{U3}
V_{L9}	lower vertical tail used with differentially deflected speed brakes J_{L3}
W_2	wing of configurations 2 and 3
X_4	shortened side fairings of configuration 3
X_{14}	fairings X_4 with wing moved forward 0.0734 inch on model

Subscripts:

L	indicates left horizontal tail, lower or left speed brake, or lower vertical tail
R	indicates right horizontal tail or right speed brake
U	indicates upper vertical tail or upper speed brake
s	stability-axis system

MODEL

A photograph of the model used for most of the present tests is shown in figure 1. This 0.02-scale model of the final configuration of the X-15 research airplane is known as configuration 3 and is designated $B_4W_2X_{14}H_9V_{U5}V_{L7}$. A three-view drawing of the model is presented in figure 2 and geometric characteristics are given in table I. The model was of conventional tail-rearward design, having an ogival nose and a cylindrical fuselage with side fairings. The cylindrical portion of the model was slightly boattailed at the base. The model had a trapezoidal wing with 25.64° sweep of the quarter-chord line and had an all-movable horizontal tail for pitch control. This tail, which could be operated differentially for lateral control, was swept back 45° at the quarter-chord line and had 15° of negative dihedral. Both the wing and the horizontal tail had modified NACA 66-005 airfoil sections; the ordinates are presented in table II. Figure 3 presents details of the vertical-tail surfaces and speed brakes. The vertical-tail surfaces had 10° included angle wedge airfoil sections and a plan-form-area distribution of 55 percent of the total vertical-tail area for the dorsal fin and 45 percent for the ventral fin. The directional controls consisted of the outer panels of both upper and lower vertical-tail surfaces. The inside part of each tail surface was fixed and supported the speed brakes.

A few tests were made on a modification of configuration 3. This modified configuration (designated $B_2W_2X_4H_3V_{U8}V_{L9}$) is similar to configuration 3 (designated $B_4W_2X_{14}H_9V_{U5}V_{L7}$) except for minor shifts of the wing and horizontal tail (as noted in the definition of component-designation symbols) and a major alteration of the vertical tail and directional controls. This modified vertical tail is shown in detail in figure 3(b) and had a 10° included angle wedge airfoil section and a plan-form-area distribution of 60 percent of the total vertical-tail area for the dorsal fin and 40 percent for the ventral fin. The directional control consisted of differentially deflected speed brakes.

Figure 3(b) shows a differential deflection of the speed brakes to give -5° directional control and an average speed-brake deflection of 10°.

APPARATUS AND TEST CONDITIONS

The tests were conducted in the Mach number 6.86 test section of the Langley 11-inch hypersonic tunnel. The tunnel-wall boundary-layer thickness and likewise the free-stream Mach number of this test section are dependent upon the stagnation pressure. For the tests, an average stagnation pressure of 26 atmospheres and an average stagnation temperature of 675° F (to avoid liquefaction) were maintained. The average free-stream Mach number was 6.83 and the Reynolds number was 640,000 based on the model wing mean aerodynamic chord. The absolute humidity was kept to less than 1.9×10^{-5} pounds of water per pound of dry air for all tests. Force and moment data were obtained by use of a six-component strain-gage balance through an angle-of-attack range from -20° to 24° at angles of sideslip of 0° and -4.5°. The horizontal-tail deflection was varied from -35° to 15°, the vertical-tail deflection from 0° to -7.5°, and the speed-brake deflection from 0° to 50°. One test was made at an angle of attack of 0° and a range of sideslip angles from -2° to 21°. The balance and model were mounted in the tunnel test section on a movable strut which was rotated through an angle of attack during the run for each test point. Angles of sideslip were obtained by offsetting the model and balance support to the desired sideslip angle prior to each run. Thus the data were obtained at an essentially constant sideslip angle over the angle-of-attack range.

The true angles of attack were set optically by use of a point source of light and a small lens-prism assembly mounted in the model behind the fuselage fairings. The image of the light source was reflected by the prism and focused by the lens onto a calibrated chart. Model base pressures were measured during all tests and the axial-force component was adjusted to correspond to a base pressure equal to stream static pressure.

ACCURACY OF DATA

The probable uncertainties in the force and moment coefficients for the individual test points due to the force balance system and variations in dynamic pressure are presented as follows:

C_L	±0.02
C_D	±0.006
C_m	±0.006
C_l	±0.0005
C_n	±0.001
C_Y	±0.005

The errors in the positioning of the angle of attack, angle of sideslip, and horizontal-tail, vertical-tail, and speed-brake deflections were no greater than ±0.10°. The stagnation pressure was measured to an accuracy of ±2 inches of mercury out of about 800 inches and the variation of the Mach number used in calculating dynamic pressure was no greater than ±0.01.

RESULTS AND DISCUSSION

The results of the tests are presented as coefficients of forces and moments as defined in the section entitled Symbols. The longitudinal data are referred to the stability-axis system and the directional and lateral data are referred to the body-axis system. The body- and stability-axis systems are illustrated in figure 4. The moment reference was at 20 percent of the wing mean aerodynamic chord. All tests were made at a Mach number of 6.83 and a Reynolds number of 640,000 based on the wing mean aerodynamic chord. Typical schlieren photographs of configuration 3 are presented in figure 5.

The data are presented in the form of comparison plots to show the effects of component breakdown and control deflection. For convenience in locating these various effects and configurations, an index to the data figures is presented in table III. The basic longitudinal stability characteristics (C_L, C_D, and C_m) are presented in figures 6 to 22.

With the exception of one test at $\alpha = 0°$, no variations of the basic lateral and directional stability data (C_Y, C_n, and C_l) with sideslip angle are presented since most of the tests were made through the angle-of-attack range only at sideslip angles of 0° and -4.5°. Straight-line slopes between the basic data at these sideslip angles were then used to obtain the lateral and directional stability parameters. This method is believed to yield sufficiently accurate results since the slopes so obtained agree very well with those obtained from a limited number of tests wherein the model was tested over a sideslip-angle range at $\alpha = 0°$ and in all tests the values of the lateral

forces and moments were zero within the accuracy of the results at $\beta = 0^\circ$. Six-component body-axis data at $\alpha = 0^\circ$ and $\beta = -2^\circ$ to 21° are presented in figure 23 and show essentially linear variations of the coefficients C_Y, C_n, and C_l with sideslip angle near $\beta = 0^\circ$. The lateral and directional stability parameters $\left(C_{Y_\beta}, C_{n_\beta}, \text{and } C_{l_\beta}\right)$ are presented in figures 24 to 35. The straight-line-slope method was also used to obtain the lateral and directional control parameters presented in figures 36 to 48.

Although an analysis of the data has been omitted from this report, a few comments concerning parts of the test results are in order. A comparison of the aerodynamic characteristics presented in figures 8 and 9, particularly the pitching-moment coefficients C_m, shows that marked nonlinearities occur at low angles of attack for the configuration with the wing because of wing wake impingement and interference on the horizontal tail. This phenomenon has been reported previously in references 5 and 18. Tests at Reynolds numbers other than that used in the present investigation indicate that this pitching-moment nonlinearity is aggravated at lower Reynolds numbers and diminishes at higher Reynolds numbers. Although to a lesser degree, the results of tests with speed-brake deflection are also affected to some extent by the Reynolds number level of the tests inasmuch as some flow separation occurred over and ahead of the brake surfaces in the vicinity of the hinge line.

For the remaining tests with undeflected horizontal tails and speed brakes, no significant effects of Reynolds number on the longitudinal, lateral, and directional stability and control characteristics were observed.

Langley Research Center,
National Aeronautics and Space Administration,
Langley Field, Va., November 5, 1959.

REFERENCES

1. Penland, Jim A., Ridyard, Herbert W., and Fetterman, David E., Jr.: Lift, Drag, and Static Longitudinal Stability Data From an Exploratory Investigation at a Mach Number of 6.86 of an Airplane Configuration Having a Wing of Trapezoidal Plan Form. NACA RM L54L03b, 1955.

2. Ridyard, Herbert W., Fetterman, David E., Jr., and Penland, Jim A.: Static Lateral Stability Data From an Exploratory Investigation at a Mach Number of 6.86 of an Airplane Configuration Having a Wing of Trapezoidal Plan Form. NACA RM L55A21a, 1955.

3. Dunning, Robert W., and Ulmann, Edward F.: Static Longitudinal and Lateral Stability Data From an Exploratory Investigation at Mach Number 4.06 of an Airplane Configuration Having a Wing of Trapezoidal Plan Form. NACA RM L55A21, 1955.

4. Dunning, Robert W., and Ulmann, Edward F.: Exploratory Investigation at Mach Number 4.06 of an Airplane Configuration Having a Wing of Trapezoidal Plan Form - Longitudinal and Lateral Control Characteristics. NACA RM L55B28, 1955.

5. Fetterman, David E., Jr., Penland, Jim A., and Ridyard, Herbert W.: Static Longitudinal and Lateral Stability and Control Data From an Exploratory Investigation at a Mach Number of 6.86 of an Airplane Configuration Having a Wing of Trapezoidal Plan Form. NACA RM L55C04, 1955.

6. Dunning, Robert W., and Ulmann, Edward F.: Exploratory Investigation at Mach Number 4.06 of an Airplane Configuration Having a Wing of Trapezoidal Plan Form - Effects of Various Tail Arrangements on Wing-On and Wing-Off Static Longitudinal and Lateral Stability Characteristics. NACA RM L55D08, 1955.

7. Penland, Jim A., Fetterman, David E., Jr., and Ridyard, Herbert W.: Static Longitudinal and Lateral Stability and Control Characteristics of an Airplane Configuration Having a Wing of Trapezoidal Plan Form With Various Tail Airfoil Sections and Tail Arrangements at a Mach Number of 6.86. NACA RM L55F17, 1955.

8. Osborne, Robert S.: Aerodynamic Characteristics of a 0.0667-Scale Model of the North American X-15 Research Airplane at Transonic Speeds. NASA TM X-24, 1959.

9. Leupold, Mathias J., and Freeman, Elizabeth M.: Supersonic Force Tests for Stabilizer-Control Effectiveness on the Full-Span Model X-15 for North American Aviation, Inc., Wind Tunnel Rep. 164, Naval Supersonic Lab., M.I.T., Oct. 1957.

10. Leupold, Mathias J., and Freeman, Elizabeth M.: A Second Series of Supersonic Force Tests on the Full-Span Model X-15 for North American Aviation, Incorporated. Wind Tunnel Rep. 200, Naval Supersonic Lab., M.I.T., Sept. 1958.

11. Leupold, Mathias J., and Freeman, Elizabeth M.: A Third Series of Supersonic Force Tests on the Full-Span Model X-15 for North American Aviation, Incorporated. Wind Tunnel Rep. 228, Naval Supersonic Lab., M.I.T., Nov. 1958.

12. Leupold, Mathias J., and Freeman, Elizabeth M.: A Fourth Series of Supersonic Force Tests on the Full-Span Model X-15 for North American Aviation, Incorporated. Wind Tunnel Rep. 239, Naval Supersonic Lab., M.I.T., Dec. 1958.

13. Franklin, Arthur E., and Silvers, H. Norman: Investigation of the Aerodynamic Characteristics of a 0.067-Scale Model of the X-15 Airplane (Configuration 2) at Mach Numbers of 2.29, 2.98, 3.96, and 4.65. NASA MEMO 4-27-59L, 1959.

14. Boisseau, Peter C.: Investigation of the Low-Speed Stability and Control Characteristics of a 1/7-Scale Model of the North American X-15 Airplane. NACA RM L57D09, 1957.

15. Lopez, Armando E., and Tinling, Bruce E.: The Static and Dynamic-Rotary Stability Derivatives at Subsonic Speeds of a Model of the X-15 Research Airplane. NACA RM A58F09, 1958.

16. Tunnell, Phillips J., and Latham, Eldon A.: The Static and Dynamic-Rotary Stability Derivatives of a Model of the X-15 Research Airplane at Mach Numbers From 1.55 to 3.50. NASA MEMO 12-23-58A, 1959.

17. Fetterman, David E., Jr., and Penland, Jim A.: Static Longitudinal, Directional, and Lateral Stability and Control Data From an Investigation at a Mach Number of 6.83 of Two Developmental X-15 Airplane Configurations. NASA TM X-209, 1960.

18. Ulmann, Edward F., and Ridyard, Herbert W.: Flow-Field Effects on Static Stability and Control at High Supersonic Mach Numbers. NACA RM L55L19a, 1956.

TABLE I.- GEOMETRIC CHARACTERISTICS OF MODEL

Wing, W_2:	
Area, total, sq in.	11.520
Area, exposed, sq in.	6.050
Span, in.	5.366
Aspect ratio	2.500
Root chord, fuselage center line, in.	3.578
Root chord, exposed, in.	2.64
Tip chord, in.	0.716
Mean aerodynamic chord, in.	2.465
Sweepback angles, deg -	
Leading edge	36.75
25-percent-chord line	25.64
Trailing edge	-17.74
Taper ratio	0.200
Dihedral angle, deg	0
Incidence angle, deg	0
Airfoil section, parallel to fuselage center line	Modified NACA 66-005
Leading-edge radius, in. -	
Tip	0.008
Fuselage-line chord	0.014
Horizontal tail, H_3 and H_9:	
Area, exposed, sq in.	2.878
Semispan (panel span), in.	1.330
Aspect ratio of exposed area	1.229
Taper ratio of exposed area	0.328
Root chord, exposed, in.	1.658
Tip chord, in.	0.506
Mean aerodynamic chord, exposed area, in.	1.184
Sweepback angles, deg -	
Leading edge	50.58
25-percent-chord line	45.00
Trailing edge	19.28
Dihedral, deg	-15.000
Airfoil section, parallel to fuselage center line	Modified NACA 66-005
Leading-edge radius, in. -	
Tip	0.005
Fuselage-line chord	0.010
Upper vertical tail, V_{U5}:	
Area, exposed, sq in.	2.356
Span, in.	1.10
Aspect ratio of exposed area	0.516
Taper ratio of exposed area	0.738
Root chord, fuselage surface line, in.	2.450
Tip chord, in.	1.81
Mean aerodynamic chord of exposed area, in.	2.148
Sweepback angles, deg -	
Leading edge	30.000
25-percent-chord line	23.413
Trailing edge	0
Airfoil section, parallel to fuselage center line	10° full wedge
Leading-edge radius, in.	0.010
Control surface -	
Area, sq in.	1.521
Root chord, in.	2.250
Mean aerodynamic chord, in.	2.039

L-139

TABLE I.- GEOMETRIC CHARACTERISTICS OF MODEL - Concluded

Lower vertical tail, V_{L7}:	
Area, exposed, sq in.	1.982
Span, exposed, in. -	
Maximum	0.920
Minimum	0.880
Average	0.900
Aspect ratio of exposed area	0.427
Taper ratio of exposed area	0.783
Root chord, in.	2.450
Tip chord, in.	1.919
Mean aerodynamic chord of exposed area, in.	2.200
Sweepback angles, deg -	
Leading edge	30.000
25-percent-chord line	23.413
Trailing edge	0
Airfoil section, parallel to fuselage center line	10° full wedge
Leading-edge radius, in.	0.010
Control surface -	
Area, sq in.	1.149
Root chord, in.	2.250
Mean aerodynamic chord, in.	2.093
Upper vertical tail, V_{U8}:	
Area, exposed, sq in.	1.776
Span, in.	1.11
Aspect ratio of exposed area	0.694
Taper ratio of exposed area	0.435
Root chord, fuselage surface line, in.	2.23
Tip chord, in.	0.97
Mean aerodynamic chord, in.	1.683
Sweepback angles, deg -	
Leading edge	41.5
25-percent-chord line	30.8
Trailing edge	-14.2
Airfoil section, parallel to fuselage center line	10° full wedge
Leading-edge radius, in.	0.01
Area, stabilizer (speed brakes), sq in.	0.699
Lower vertical tail, V_{L9}:	
Area, exposed, sq in.	1.19
Span, exposed, in.	0.52
Aspect ratio of exposed area	0.227
Taper ratio of exposed area	0.83
Root chord, in.	2.59
Tip chord, in.	2.15
Mean aerodynamic chord, in.	1.99
Sweepback angles, deg -	
Leading edge	43.2
25-percent-chord line	33.7
Trailing edge	0
Airfoil section, parallel to fuselage center line	10° full wedge
Leading-edge radius, in.	0.01
Area, stabilizer (speed brakes), sq in.	0.484
Fuselage, B_4X_{14}:	
Length, in.	11.76
Maximum diameter, in.	1.12
Maximum width including side fairings, in.	1.76
Fineness ratio, ratio of length to body diameter	10.50
Base diameter, in.	0.960

L-739

TABLE II.- AIRFOIL SECTION ORDINATES

[Modified NACA 66-005]

(a) Wing W_2

x, percent chord	y, percent chord	
	[1]Root	Tip
0	0	0
1.25	.358	1.048
2.5	.533	1.123
5.0	.854	1.263
7.5	1.137	1.395
10	1.382	1.523
15	1.759	1.769
20	2.001	2.001
25	2.182	2.182
30	2.318	2.318
35	2.416	2.416
40	2.476	2.476
45	2.500	2.500
50	2.485	2.485
55	2.432	2.432
60	2.332	2.332
65	2.151	2.151
67	2.085	2.085
100	.500	.500

L.E. radius: Root, 0.015 inch; tip, 0.008 inch.

Basic airfoil modifed for linear taper between root and tip forward of 17-percent-chord line and modified to straight side rearward of 67-percent-chord line to 1-percent-thick trailing edge.

[1]Exposed root chord.

(b) Horizontal tails H_3 and H_9

x, percent chord	y, percent chord	
	[1]Root	Tip
0	0	0
.1	.269	.348
.25	.408	.538
.5	.531	.728
.75	.590	.846
1.25	.650	.969
2.50	.791	1.052
5.00	1.048	1.206
7.5	1.268	1.353
10	1.458	1.495
15	1.765	1.768
20	2.001	2.001
25	2.182	2.182
30	2.318	2.318
35	2.416	2.416
40	2.476	2.476
45	2.500	2.500
50	2.485	2.485
55	2.432	2.432
60	2.332	2.332
75	1.653	1.653
90	.961	.961
100	.500	.500

L.E. radius: Root, 0.010 inch; tip, 0.005 inch.

Basic airfoil modified for linear taper between root and tip forward of 5-percent-chord line at root and 15-percent-chord line at tip and modified to straight side rearward of 67-percent-chord line to 1-percent-thick trailing edge.

[1]Exposed root chord.

TABLE III.- INDEX OF DATA FIGURES

Effects of -	Configuration	Horizontal-tail deflection, deg		Vertical-tail deflection, deg		Speed-brake deflection, deg		Data at $\beta = 0^\circ$			
								C_L, C_D, C_m		C_{Y_β}, C_{n_β}, C_{l_β}	
		δ_{H_L}	δ_{H_R}	δ_{V_U}	δ_{V_L}	δ_{J_U}	δ_{J_L}	Figure	Angle of attack, α, deg	Figure	Angle of attack, α, deg
Component parts	B_4X_{14}	---	---	----	----	------	------	6	-4 to 24	--	---------
	$B_4W_2X_{14}$	---	---	----	----	------	------			--	---------
	$B_4W_2X_{14}H_9$	0	0	----	----	------	------			24	-4 to 24
	$B_4W_2X_{14}H_9V_{U5}$	0	0	0	----	0	------			24	-4 to 24
	$B_4W_2X_{14}V_{U5}V_{L7}$	---	---	0	0	0	0			--	---------
	$B_4W_2X_{14}H_9V_{U5}V_{L7}$	0	0	0	0	0	0			24	-4 to 24
Speed brakes with and without horizontal tail	$B_4W_2X_{14}V_{U5}V_{L7}$	---	---	0	0	0	0	7	-4 to 24	--	---------
	$B_4W_2X_{14}V_{U5}V_{L7}J_{U2}$	---	---			35	0			26	-4 to 24
	$B_4W_2X_{14}H_9V_{U5}V_{L7}$	0	0			0	0			25	-20 to 24
	$B_4W_2X_{14}H_9V_{U5}V_{L7}J_{U2}$	0	0			35	0			26	-4 to 24
	$B_4W_2X_{14}V_{U5}V_{L7}J_{U2}J_{L2}$	---	---			35	35			26	-4 to 24
	$B_4W_2X_{14}H_9V_{U5}V_{L7}J_{U2}J_{L2}$	0	0			35	35			25	-20 to 24
Horizontal-tail deflection on configuration without wing	$B_4X_{14}H_9V_{U5}V_{L7}$	0	0	0	0	0	0	8	-20 to 24	24	-4 to 24
		-10	-10							--	---------
		-20	-20							--	---------
		-35	-35							--	---------
Horizontal-tail deflection on configuration with wing	$B_4W_2X_{14}H_9V_{U5}V_{L7}$	0	0	0	0	0	0	9	-20 to 24	27	-4 to 24
		-10	-10								
		-20	-20								
		-30	-30								
		-35	-35								
		15	15								
Vertical-tail deflection	$B_4W_2X_{14}H_9V_{U5}V_{L7}$	0	0	0	0	0	0	10	-4 to 24	28	-4 to 24
				-2.5	-2.5					--	---------
				-5	-5					28	-4 to 24
				-7.5	-7.5					28	-4 to 24
Differential horizontal-tail deflection	$B_4W_2X_{14}H_9V_{U5}V_{L7}$	0	0	0	0	0	0	11	-4 to 24	29	-20 to 24
		-5	-15							--	---------
		-15	-25							--	---------
		10	-10							29	-20 to 24
		-10	-30							29	-20 to 24
		0	-20							--	---------
		20	0							--	---------
Horizontal-tail deflection with speed-brake deflection	$B_4W_2X_{14}H_9V_{U5}V_{L7}J_{U2}J_{L2}$	0	0	0	0	35	35	12	-4 to 24	30	-4 to 24
		-10	-10			35	35				
		-20	-20			35	35				
		-20	-20			25	25				
		-20	-20			50	50				
Horizontal-tail deflection with upper speed-brake deflection	$B_4W_2X_{14}H_9V_{U5}V_{L7}J_{U2}$	0	0	0	0	35	0	13	-4 to 24	31	-4 to 24
		-10	-10								
		-20	-20								
Speed-brake deflection with differential horizontal-tail deflection	$B_4W_2X_{14}H_9V_{U5}V_{L7}J_{U2}J_{L2}$	10	-10	0	0	0	0	14	-4 to 24		
						35	0				
						35	35				
Differential horizontal-tail deflection with and without speed-brake deflection	$B_4W_2X_{14}H_9V_{U5}V_{L7}J_{U2}J_{L2}$	0	0	0	0	0	0	15	-20 to 24		
		10	-10			0	0				
		20	0			0	0				
		20	0			35	35				
Vertical-tail deflection with horizontal-tail deflection	$B_4W_2X_{14}H_9V_{U5}V_{L7}J_{U2}J_{L2}$	-20	-20	0	0	0	0	16	-2 to 24		
				-2.5	-2.5						
				-5	-5						
				-7.5	-7.5						
Horizontal-tail deflection with upper vertical-tail and speed-brake deflections	$B_4W_2X_{14}H_9V_{U5}V_{L7}J_{U2}J_{L2}$	0	0	-5	0	35	35	17	-4 to 24	32	-4 to 24
		-10	-10								
		-20	-20								
Horizontal-tail deflection with vertical-tail and speed-brake deflections	$B_4W_2X_{14}H_9V_{U5}V_{L7}J_{U2}J_{L2}$	0	0	-5	-5	35	35	18	-4 to 24	33	-20 to 24
		-10	-10								
		-20	-20								
Upper vertical-tail deflection	$B_4W_2X_{14}H_9V_{U5}V_{L7}$	0	0	0	0	0	0	19	-4 to 24	34	-20 to 24
				-5	0						
				-5	-5						
Speed-brake and horizontal-tail deflections with and without horizontal tail	$B_2W_2X_4H_3V_{L9}J_{L3}$	0	0			0	10	20	-20 to 24	--	---------
	$B_2W_2X_4V_{U8}V_{L9}J_{U3}J_{L3}$	---	---			10	10			--	---------
	$B_2W_2X_4H_3V_{U8}V_{L9}$	0	0	0	0	0	0			35	-4 to 24
	$B_2W_2X_4H_3V_{U8}V_{L9}J_{U3}J_{L3}$	0	0			10	10			35	-4 to 24
	$B_2W_2X_4H_3V_{U8}V_{L9}J_{U3}J_{L3}$	-10	-10			10	10			—	---------
Differential speed-brake deflection	$B_2W_2X_4H_3V_{U8}V_{L9}J_{U3}J_{L3}$	0	0	Effective		L R	L R	21	-4 to 24		
				0	0	10 10	10 10				
				-5	-5	5 15	5 15				
				-10	-10	0 20	0 20				
Differential horizontal-tail deflection with speed-brake deflection	$B_2W_2X_4H_3V_{U8}V_{L9}J_{U3}J_{L3}$	0	0	Effective		L R	L R	22	-4 to 24		
		5	-5	0	0	10 10	10 10				
		10	-10								

L-739

TABLE III.- INDEX OF DATA FIGURES - Concluded

Effects of -	Configuration	Horizontal-tail deflection, deg		Vertical-tail deflection, deg		Speed-brake deflection, deg		Figure	Angle of attack, α, deg	Angle of sideslip, β, deg
		δ_{H_L}	δ_{H_R}	δ_{V_U}	δ_{V_L}	δ_{J_U}	δ_{J_L}			
Data: C_N, C_A, C_m, C_Y, C_n, C_l										
Angle of sideslip	$B_4W_2X_{14}H_9V_{U5}V_{L7}$	0	0	0	0	0	0	23	0	-2 to 21
Data: $C_{Y_{\delta v}}$, $C_{n_{\delta v}}$, $C_{l_{\delta v}}$										
Upper or upper and lower vertical-tail and speed-brake deflections	$B_4W_2X_{14}H_9V_{U5}V_{L7}J_{U2}J_{L2}$	0	0	-5	0 -5 0 -5	0 0 35 35	0 0 35 35	36	-4 to 24	0
Horizontal-tail deflection with upper vertical-tail and speed-brake deflections	$B_4W_2X_{14}H_9V_{U5}V_{L7}J_{U2}J_{L2}$	0 -10 -20	0 -10 -20	-5	0	35	35	37	-4 to 24	0
Horizontal-tail deflection with vertical-tail and speed-brake deflections	$B_4W_2X_{14}H_9V_{U5}V_{L7}J_{U2}J_{L2}$	0 -10 -20	0 -10 -20	-5	-5	35	35	38	-4 to 24	0
Speed-brake deflection at angle of sideslip	$B_4W_2X_{14}H_9V_{U5}V_{L7}J_{U2}J_{L2}$	0	0	-5	-5	0 0 35 35	0 0 35 35	39	-20 to 24	0 -4.5 0 -4.5
Horizontal-tail deflection with upper vertical-tail and speed-brake deflections at angle of sideslip	$B_4W_2X_{14}H_9V_{U5}V_{L7}J_{U2}J_{L2}$	0 -10 -20	0 -10 -20	-5	0	35	35	40	-4 to 24	-4.5
Horizontal-tail deflection with vertical-tail and speed-brake deflections at angle of sideslip	$B_4W_2X_{14}H_9V_{U5}V_{L7}J_{U2}J_{L2}$	0 -10 -20	0 -10 -20	-5	-5	35	35	41	-4 to 24	-4.5
Angle of sideslip with upper vertical-tail deflection	$B_4W_2X_{14}H_9V_{U5}V_{L7}$	0	0	-5	0	0	0	42	-4 to 24	0 -4.5
Differential speed-brake deflection	$B_2W_2X_4H_3V_{U8}V_{L9}J_{U3}J_{L3}$	0	0	Effective -5 -10	 -5 -10	L R 5 15 0 20	L R 5 15 0 20	43	-4 to 24	0
Data: $C_{Y_{\delta h'}}$, $C_{n_{\delta h'}}$, $C_{l_{\delta h'}}$										
Angle of sideslip	$B_4W_2X_{14}H_9V_{U5}V_{L7}$	10	-10	0	0	0	0	44	-20 to 24	0 -4.5
Angle of sideslip with equivalent horizontal-tail deflection	$B_4W_2X_{14}H_9V_{U5}V_{L7}$	-10	-30	0	0	0	0	45	-4 to 24	0 -4.5
Speed-brake deflection	$B_4W_2X_{14}H_9V_{U5}V_{L7}J_{U2}J_{L2}$	10	-10	0	0	0 35 35	0 0 35	46	-4 to 24	0
Speed-brake deflection with equivalent horizontal-tail deflection	$B_4W_2X_{14}H_9V_{U5}V_{L7}J_{U2}J_{L2}$	20	0	0	0	0 35	0 35	47	-20 to 24	0
Equivalent horizontal-tail deflection	$B_4W_2X_{14}H_9V_{U5}V_{L7}$	-5 0 -10	-15 -20 -30	0	0	0	0	48	-4 to 24	0

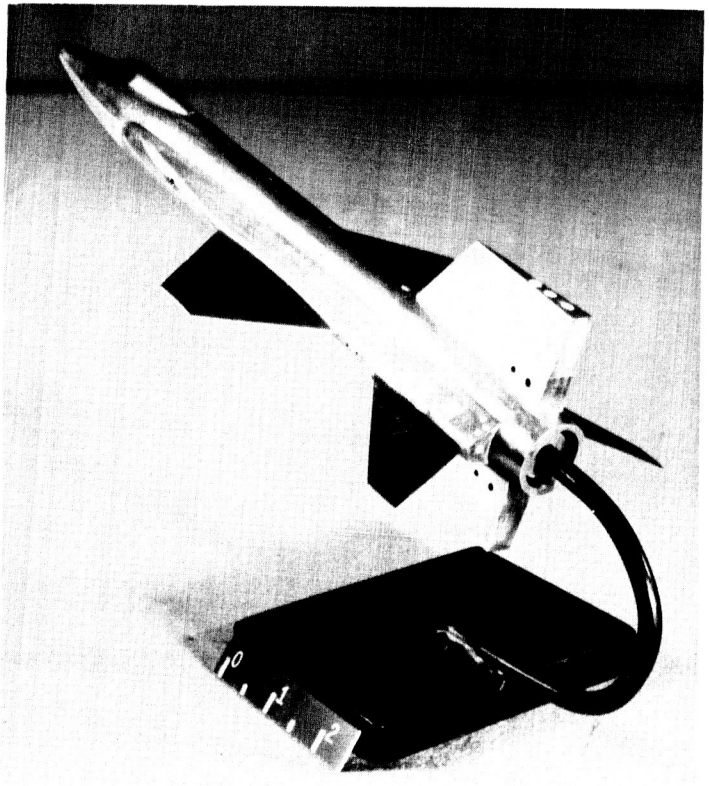

(a) Speed brakes closed.
Model $B_4W_2X_{14}H_9V_{U5}V_{L7}$.

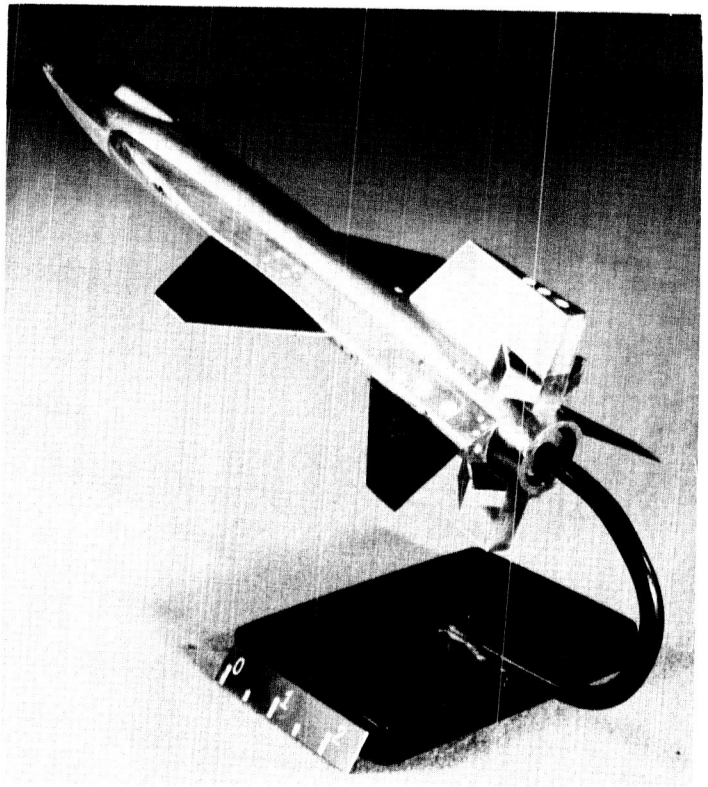

L-59-6481
(b) Speed brakes deflected 35°.
Model $B_4W_2X_{14}H_9V_{U5}V_{L7}J_{U2}J_{L2}$.

Figure 1.- Photographs of 0.02-scale model of configuration 3.

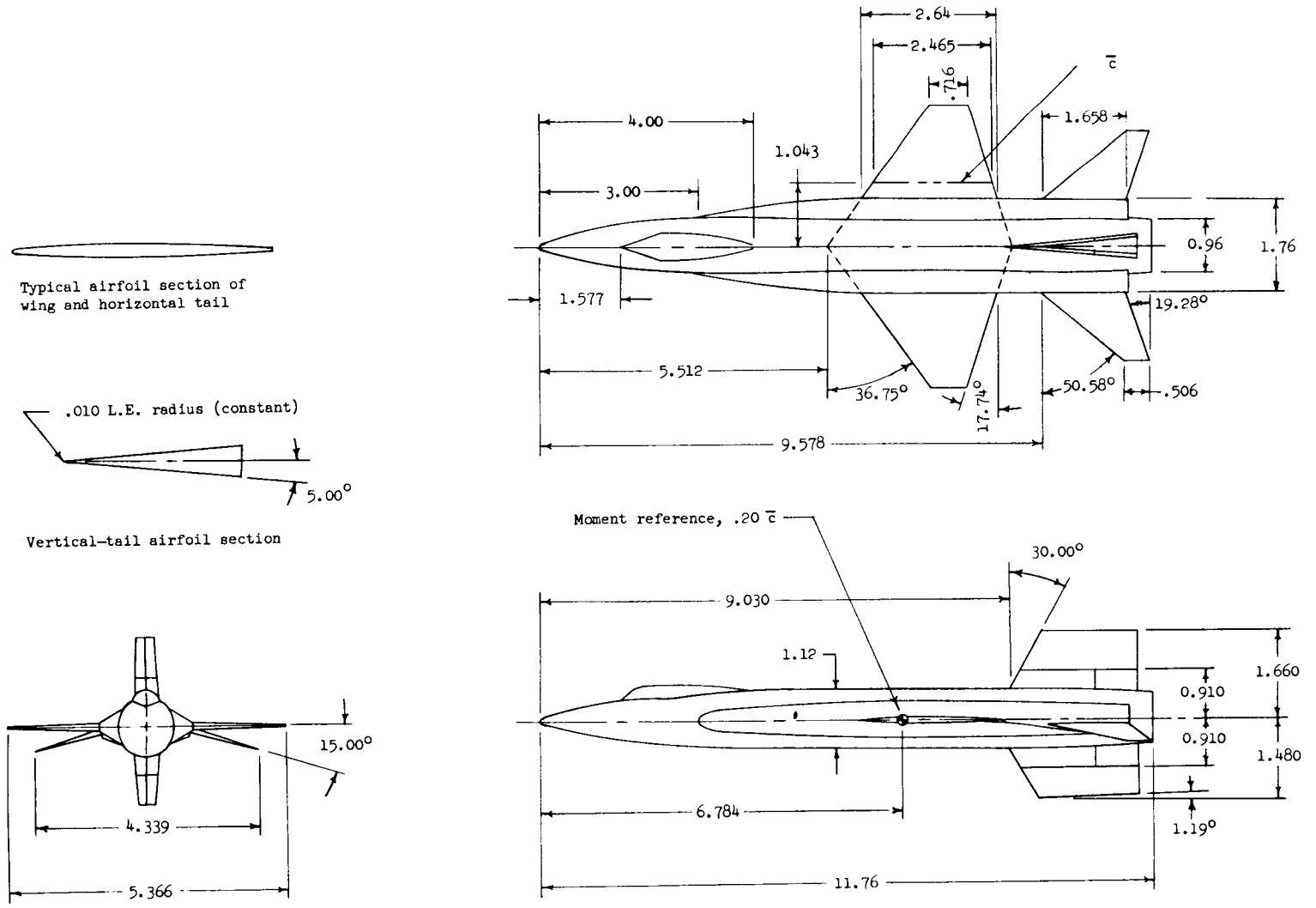

Figure 2.- Details of model of configuration 3, $B_4W_2X_{14}H_9V_{U5}V_{L7}$. All dimensions in inches.

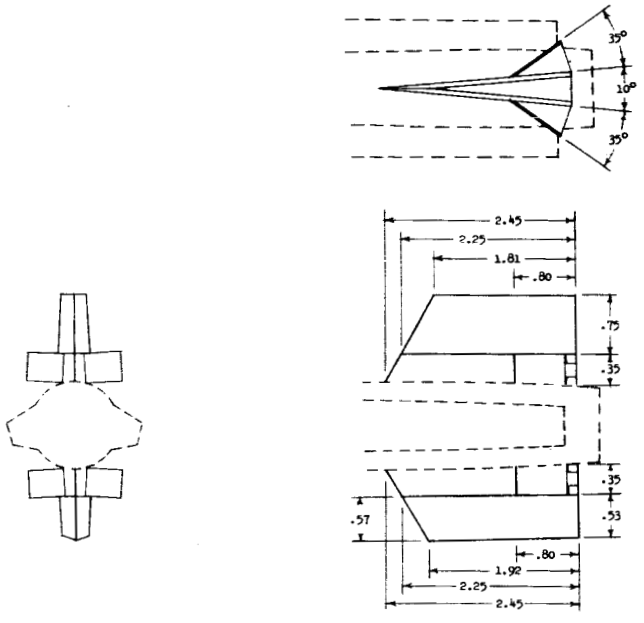

(a) Vertical tails $V_{U5}V_{L7}$ and speed brakes $J_{U2}J_{L2}$.

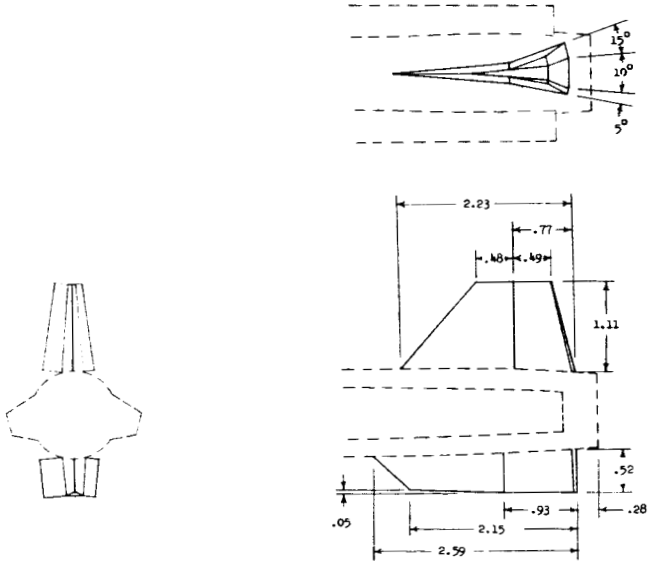

(b) Vertical tails $V_{U8}V_{L9}$ and speed brakes $J_{U3}J_{L3}$.

Figure 3.- Details of vertical tails and speed brakes showing typical symmetrical and differential speed-brake deflection. All dimensions in inches.

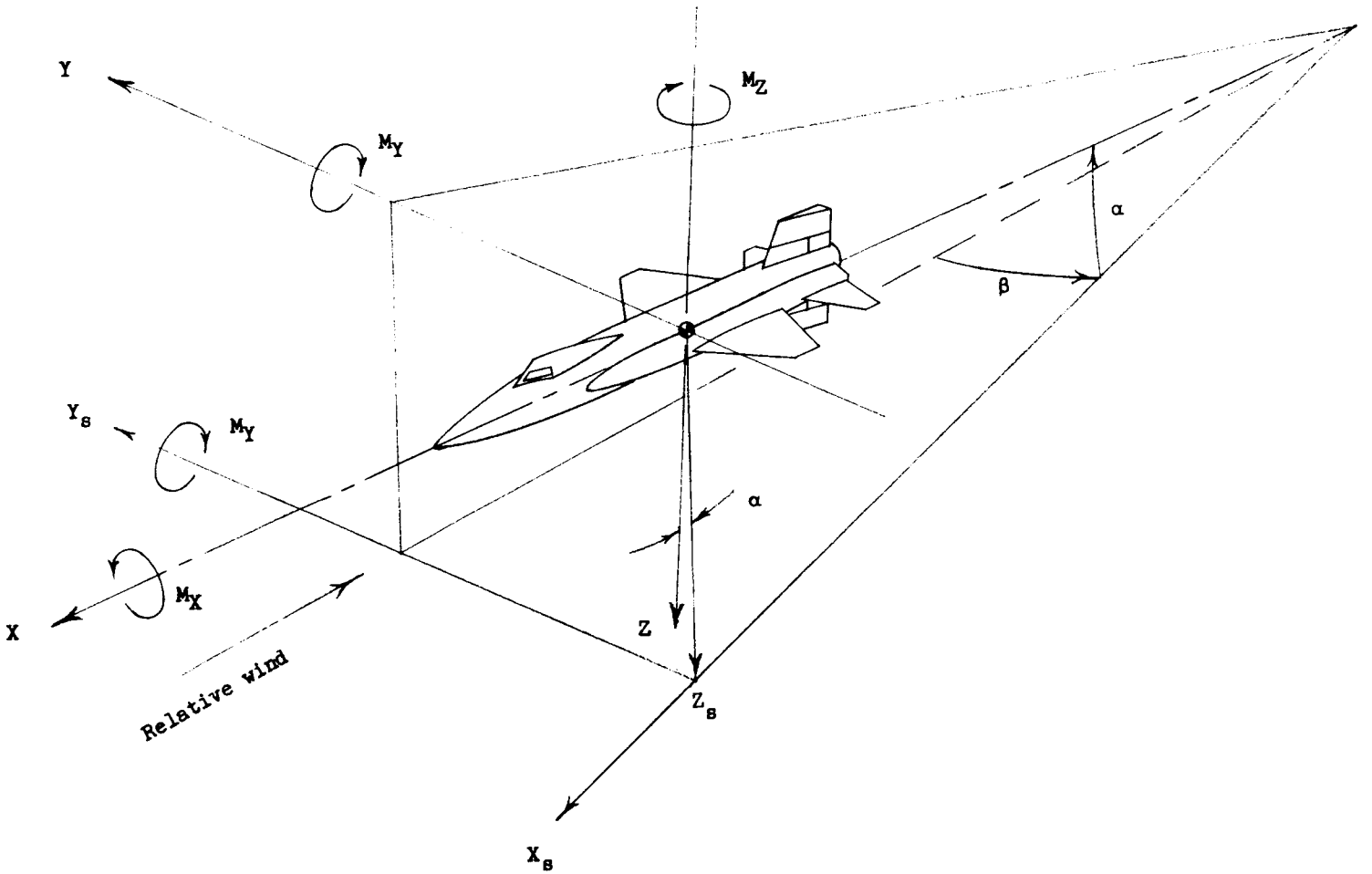

Figure 4.- Reference axis system.

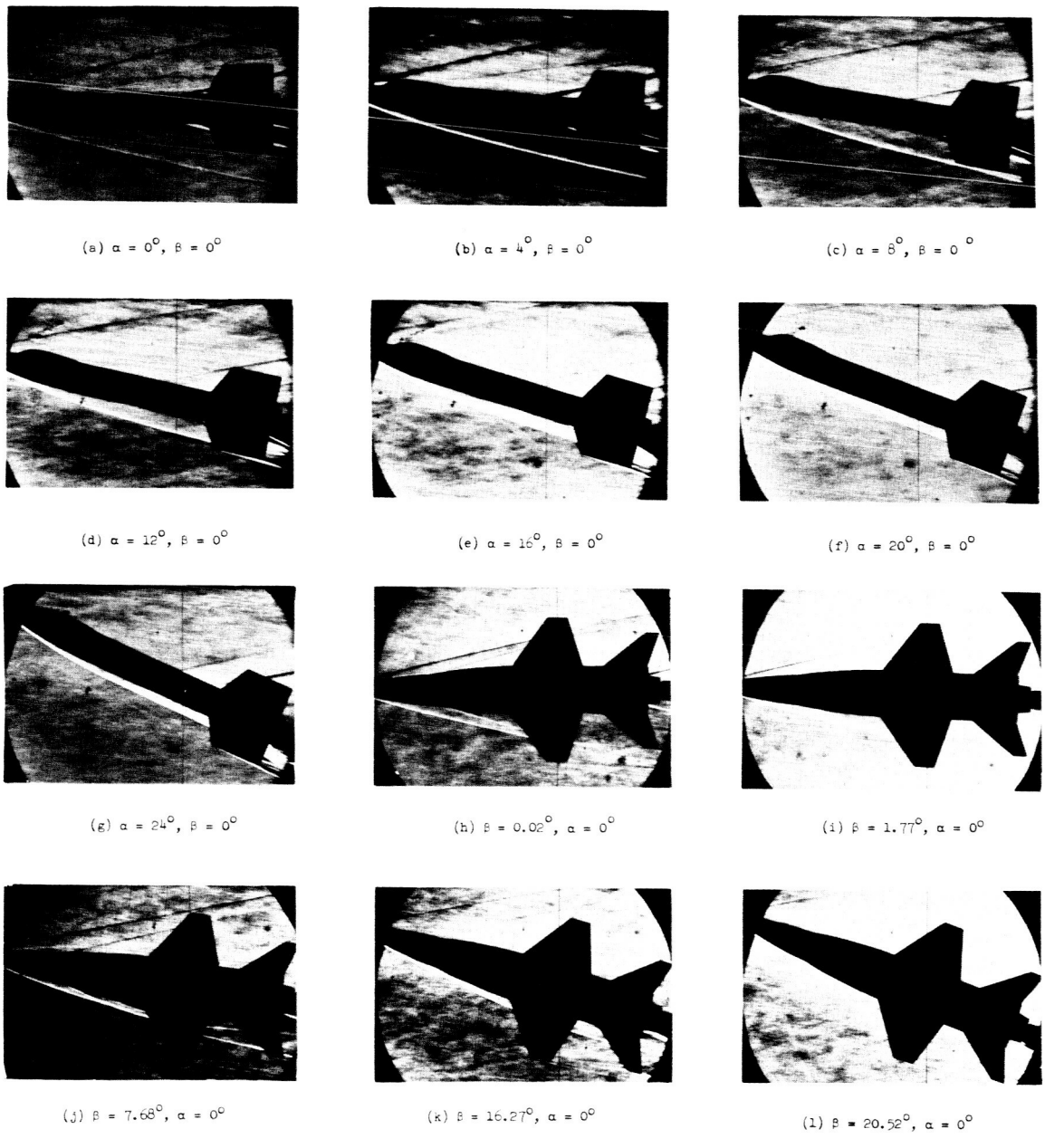

(a) $\alpha = 0^\circ$, $\beta = 0^\circ$ (b) $\alpha = 4^\circ$, $\beta = 0^\circ$ (c) $\alpha = 8^\circ$, $\beta = 0^\circ$

(d) $\alpha = 12^\circ$, $\beta = 0^\circ$ (e) $\alpha = 16^\circ$, $\beta = 0^\circ$ (f) $\alpha = 20^\circ$, $\beta = 0^\circ$

(g) $\alpha = 24^\circ$, $\beta = 0^\circ$ (h) $\beta = 0.02^\circ$, $\alpha = 0^\circ$ (i) $\beta = 1.77^\circ$, $\alpha = 0^\circ$

(j) $\beta = 7.68^\circ$, $\alpha = 0^\circ$ (k) $\beta = 16.27^\circ$, $\alpha = 0^\circ$ (l) $\beta = 20.52^\circ$, $\alpha = 0^\circ$

L-59-6482

Figure 5.- Typical schlieren photographs of configuration 3, $B_4W_2X_{14}H_9V_{U5}V_{L7}$. M = 6.83; R = 640,000.

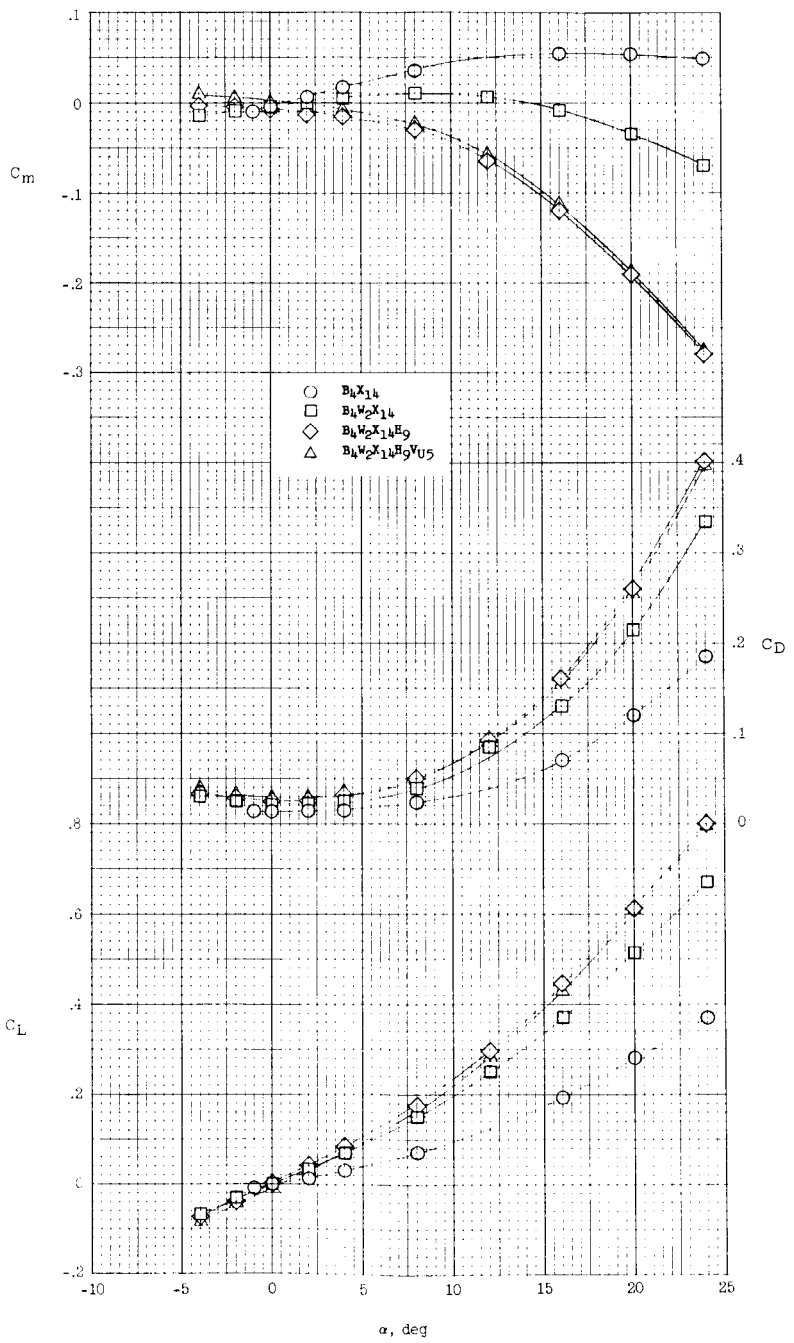

(a) Body-fairing, wing, horizontal tail, and upper vertical tail.

Figure 6.- Effect of component parts on the longitudinal stability characteristics of configuration 3. M = 6.83; R = 640,000.

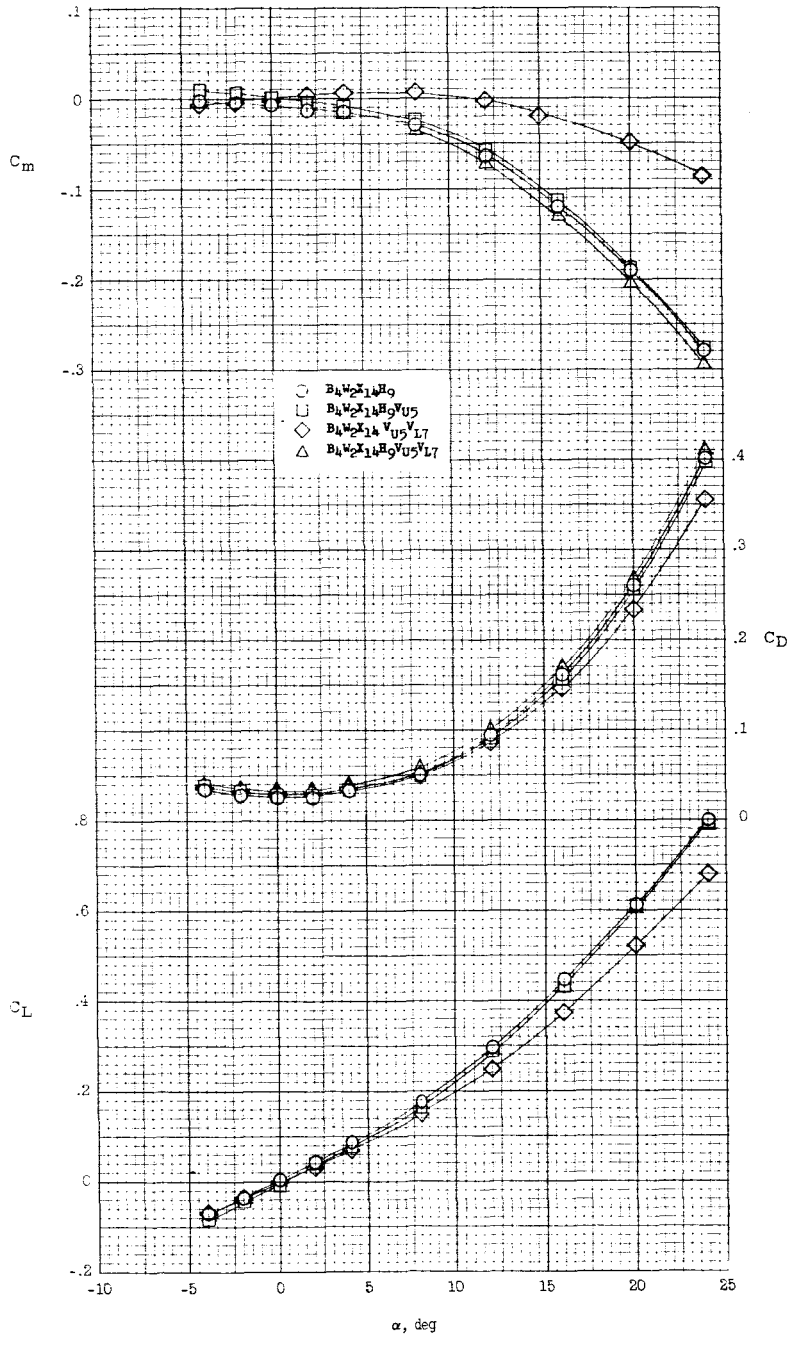

(b) Body-wing-fairing, horizontal tail, and upper and lower vertical tails.

Figure 6.- Concluded.

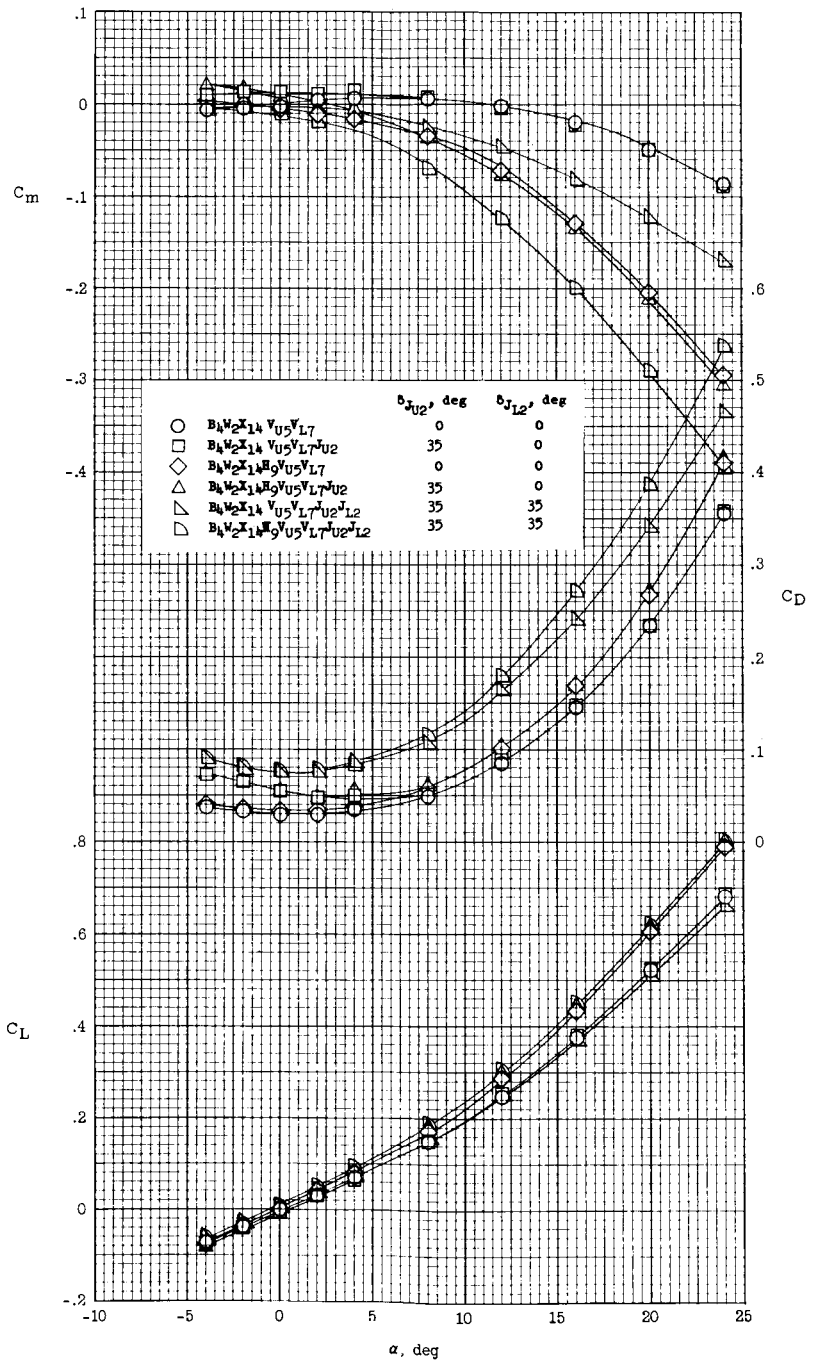

Figure 7.- Effect of speed brakes with and without the horizontal tail on the longitudinal stability characteristics of configuration 3. M = 6.83; R = 640,000.

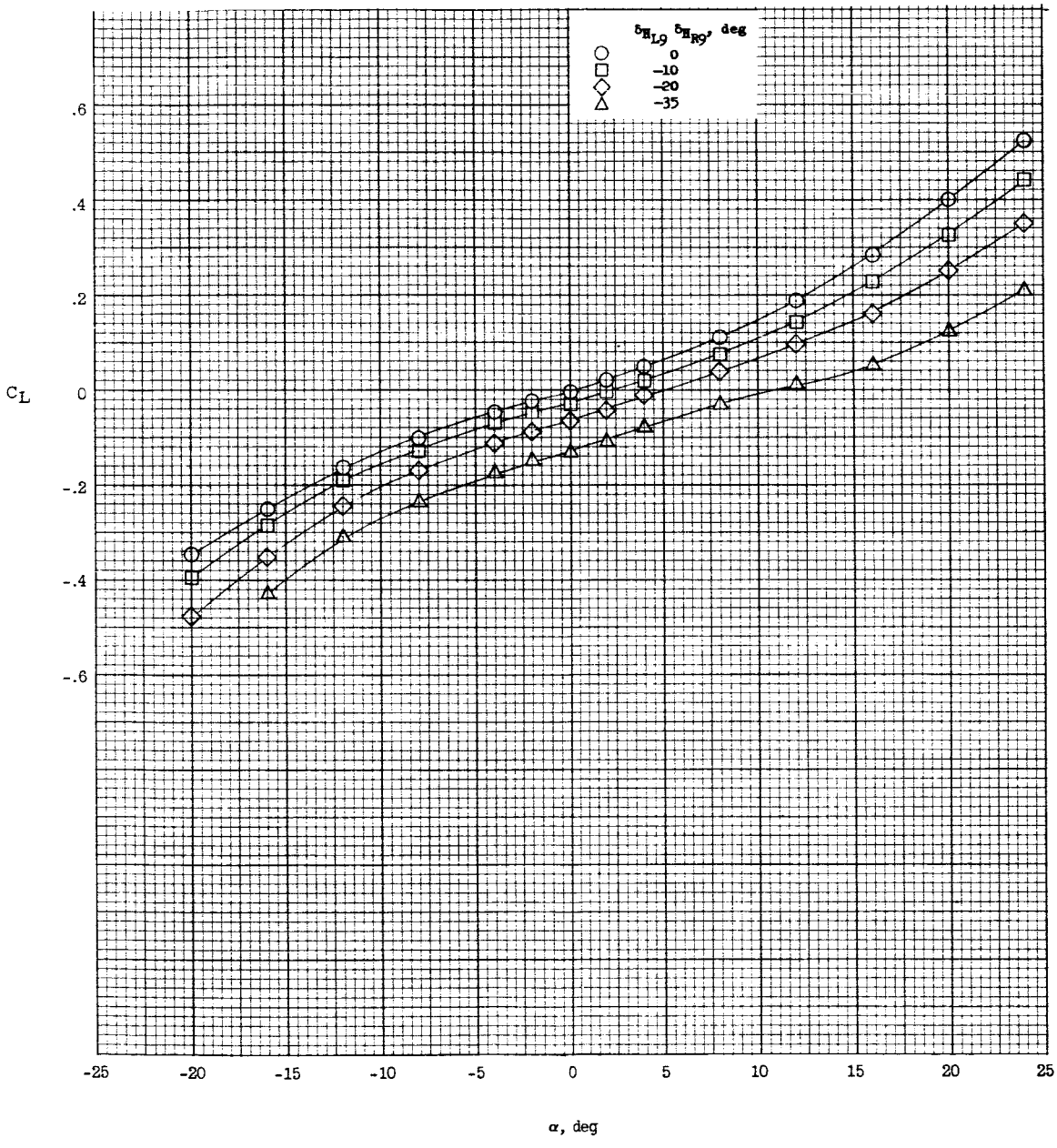

(a) Lift.

Figure 8.- Effect of horizontal-tail deflection on the longitudinal stability characteristics of configuration 3 with wing removed $(B_4X_{14}H_9V_{U5}V_{L7})$. M = 6.83; R = 640,000.

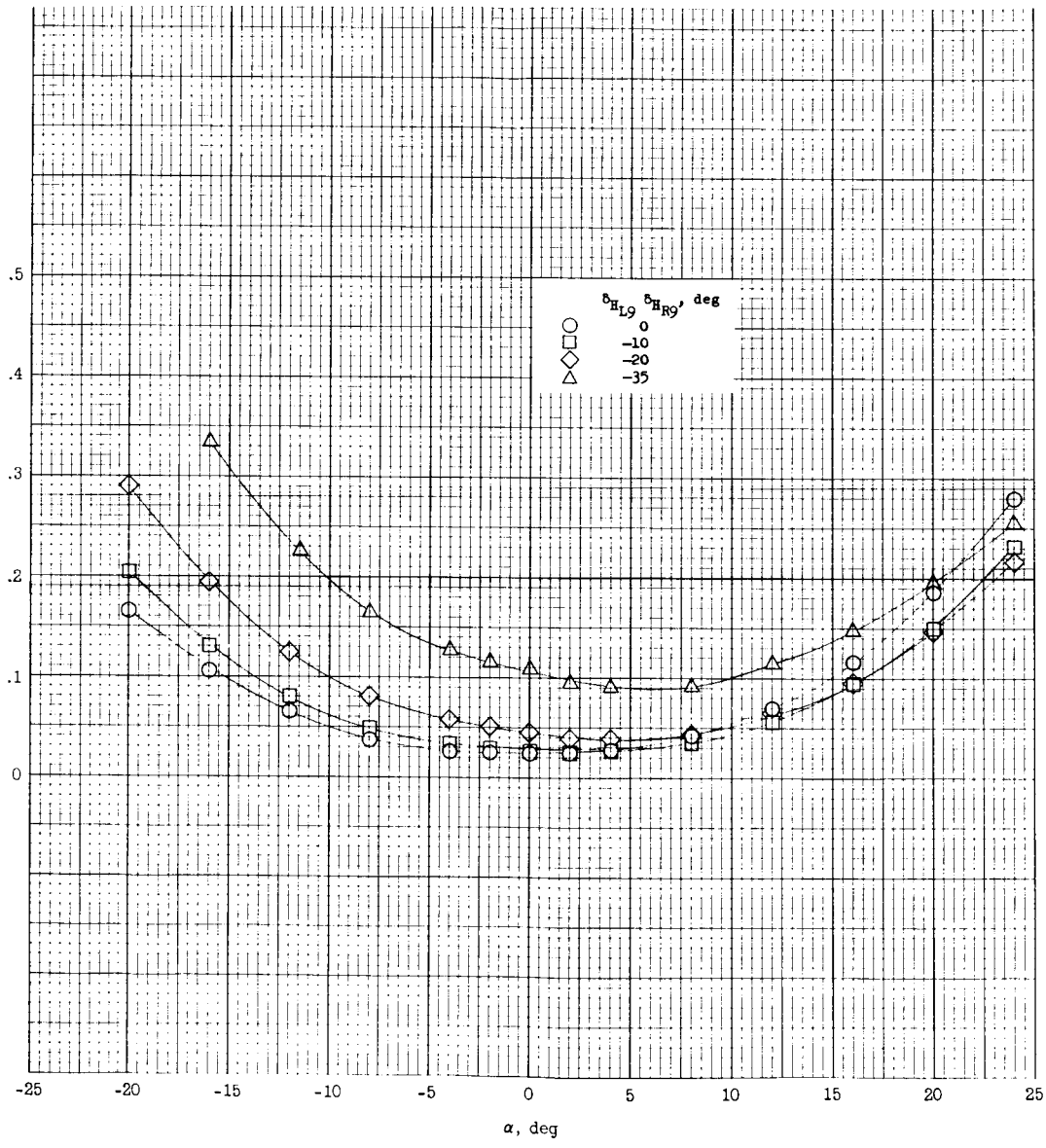

(b) Drag.

Figure 8.- Continued.

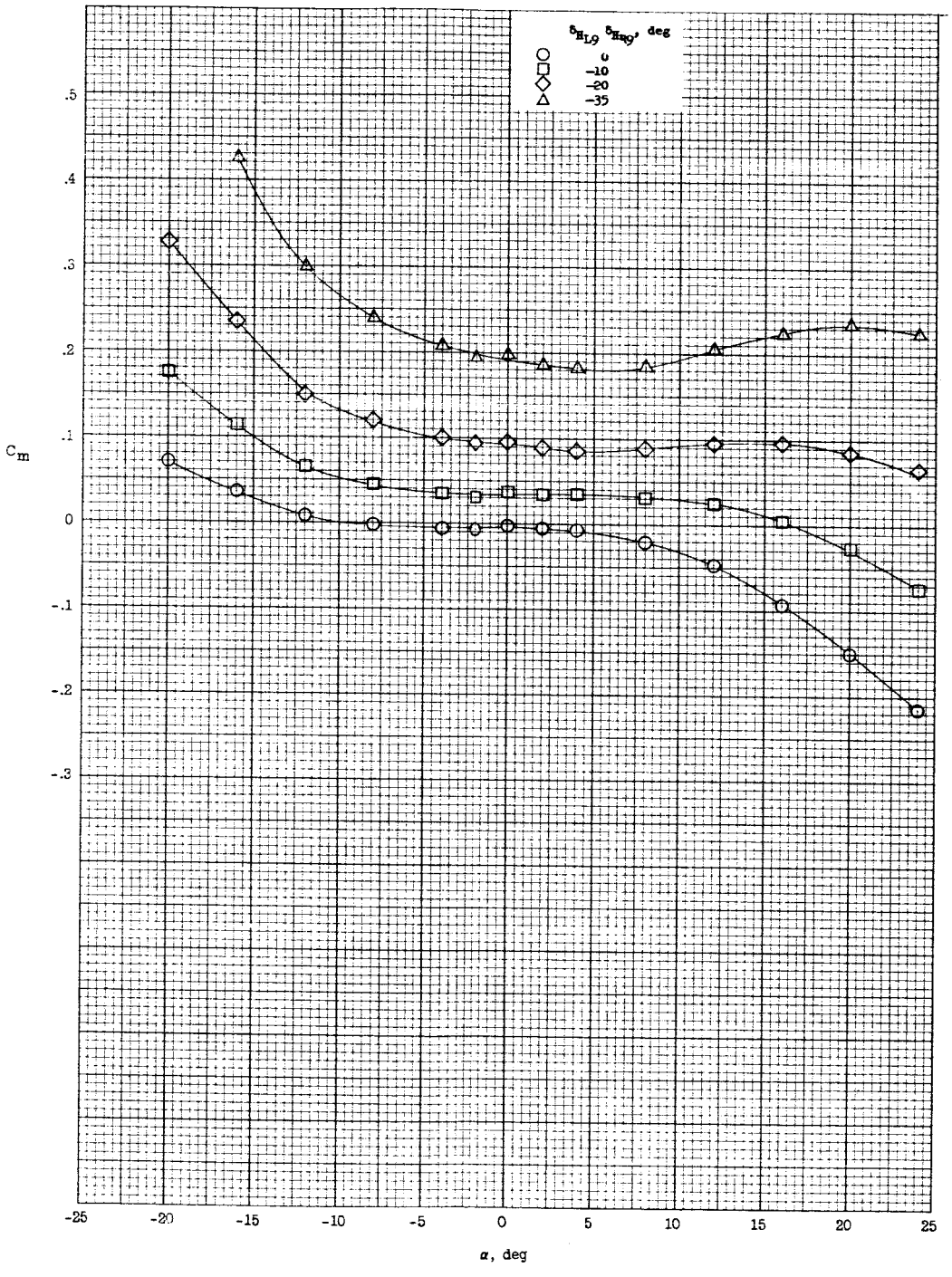

(c) Pitching moment.

Figure 8.- Concluded.

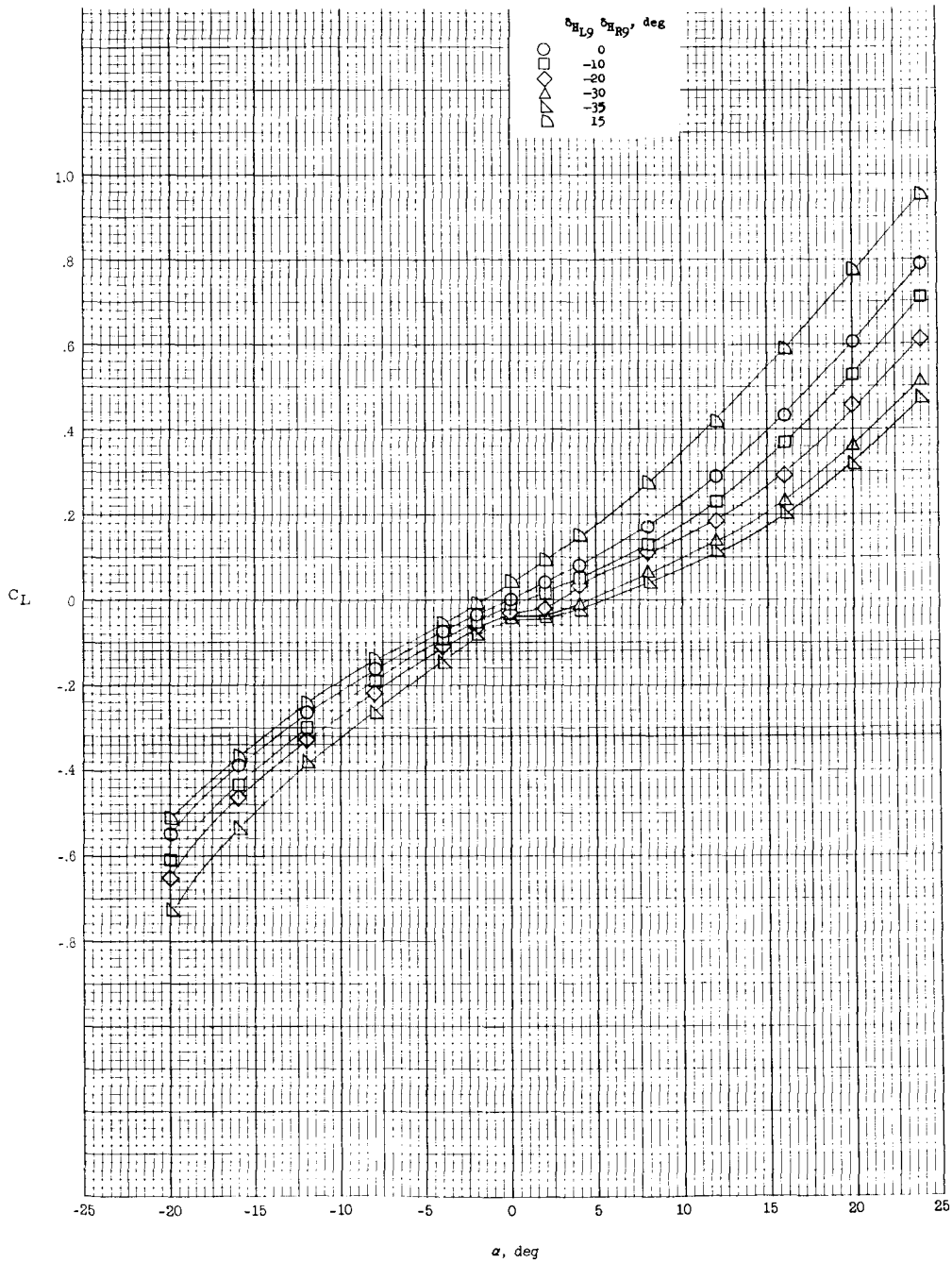

(a) Lift.

Figure 9.- Effect of horizontal-tail deflection on the longitudinal stability characteristics of configuration 3. M = 6.83; R = 640,000.

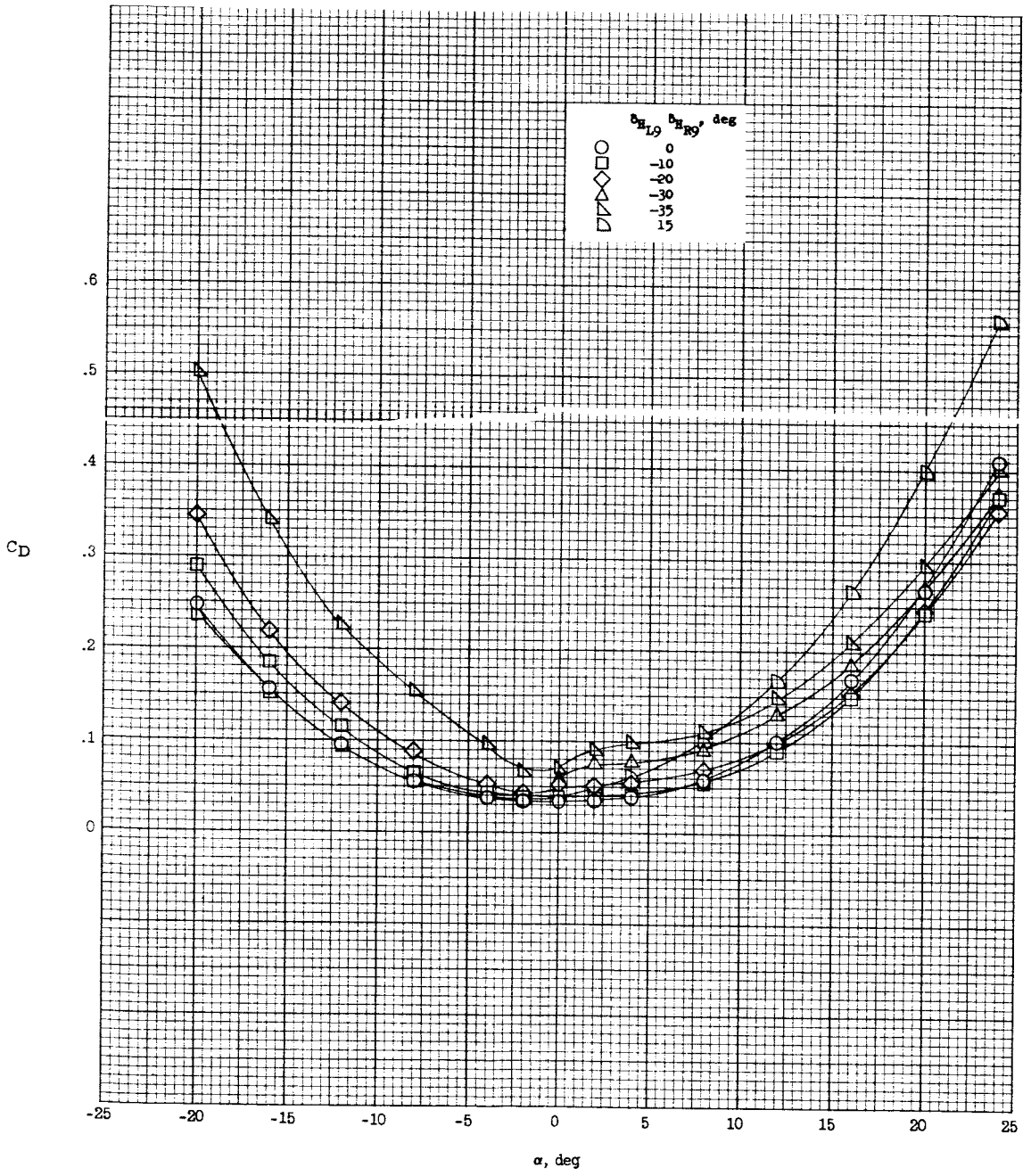

(b) Drag.

Figure 9.- Continued.

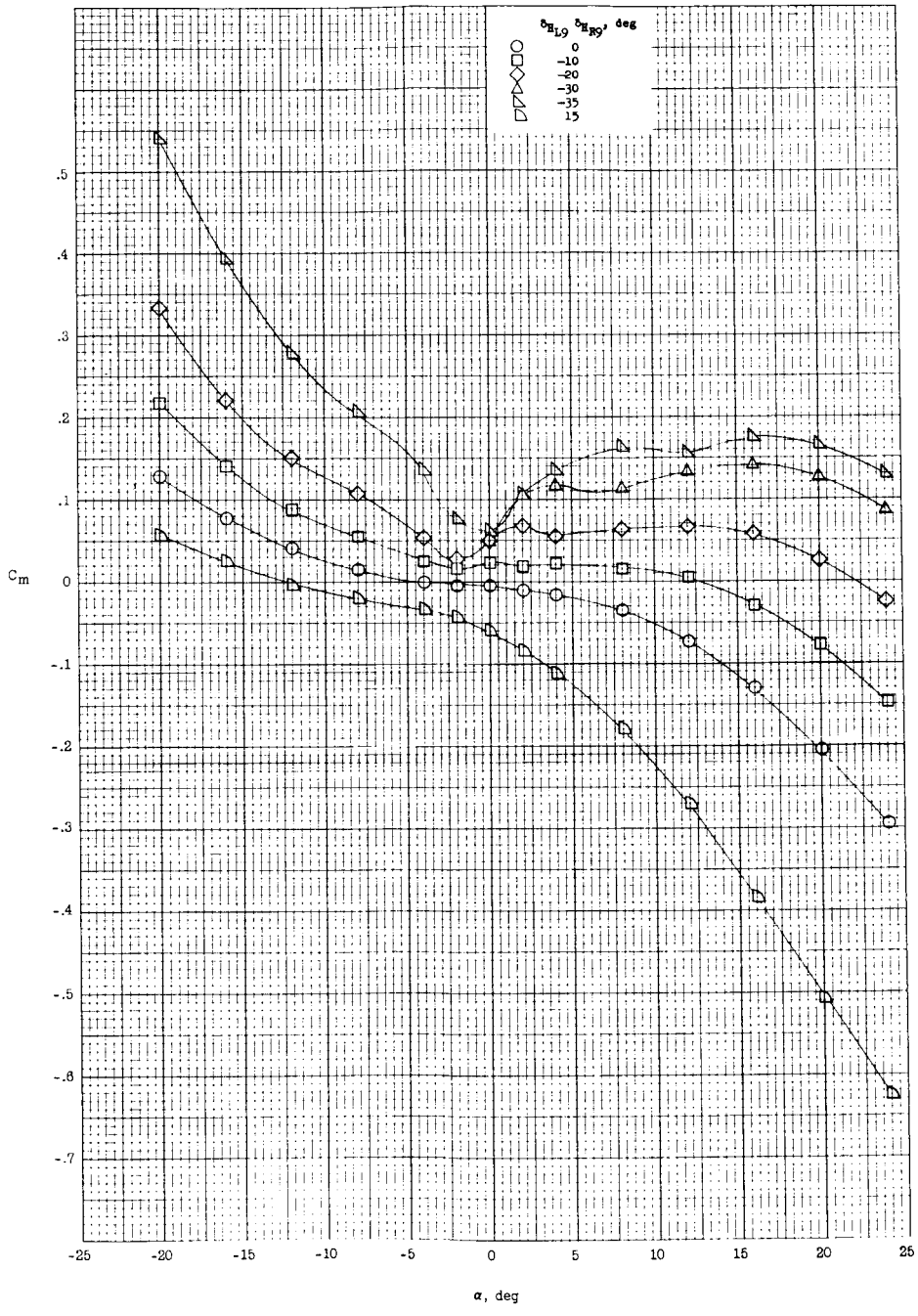

(c) Pitching moment.

Figure 9.- Concluded.

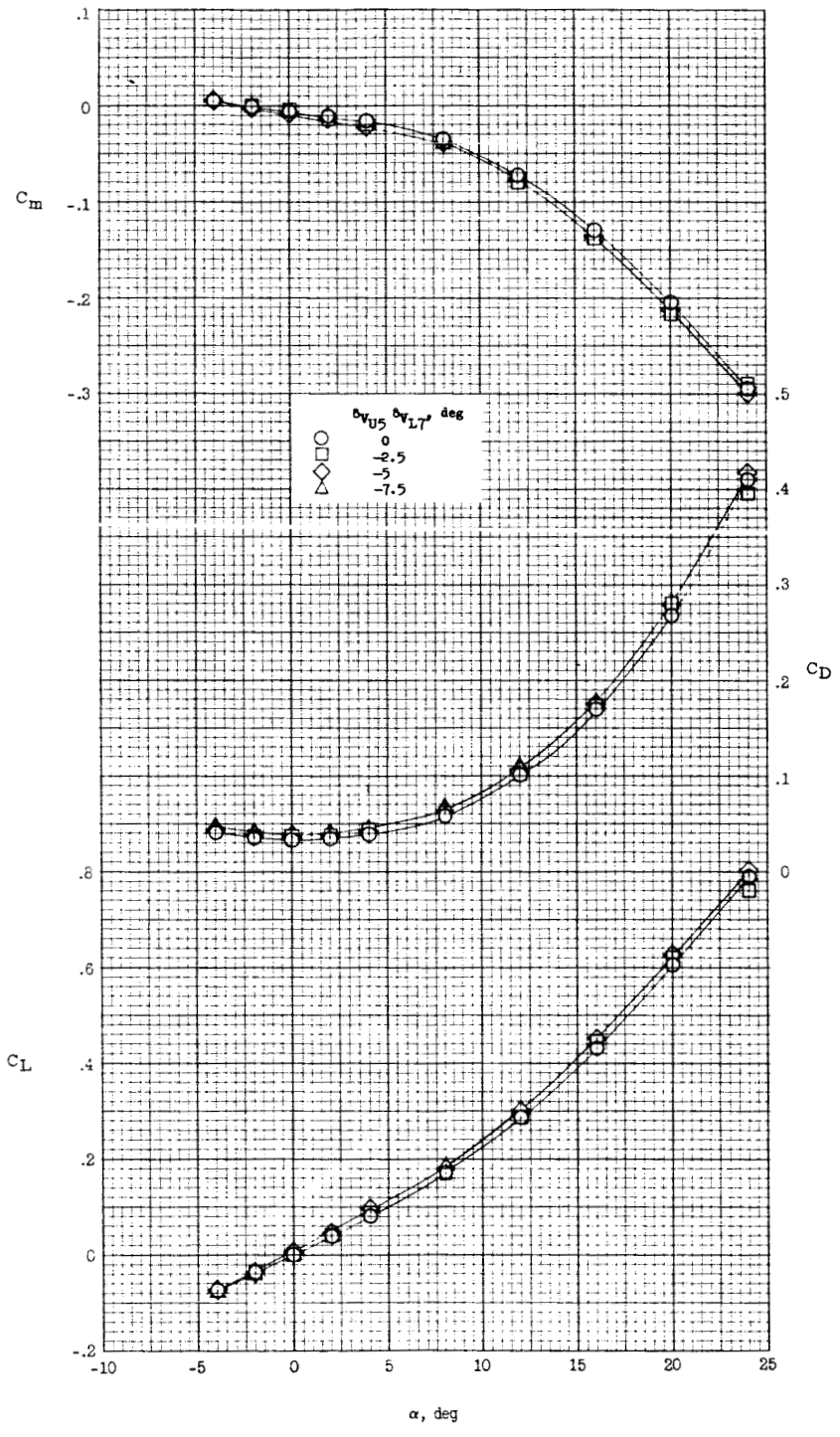

Figure 10.- Effect of vertical-tail deflection on the longitudinal stability characteristics of configuration 3. M = 6.83; R = 640,000.

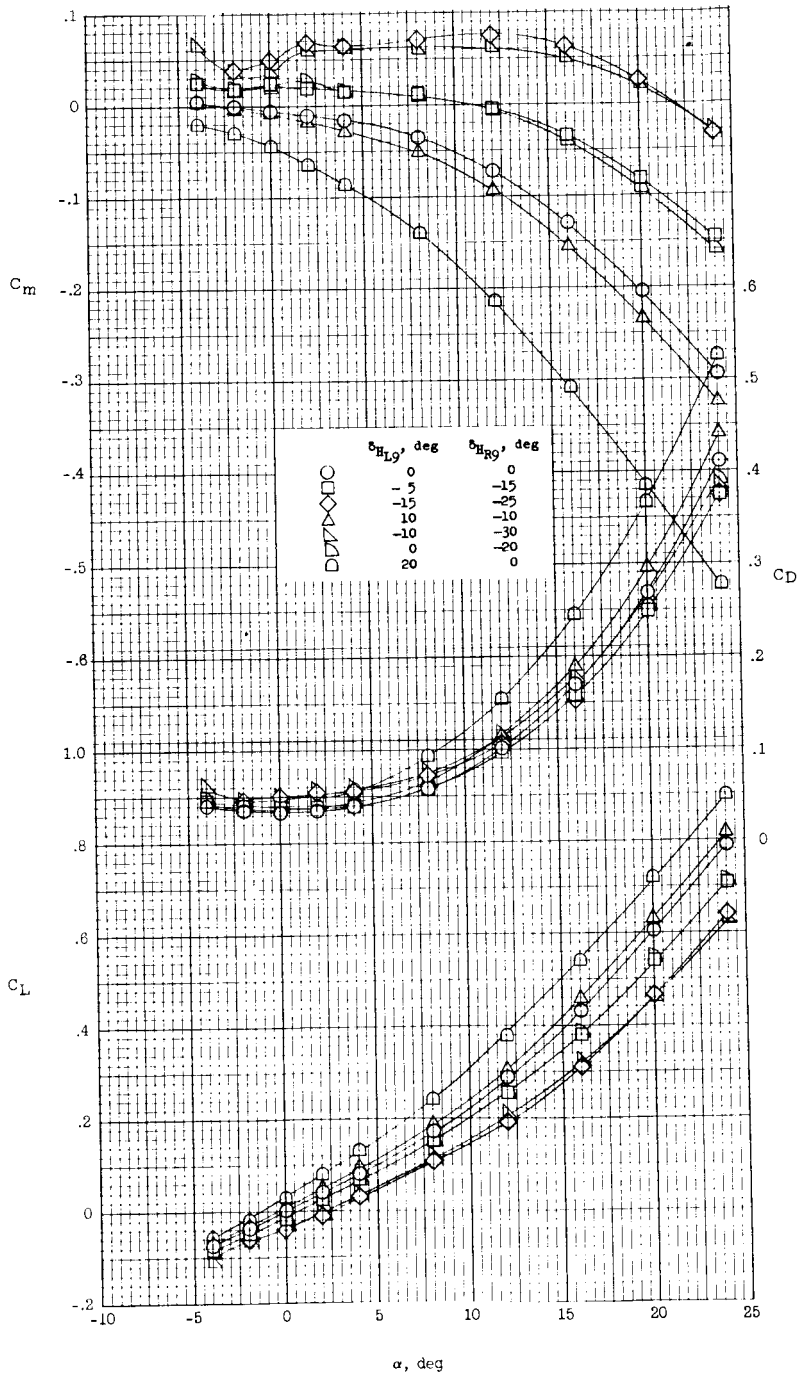

Figure 11.- Effect of differential horizontal-tail deflection on the longitudinal stability characteristics of configuration 3. M = 6.83; R = 640,000.

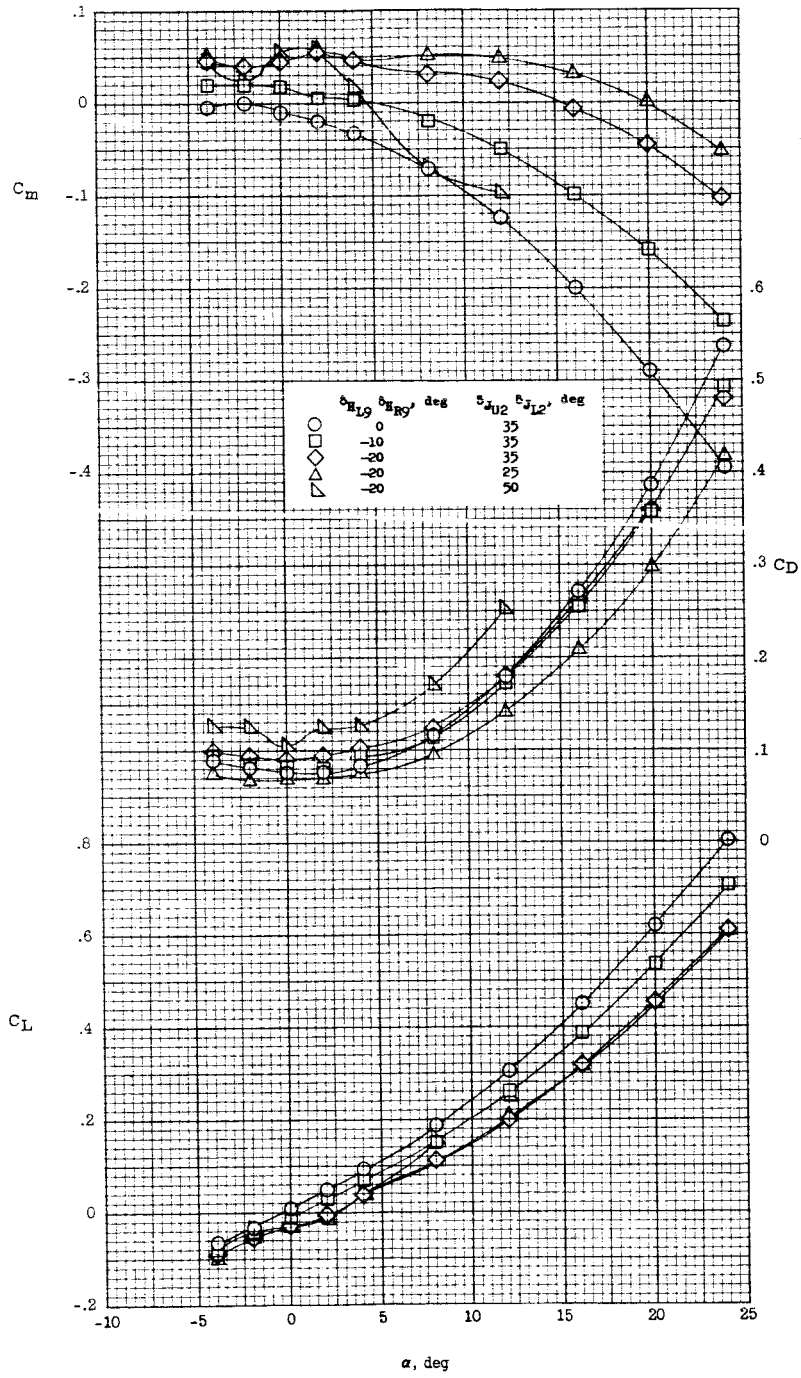

Figure 12.- Effect of horizontal-tail deflection on the longitudinal stability characteristics of configuration 3 with various speed-brake deflections. M = 6.83; R = 640,000.

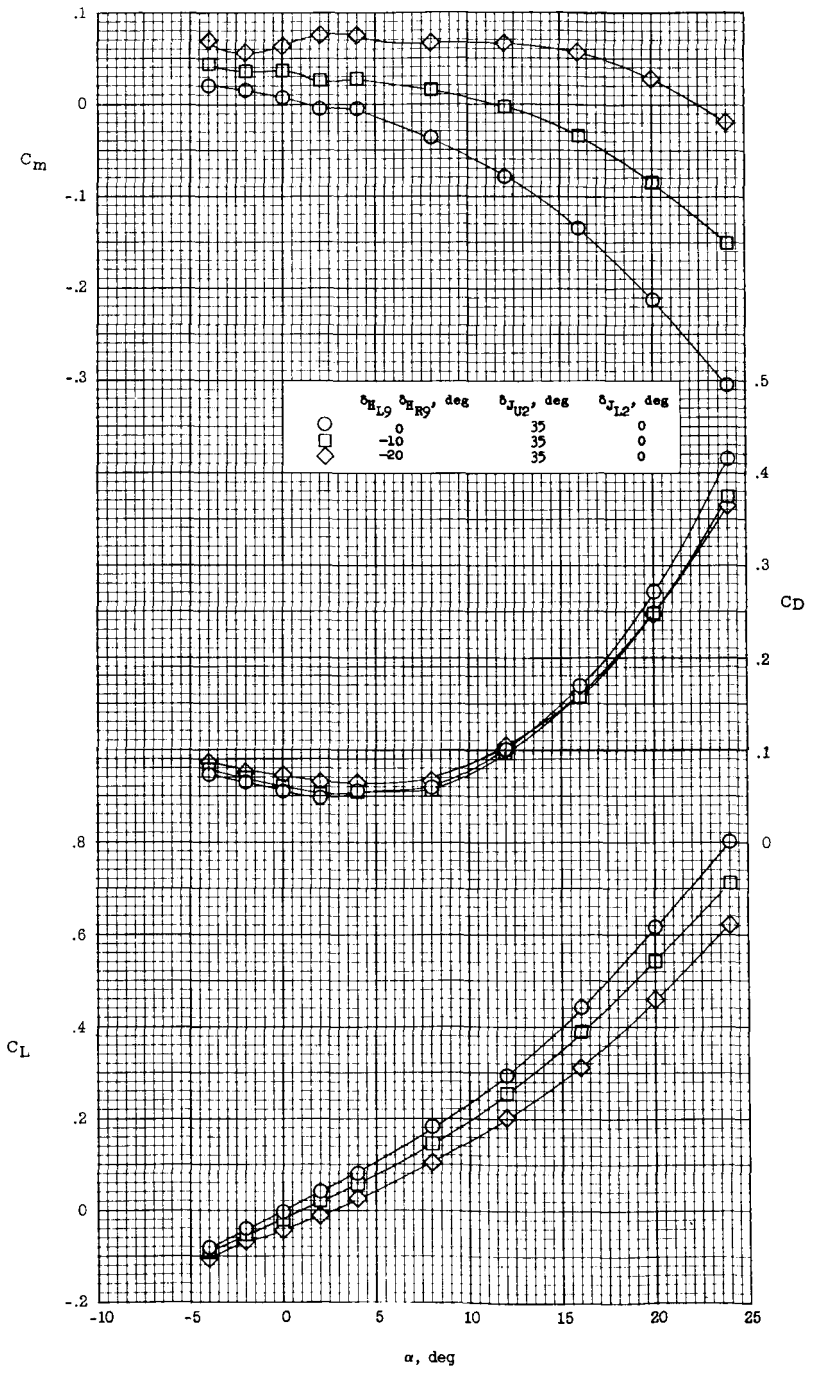

Figure 13.- Effect of horizontal-tail deflection on the longitudinal stability characteristics of configuration 3 with upper speed-brake deflection. M = 6.83; R = 640,000.

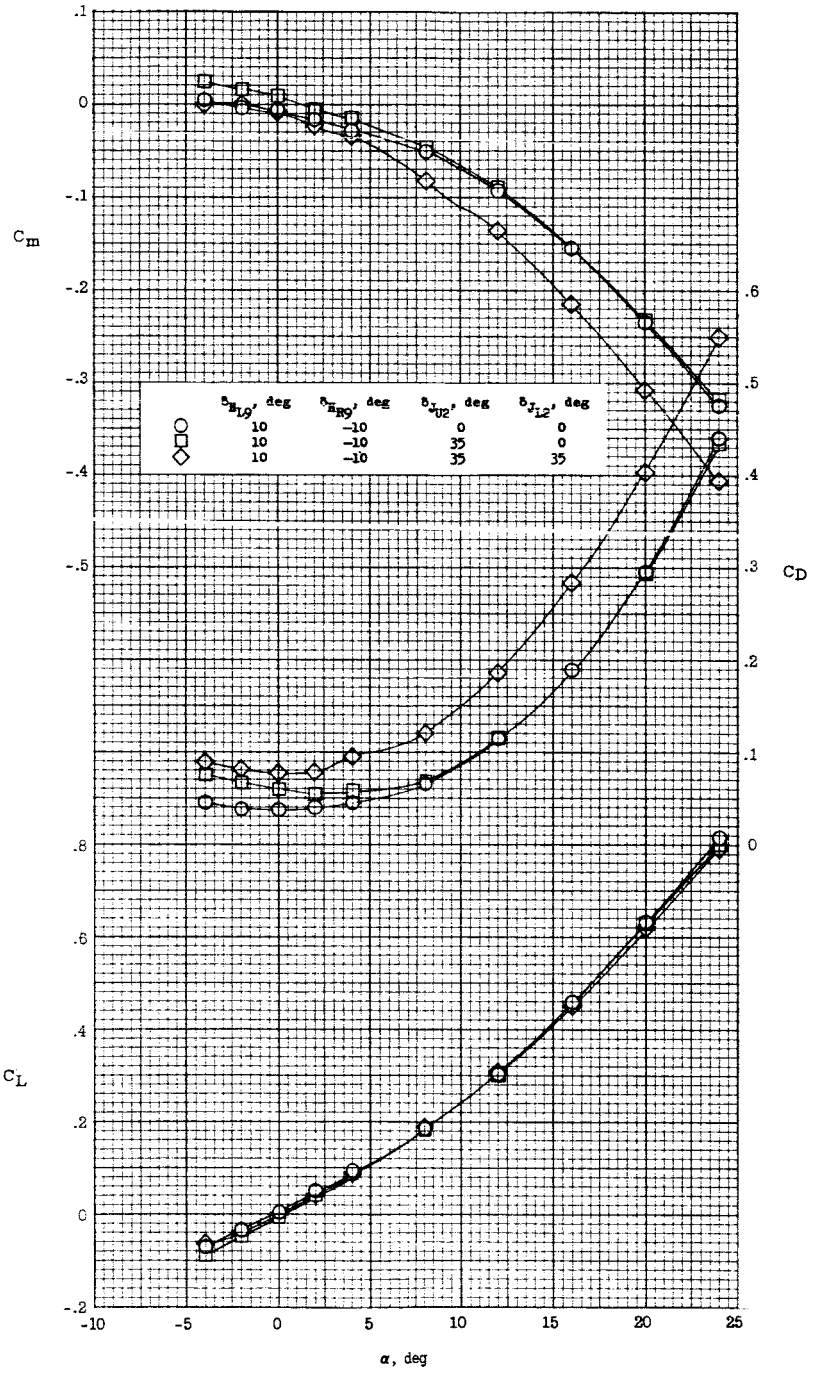

Figure 14.- Effect of speed-brake deflection on the longitudinal stability characteristics of configuration 3 with differential horizontal-tail deflection. M = 6.83; R = 640,000.

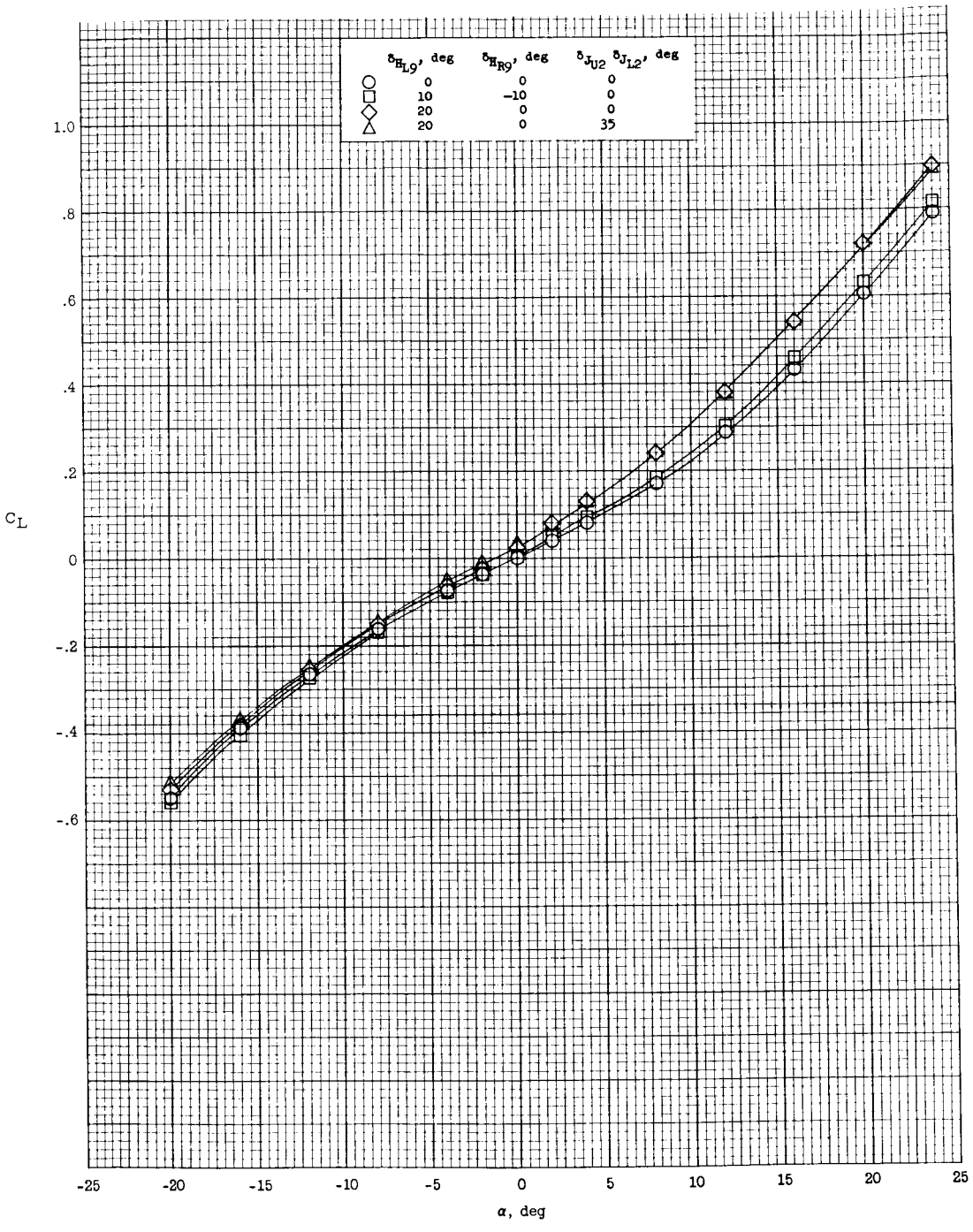

(a) Lift.

Figure 15.- Effect of differential horizontal-tail deflection on the longitudinal stability characteristics of configuration 3 with and without speed-brake deflection. M = 6.83; R = 640,000.

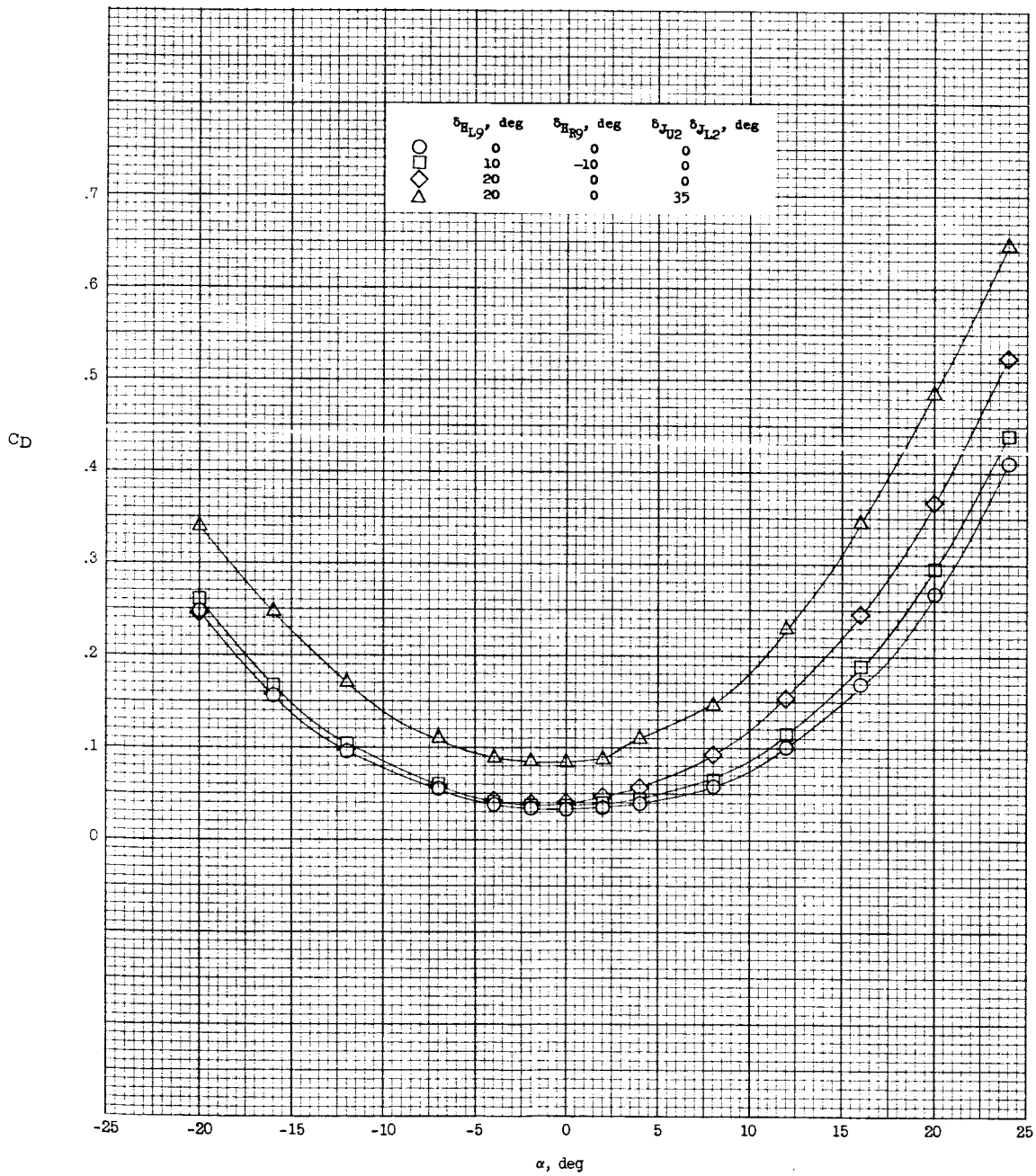

(b) Drag.

Figure 15.- Continued.

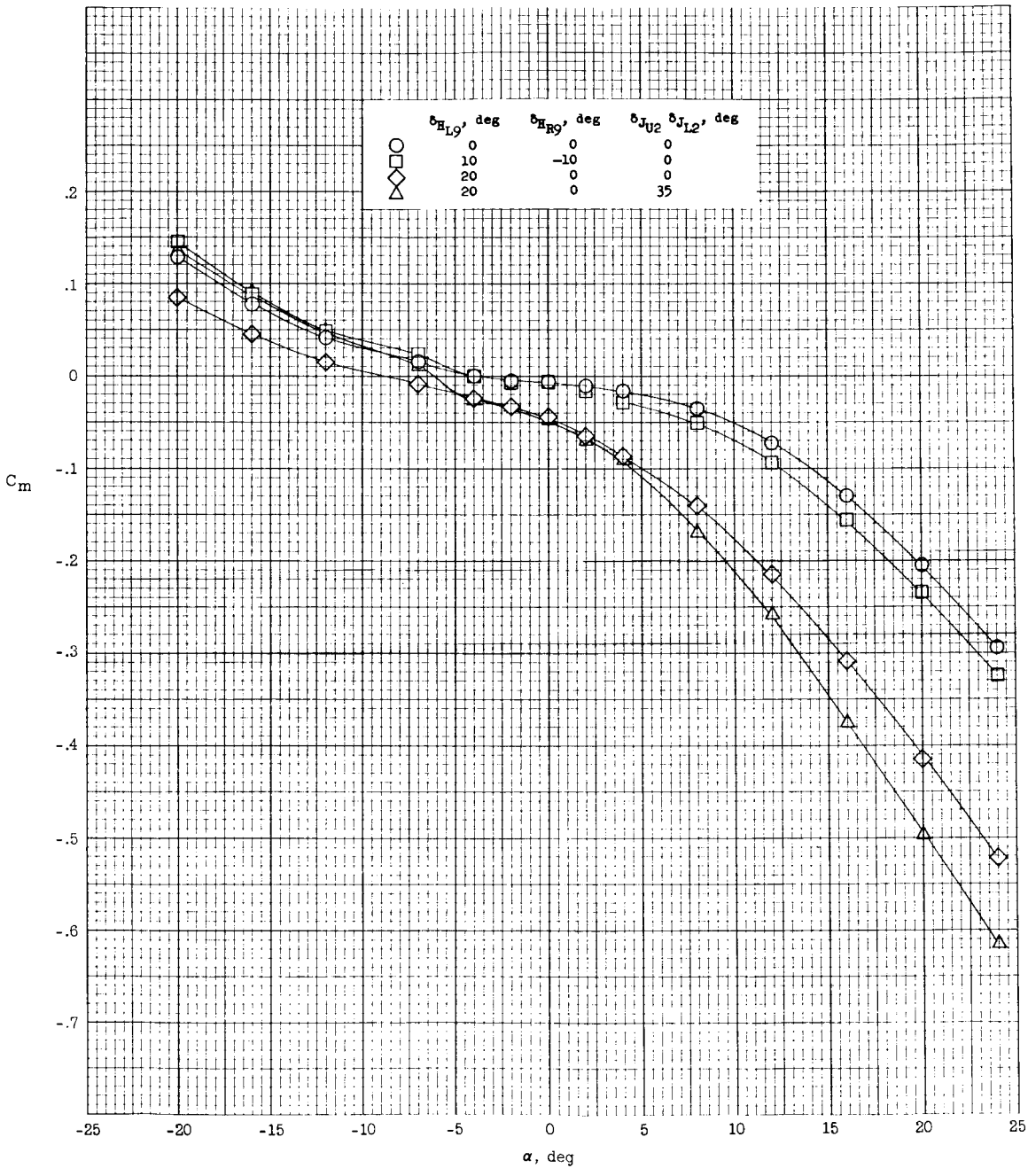

(c) Pitching moment.

Figure 15.- Concluded.

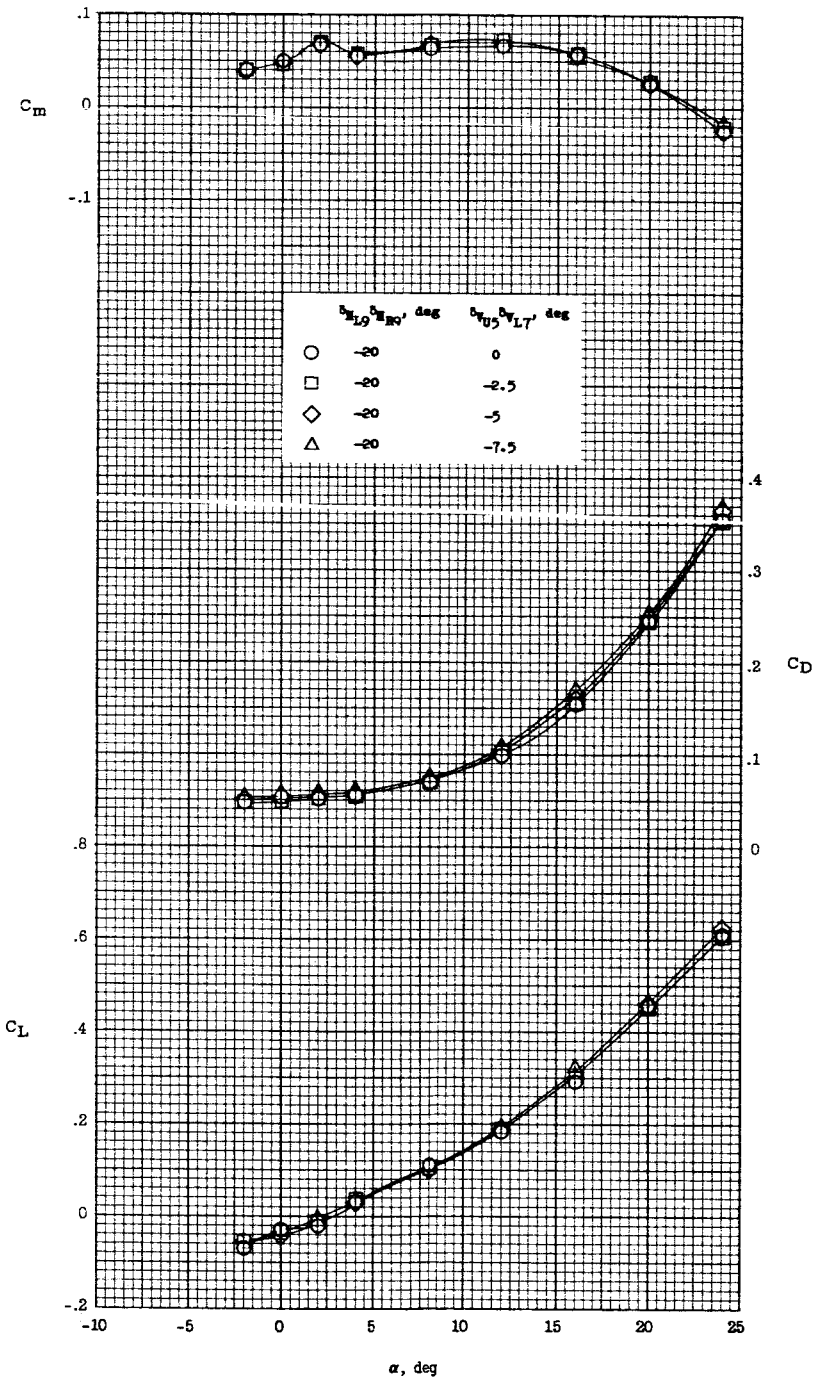

Figure 16.- Effect of vertical-tail deflection on the longitudinal stability characteristics of configuration 3 with horizontal-tail deflection. M = 6.83; R = 640,000.

L-739

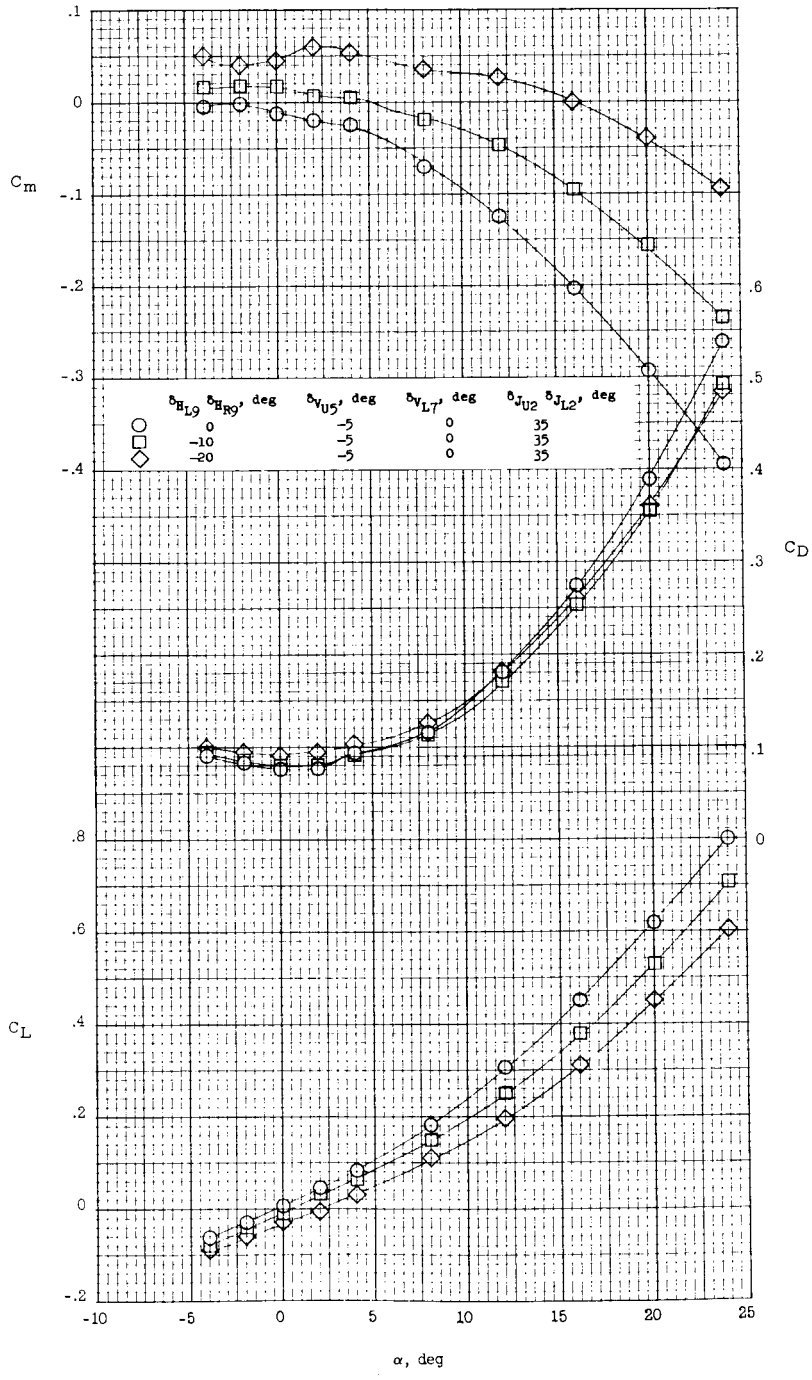

Figure 17.- Effect of horizontal-tail deflection on the longitudinal stability characteristics of configuration 3 with upper vertical-tail and speed-brake deflections. M = 6.83; R = 640,000.

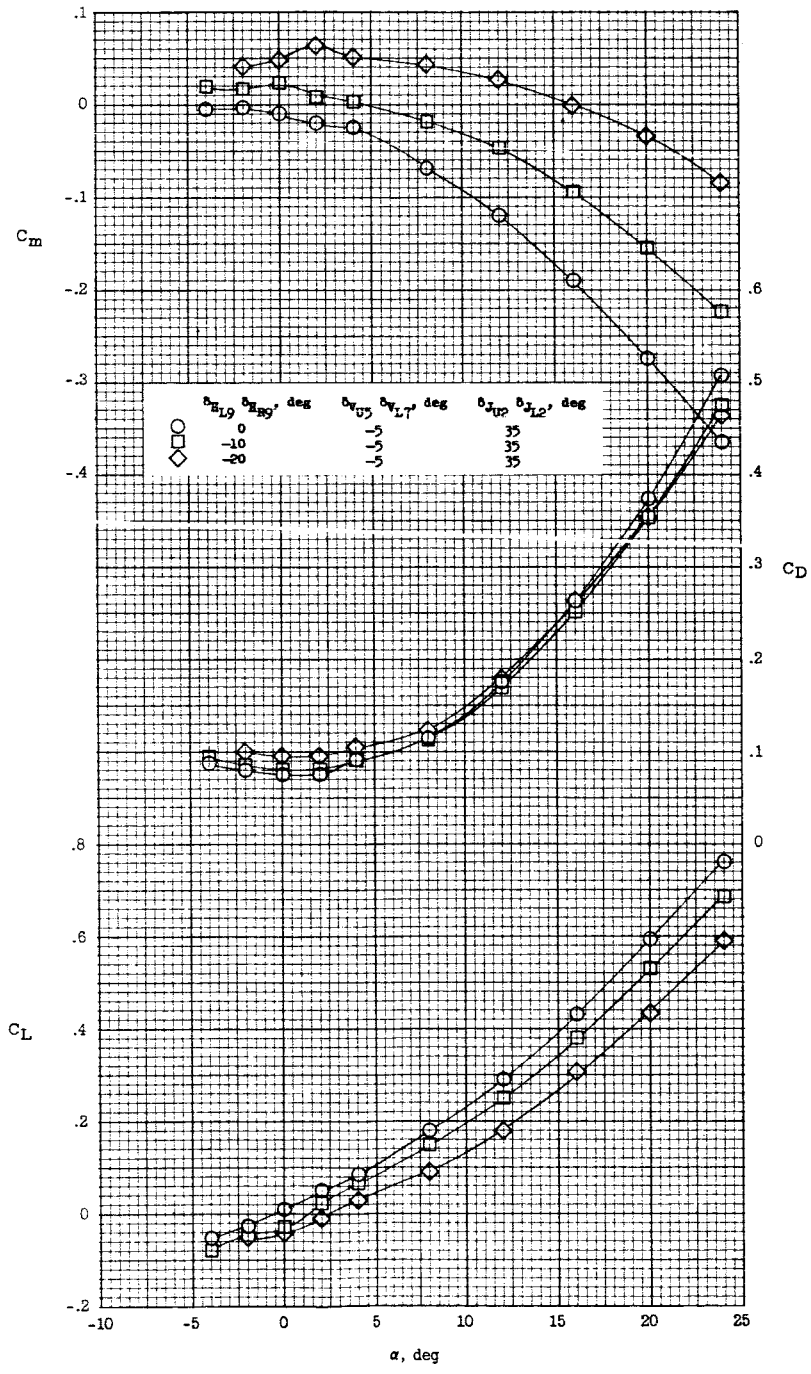

Figure 18.- Effect of horizontal-tail deflection on the longitudinal stability characteristics of configuration 3 with vertical-tail and speed-brake deflections. M = 6.83; R = 640,000.

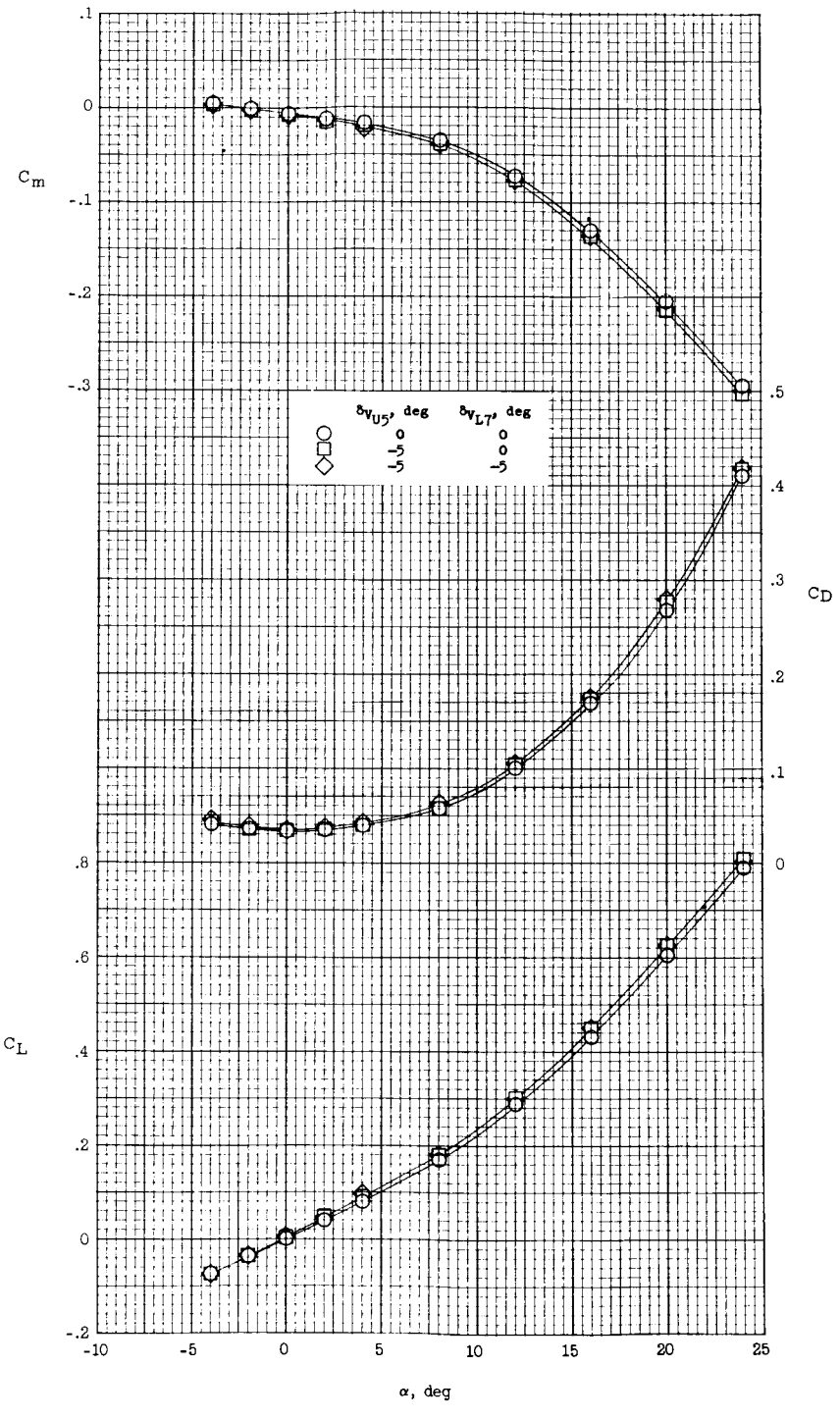

Figure 19.- Effect of upper vertical-tail deflection on the longitudinal stability characteristics of configuration 3. M = 6.83; R = 640,000.

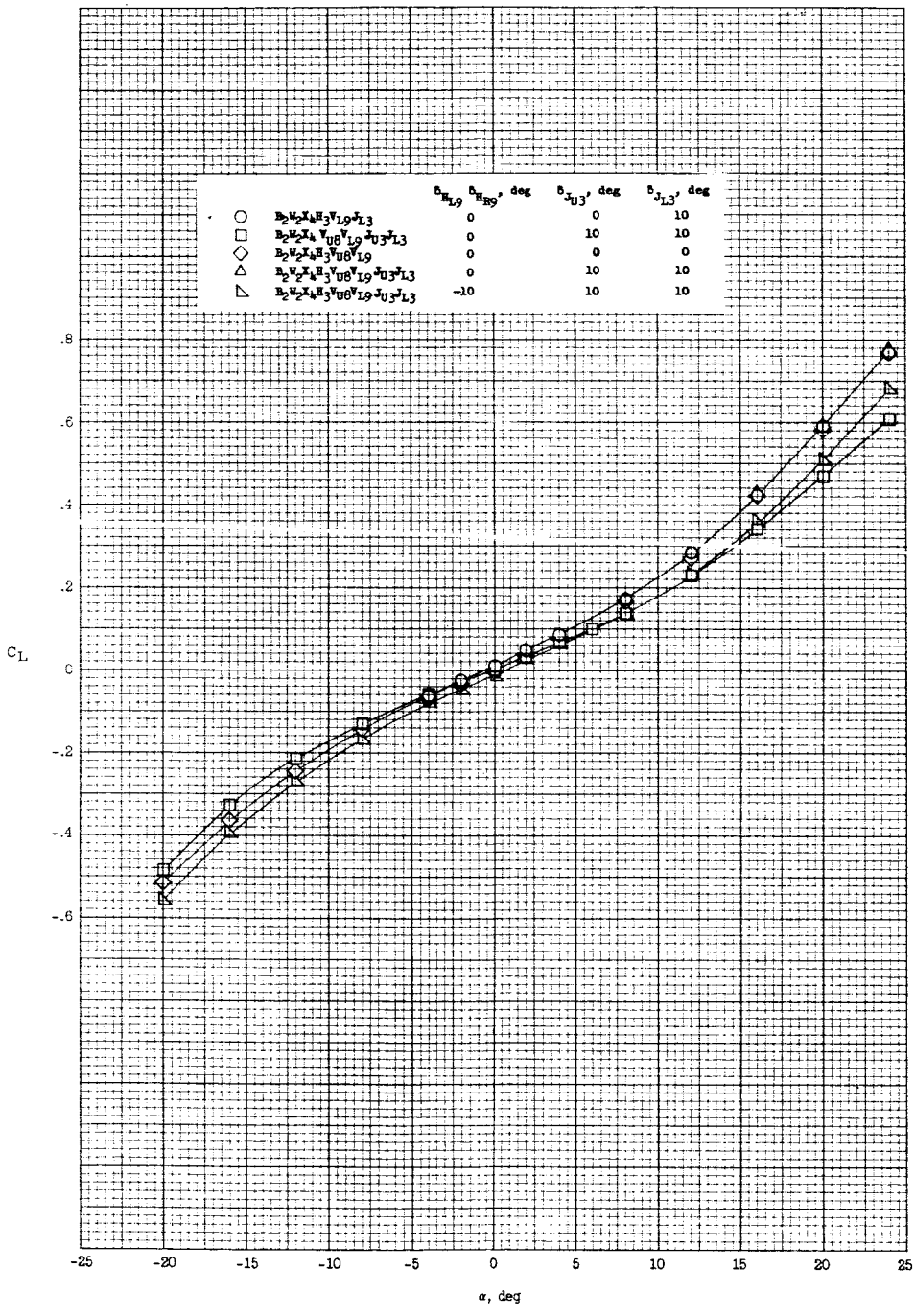

(a) Lift.

Figure 20.- Effect of speed brake and horizontal-tail deflection and the removal of the horizontal tail on the longitudinal stability characteristics of modified configuration 3, $B_2W_2X_4H_3V_{U8}V_{L9}J_{U3}J_{L3}$. M = 6.83; R = 640,000.

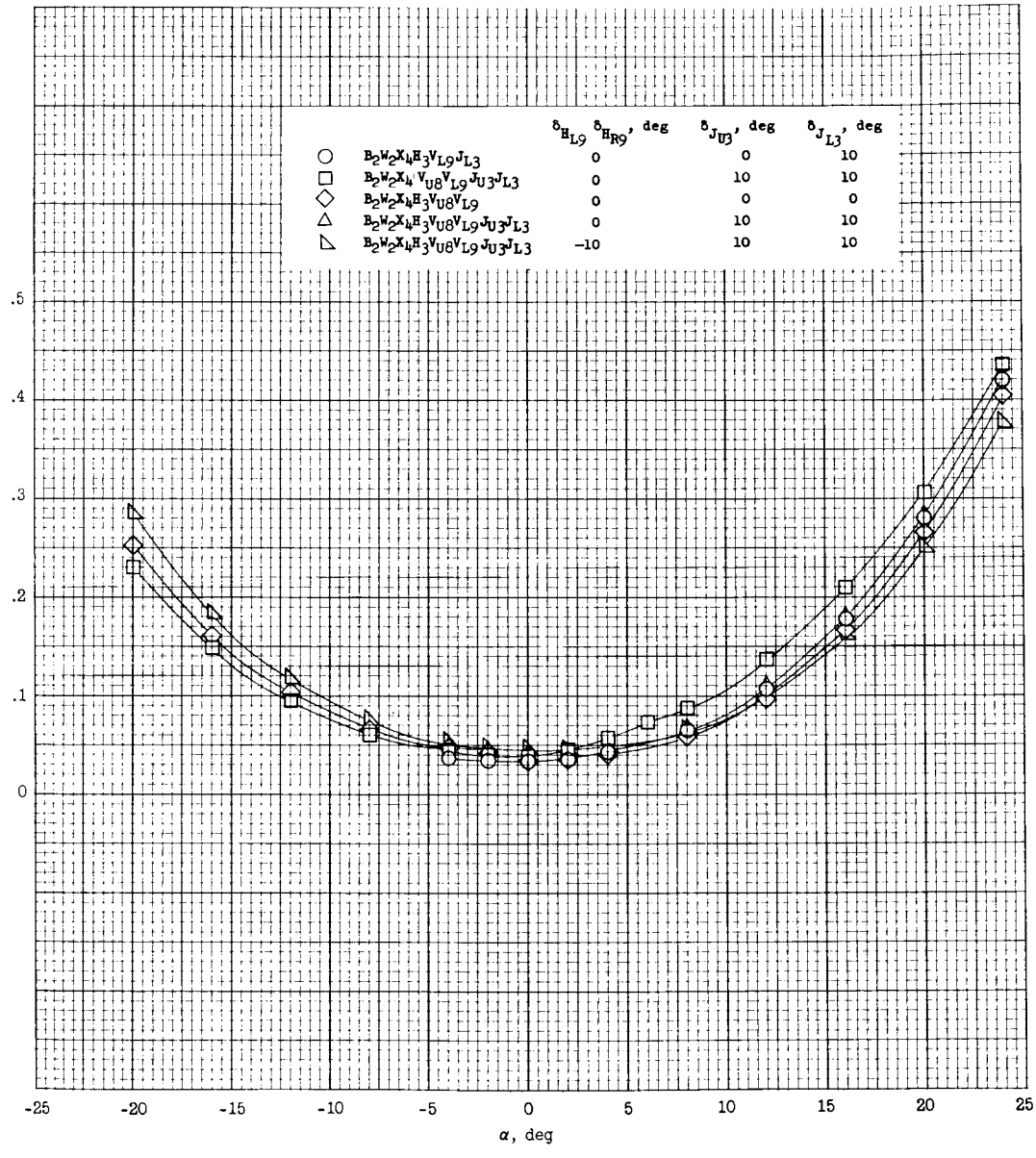

(b) Drag.

Figure 20.- Continued.

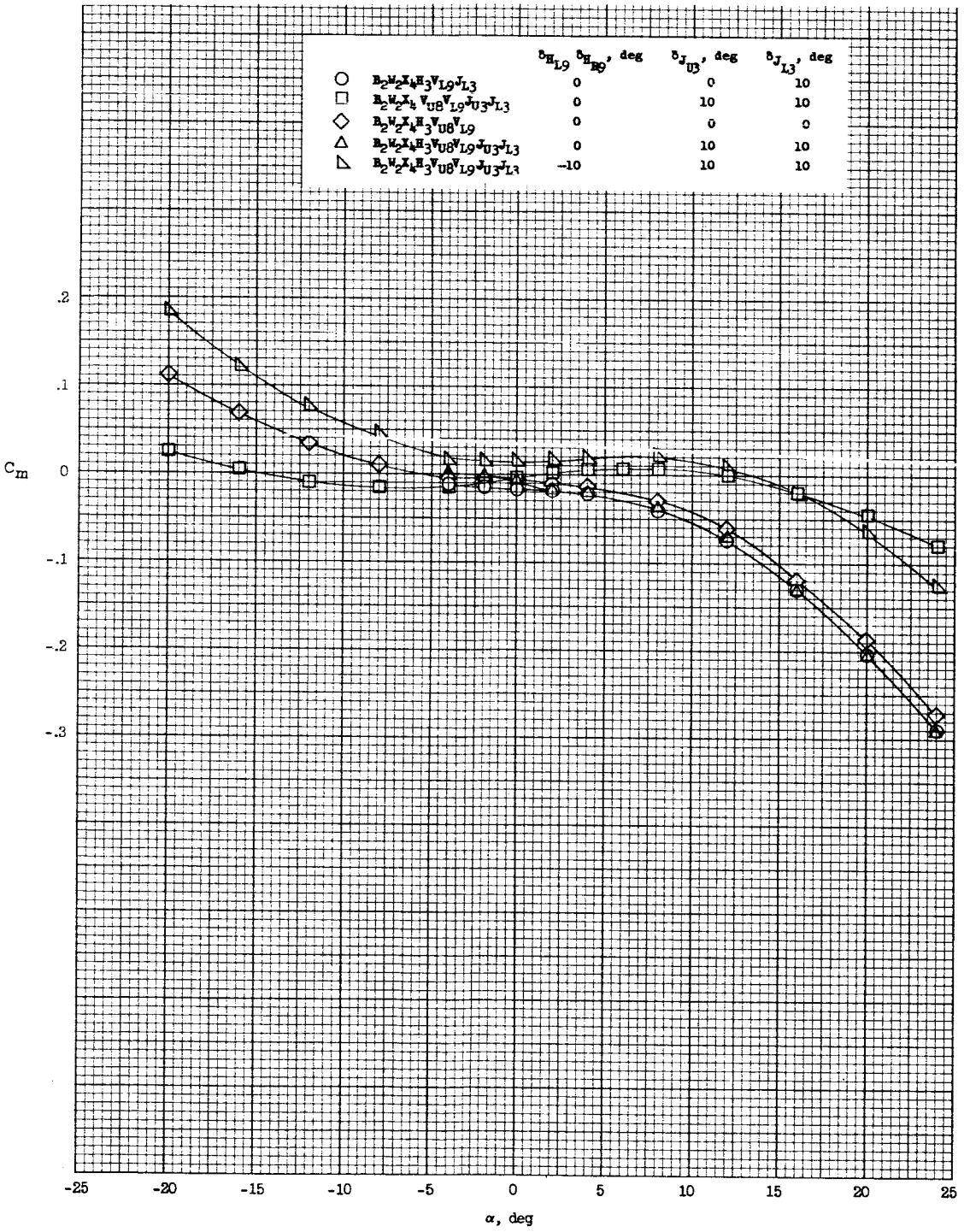

(c) Pitching moment.

Figure 20.- Concluded.

L-739

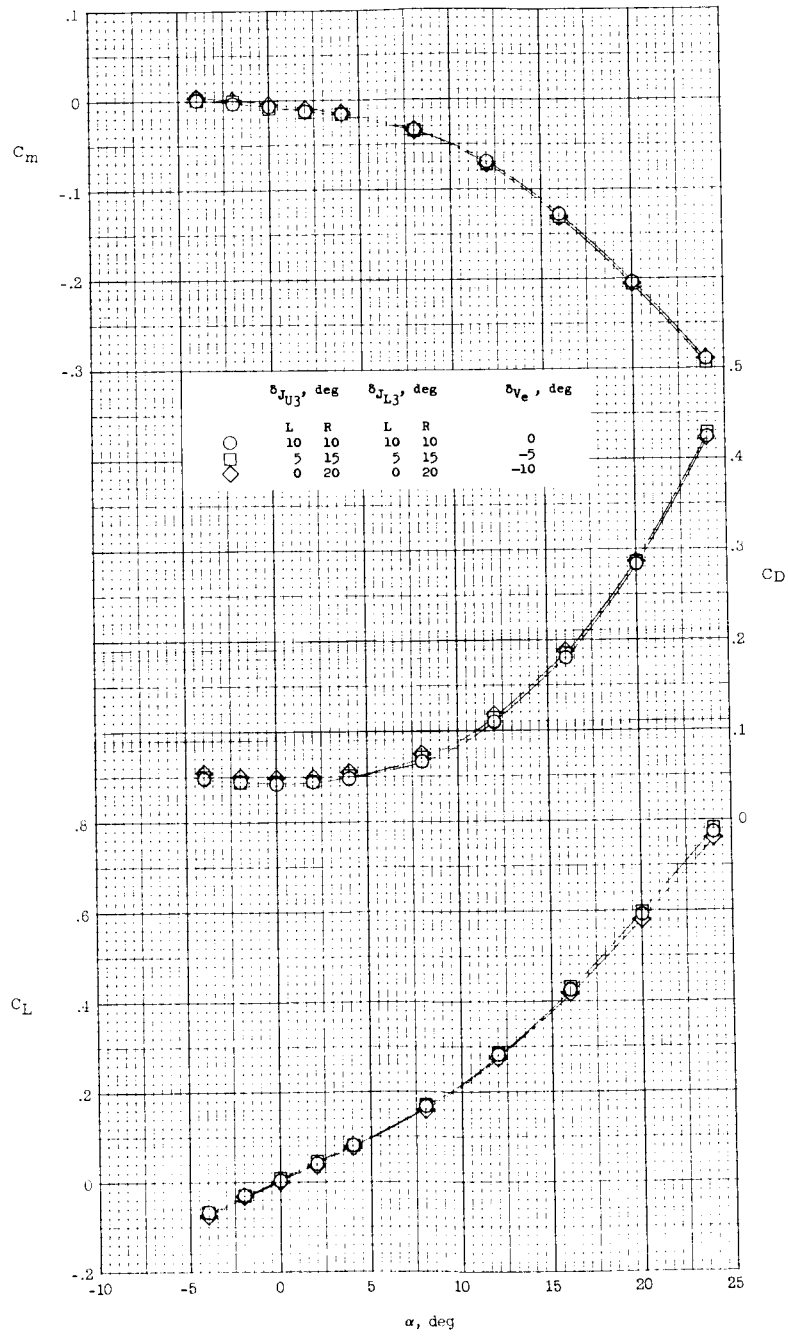

Figure 21.- Effect of differential speed-brake deflection on the longitudinal stability characteristics of modified configuration 3, $B_2W_2X_4H_3V_{U8}V_{L9}J_{U3}J_{L3}$. M = 6.83; R = 640,000.

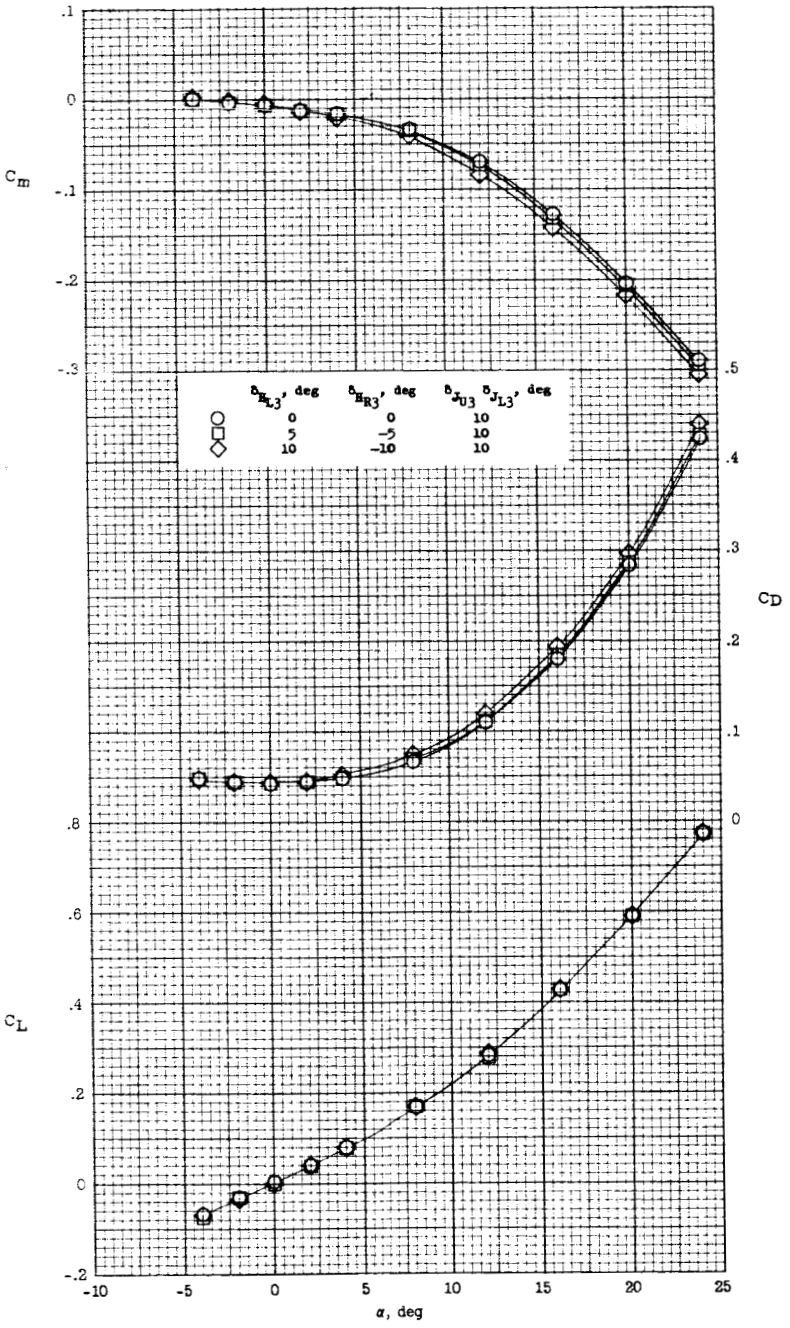

Figure 22.- Effect of differential horizontal-tail deflection on the longitudinal stability characteristics of modified configuration 3 with speed-brake deflection $(B_2W_2X_4H_3V_{U8}V_{L9}J_{U3}J_{L3})$. M = 6.83; R = 640,000.

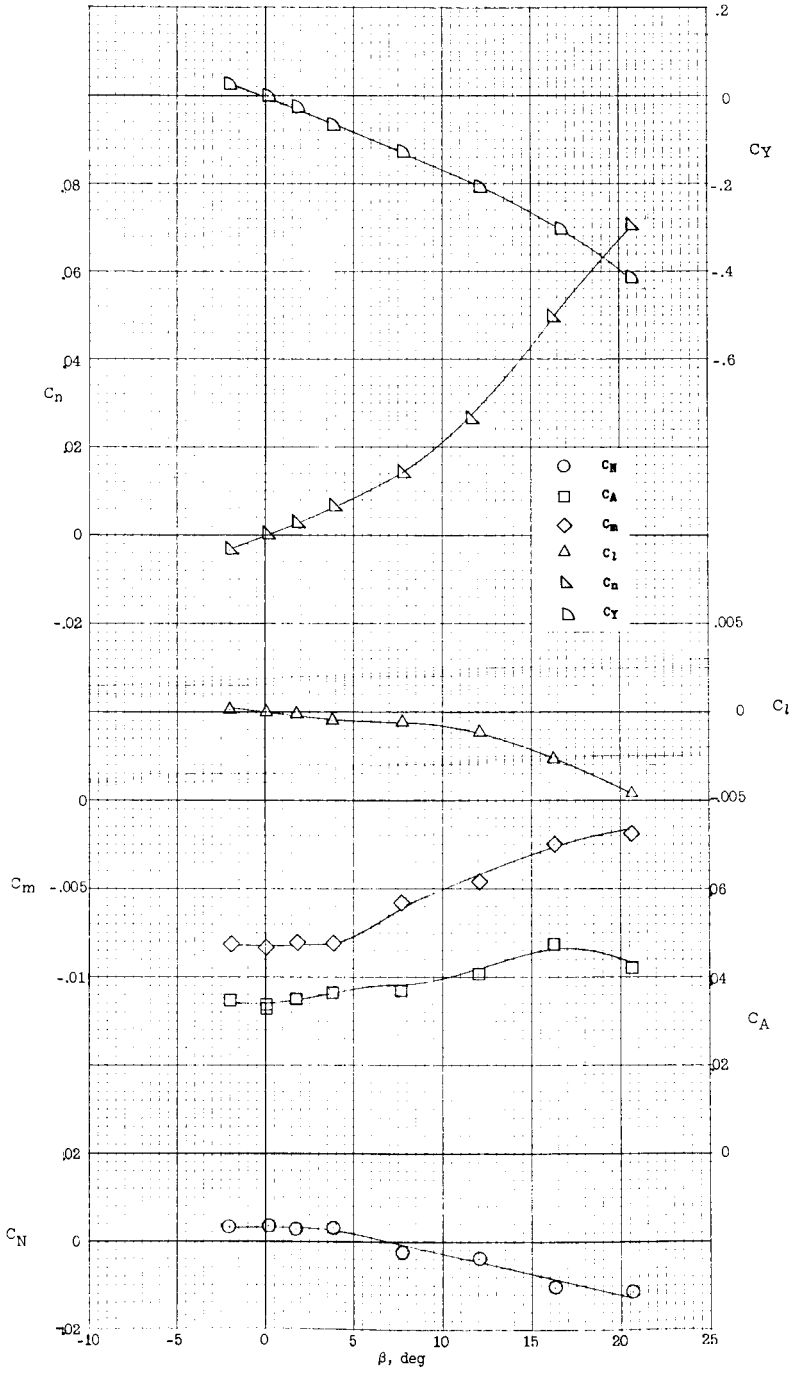

Figure 23.- Variation of longitudinal and lateral stability characteristics with angle of sideslip of configuration 3. $\alpha = 0^{\circ}$; M = 6.83; R = 640,000.

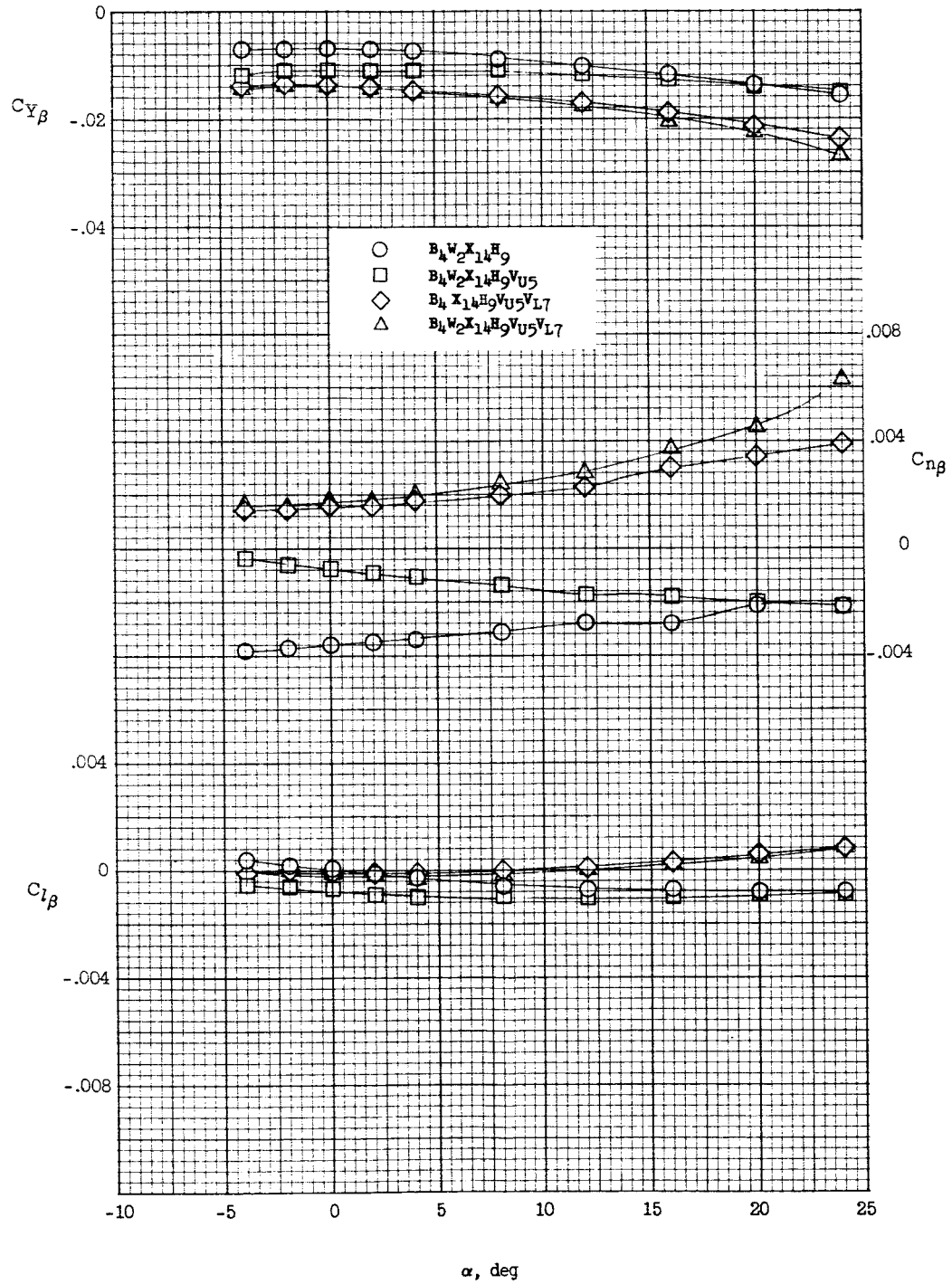

Figure 24.- Effect of component parts on the lateral and directional stability characteristics of configuration 3. M = 6.83; R = 640,000.

[redacted]

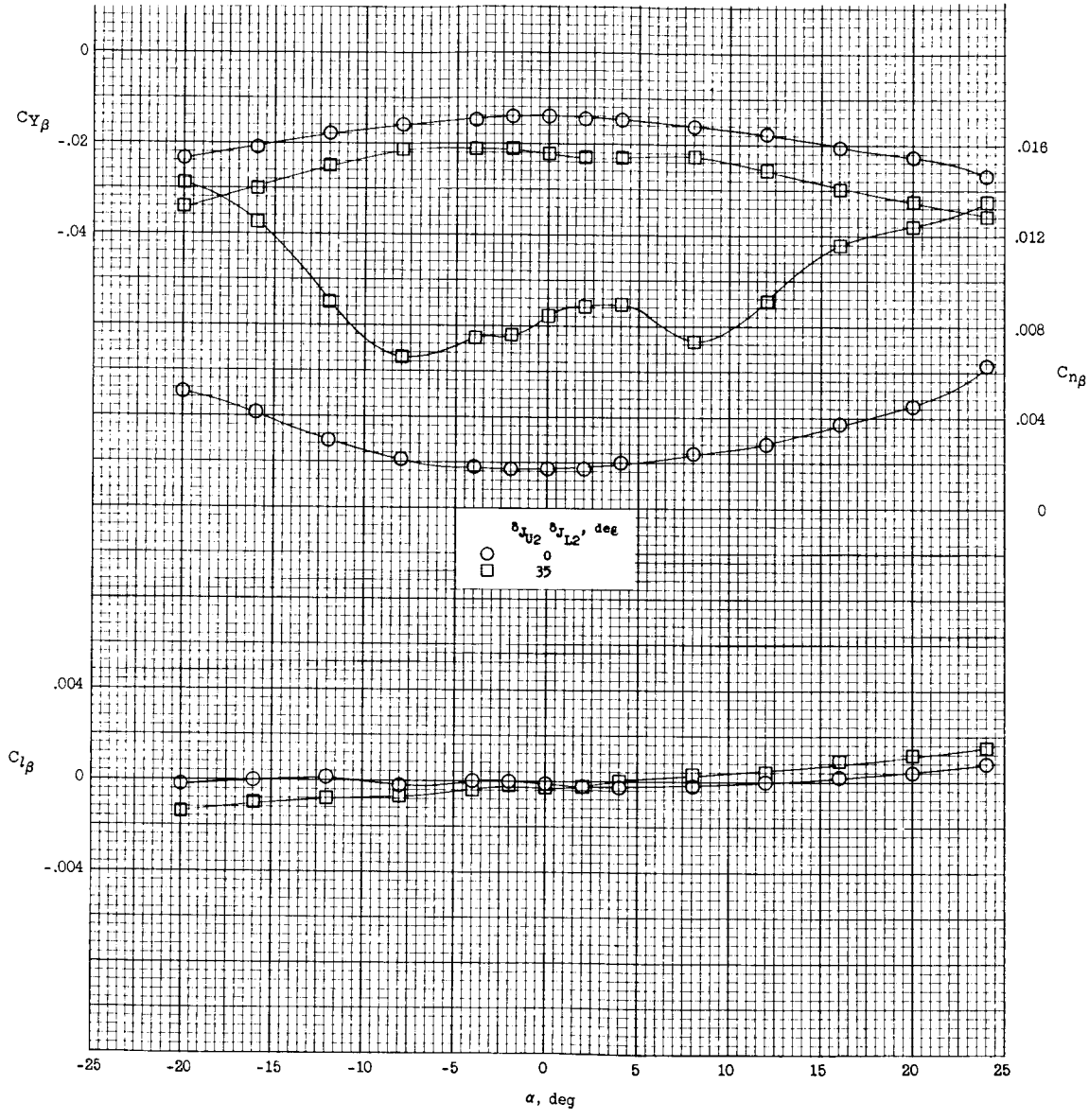

Figure 25.- Effect of speed-brake deflection on the lateral and directional stability characteristics of configuration 3. M = 6.83; R = 640,000.

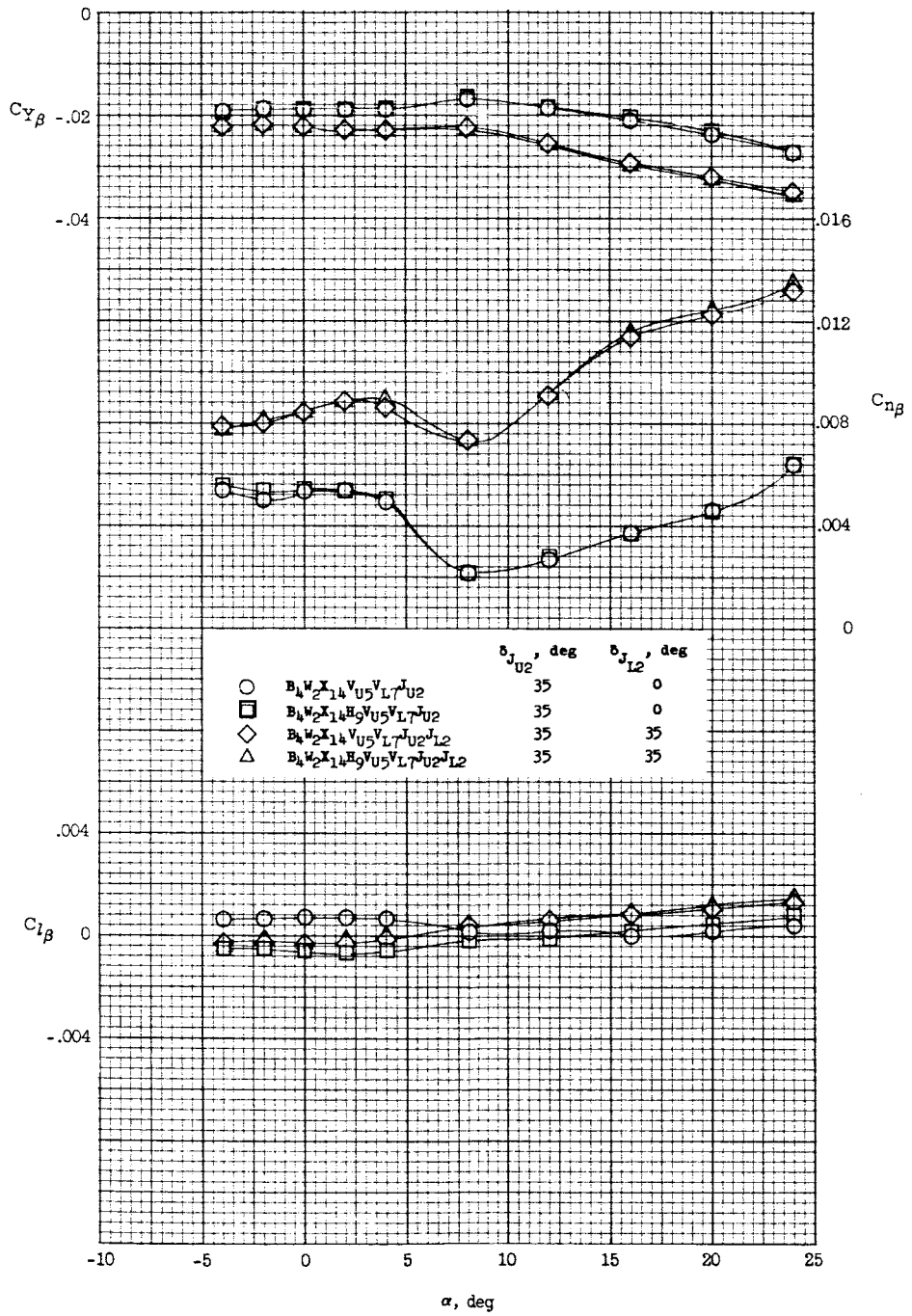

Figure 26.- Effect of speed-brake deflection on the lateral and directional stability characteristics of configuration 3 with and without horizontal tail. M = 6.83; R = 640,000.

L-739

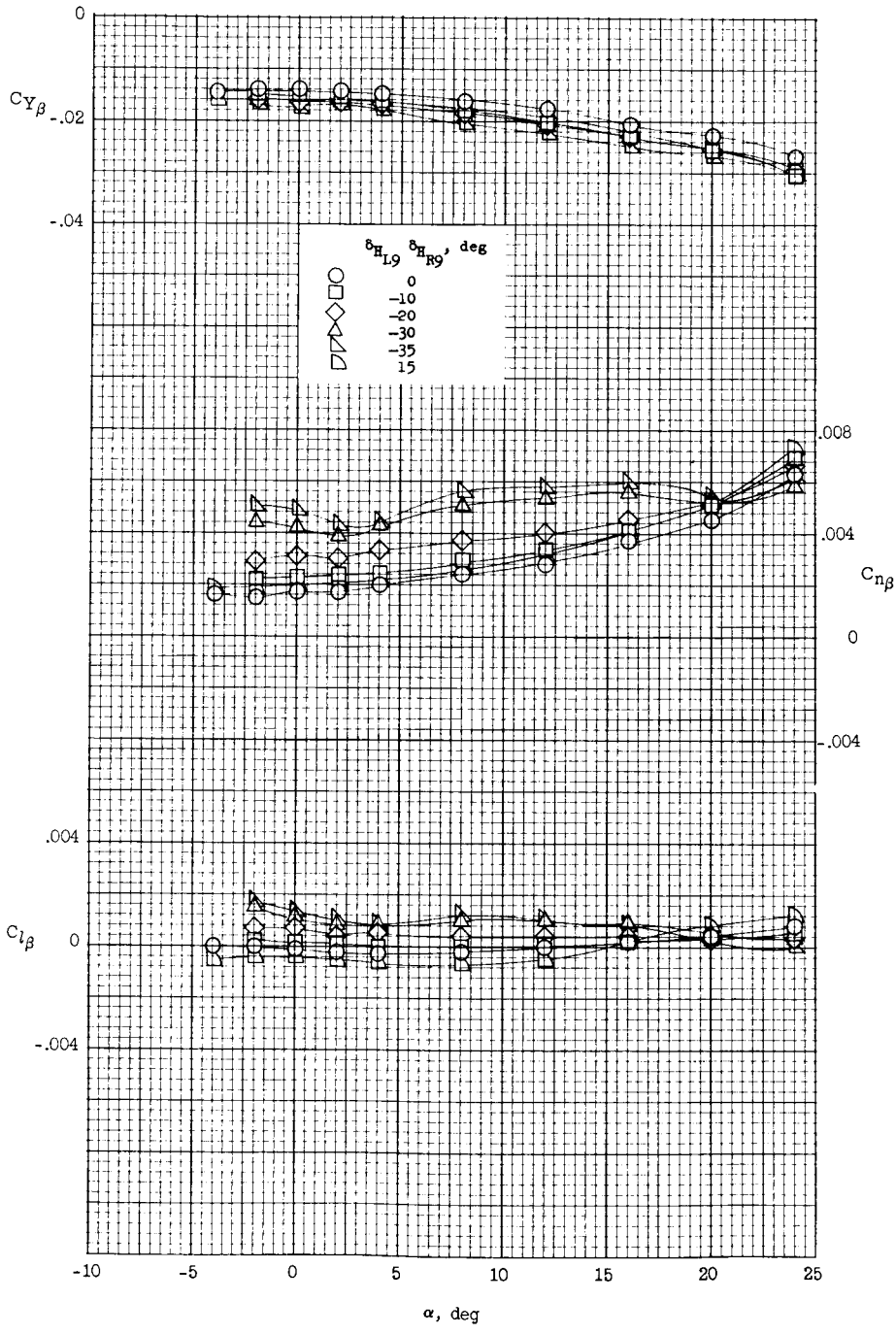

Figure 27.- Effect of horizontal-tail deflection on the lateral and directional stability characteristics of configuration 3. M = 6.83; R = 640,000.

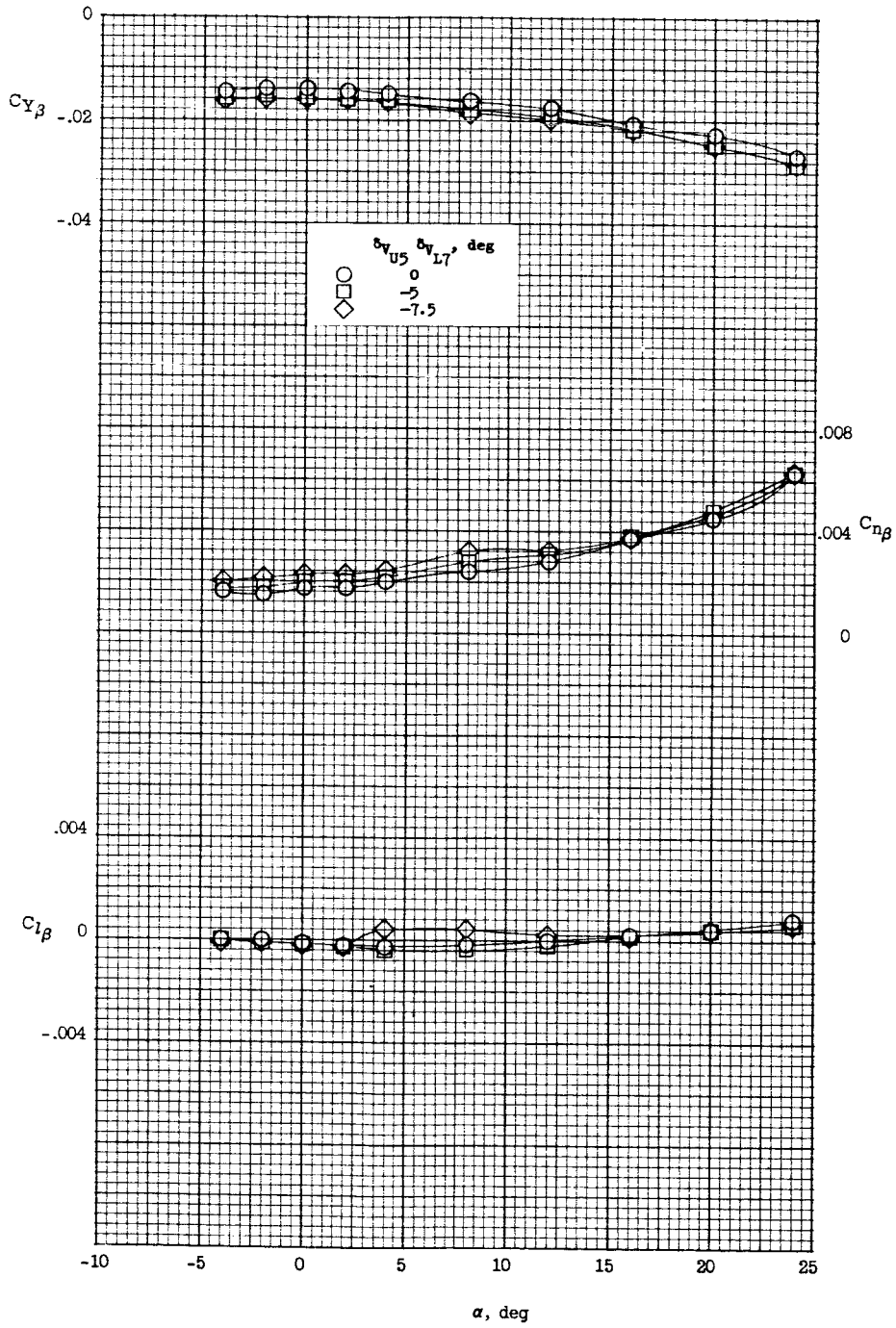

Figure 28.- Effect of vertical-tail deflection on the lateral and directional stability characteristics of configuration 3. M = 6.83; R = 640,000.

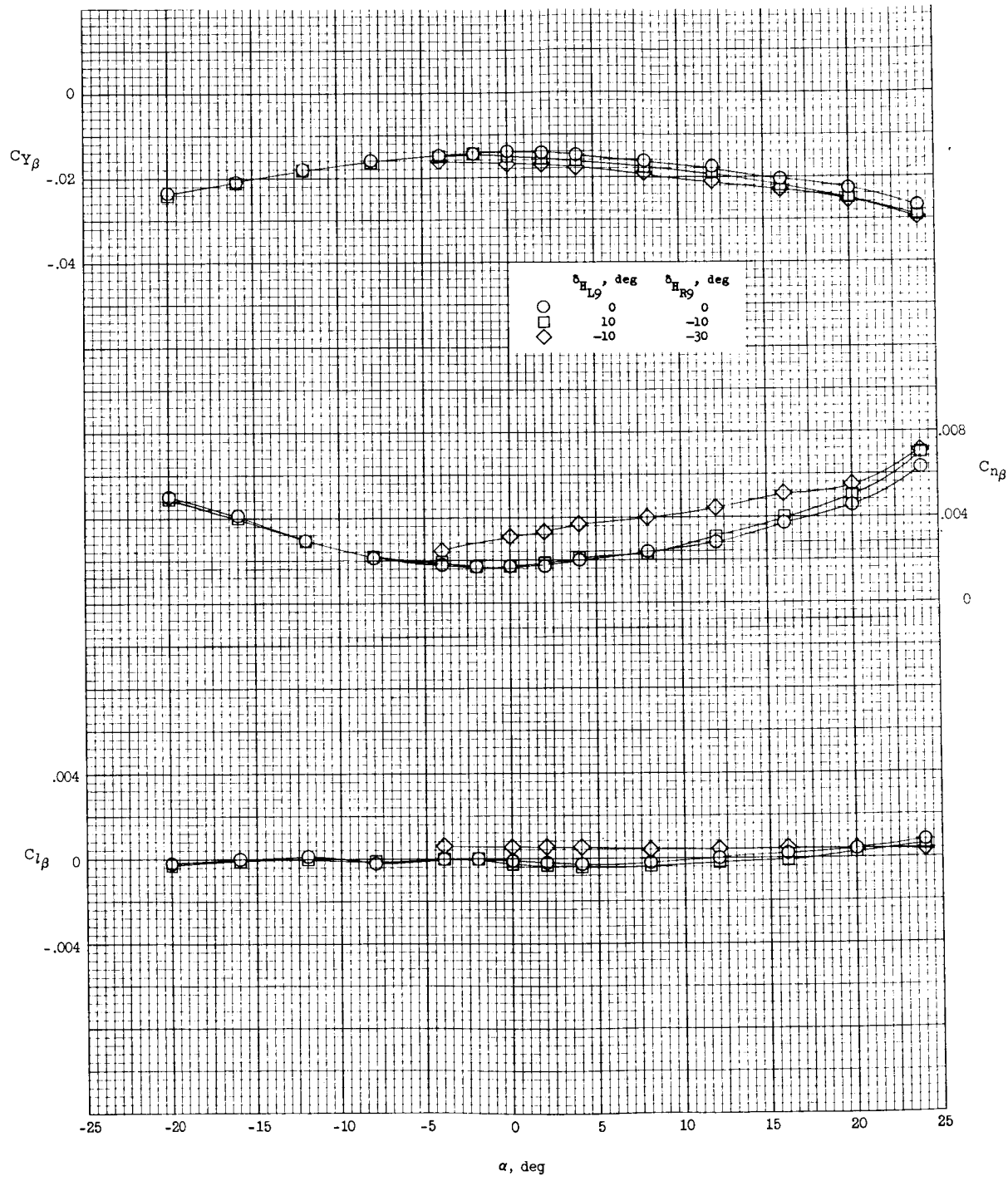

Figure 29.- Effect of differential horizontal-tail deflection on the lateral and directional stability characteristics of configuration 3. M = 6.83; R = 640,000.

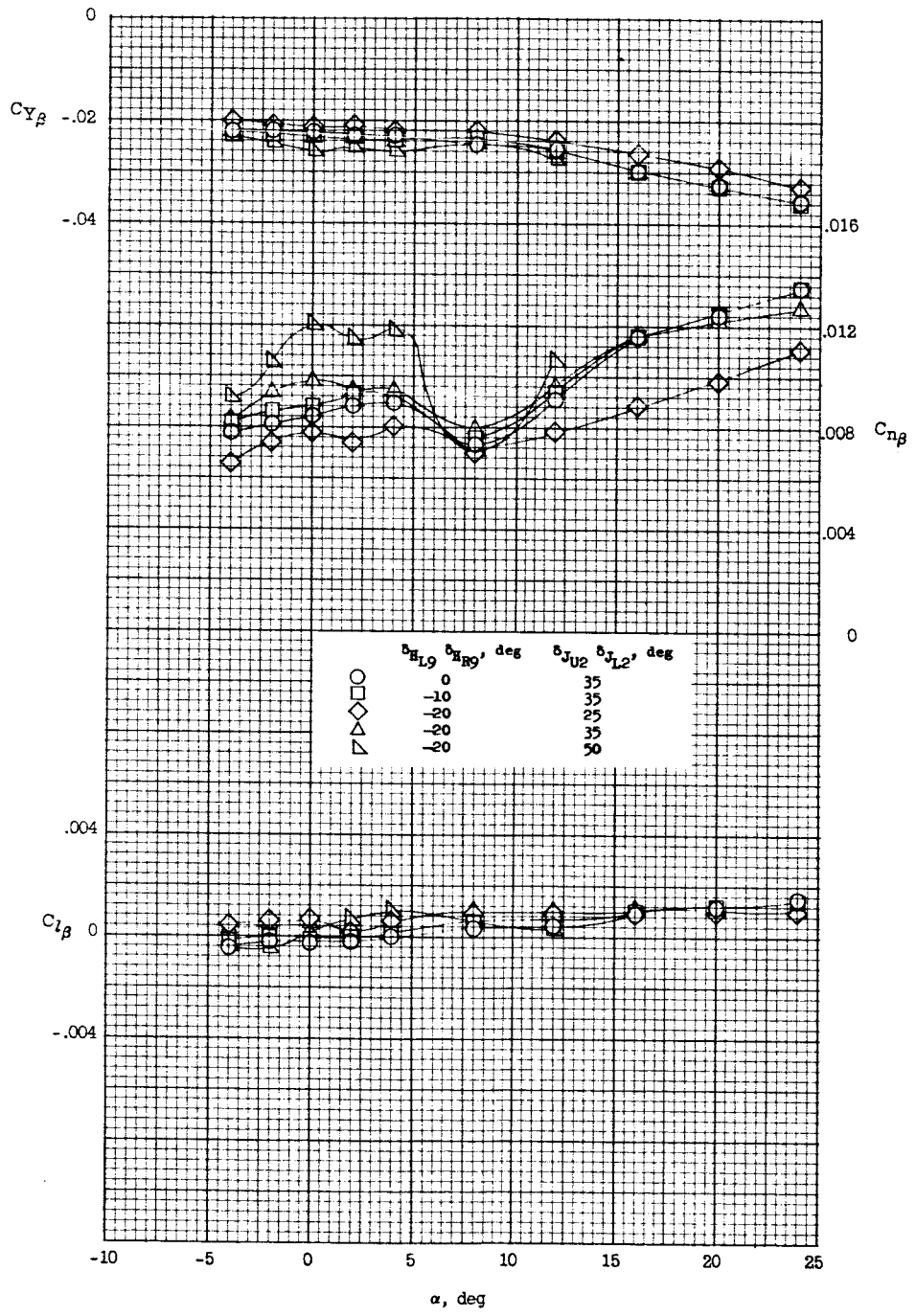

L-739

Figure 30.- Effect of horizontal-tail deflection on the lateral and directional stability characteristics of configuration 3 with various speed-brake deflections. M = 6.83; R = 640,000.

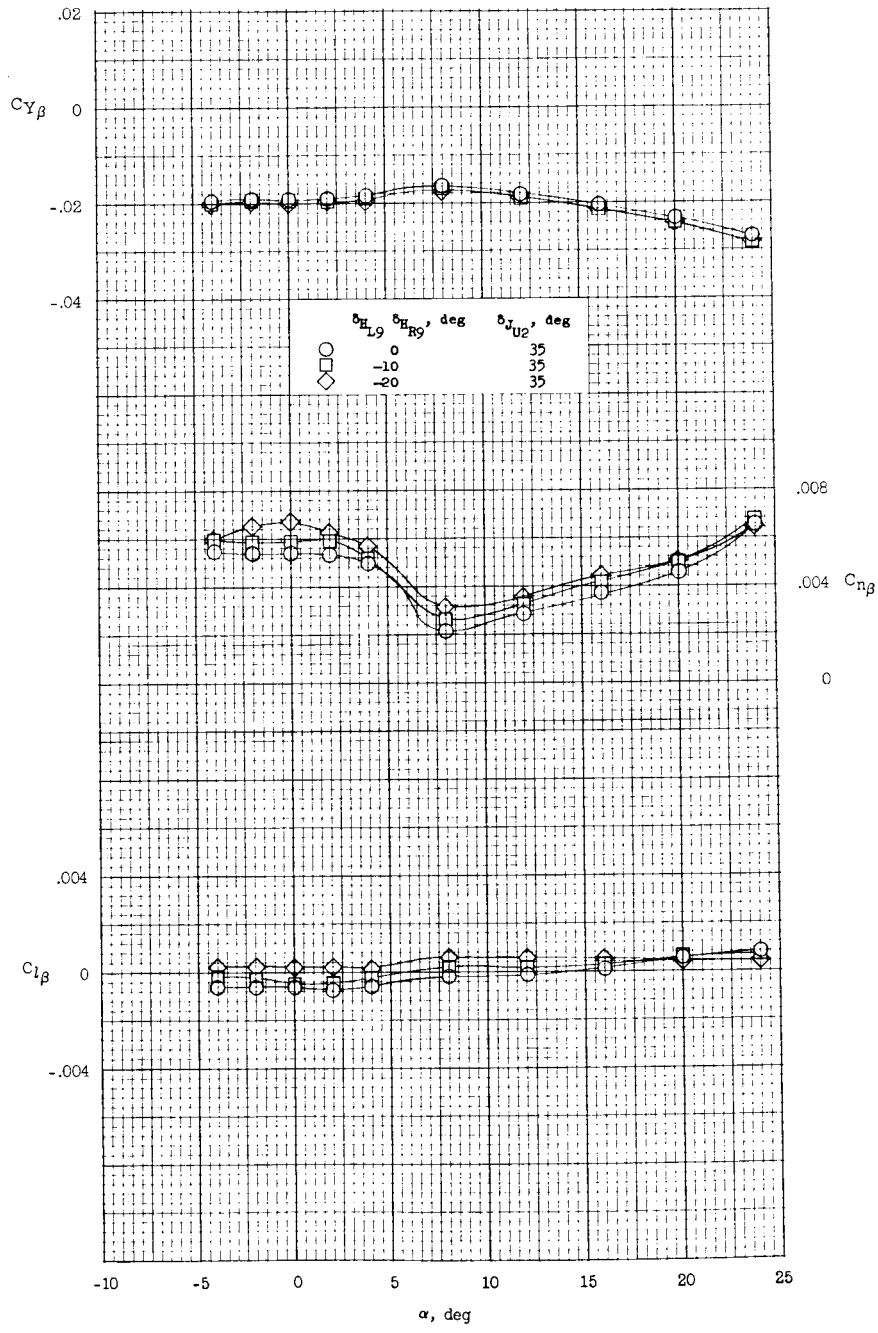

Figure 31.- Effect of horizontal-tail deflection on the lateral and directional stability characteristics of configuration 3 with upper speed-brake deflection. M = 6.83; R = 640,000.

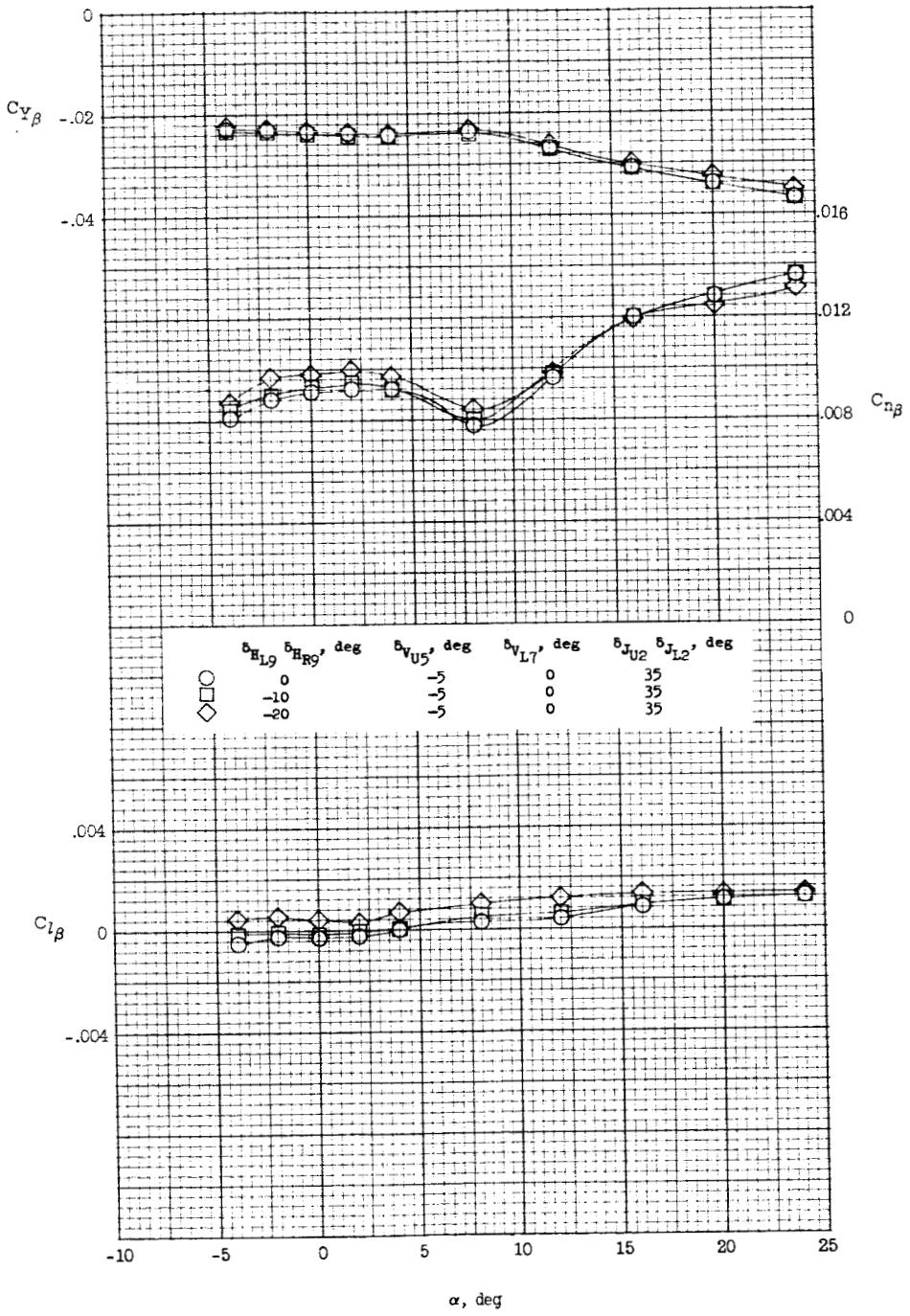

Figure 32.- Effect of horizontal-tail deflection on the lateral and directional stability characteristics of configuration 3 with upper vertical-tail and speed-brake deflections. M = 6.83; R = 640,000.

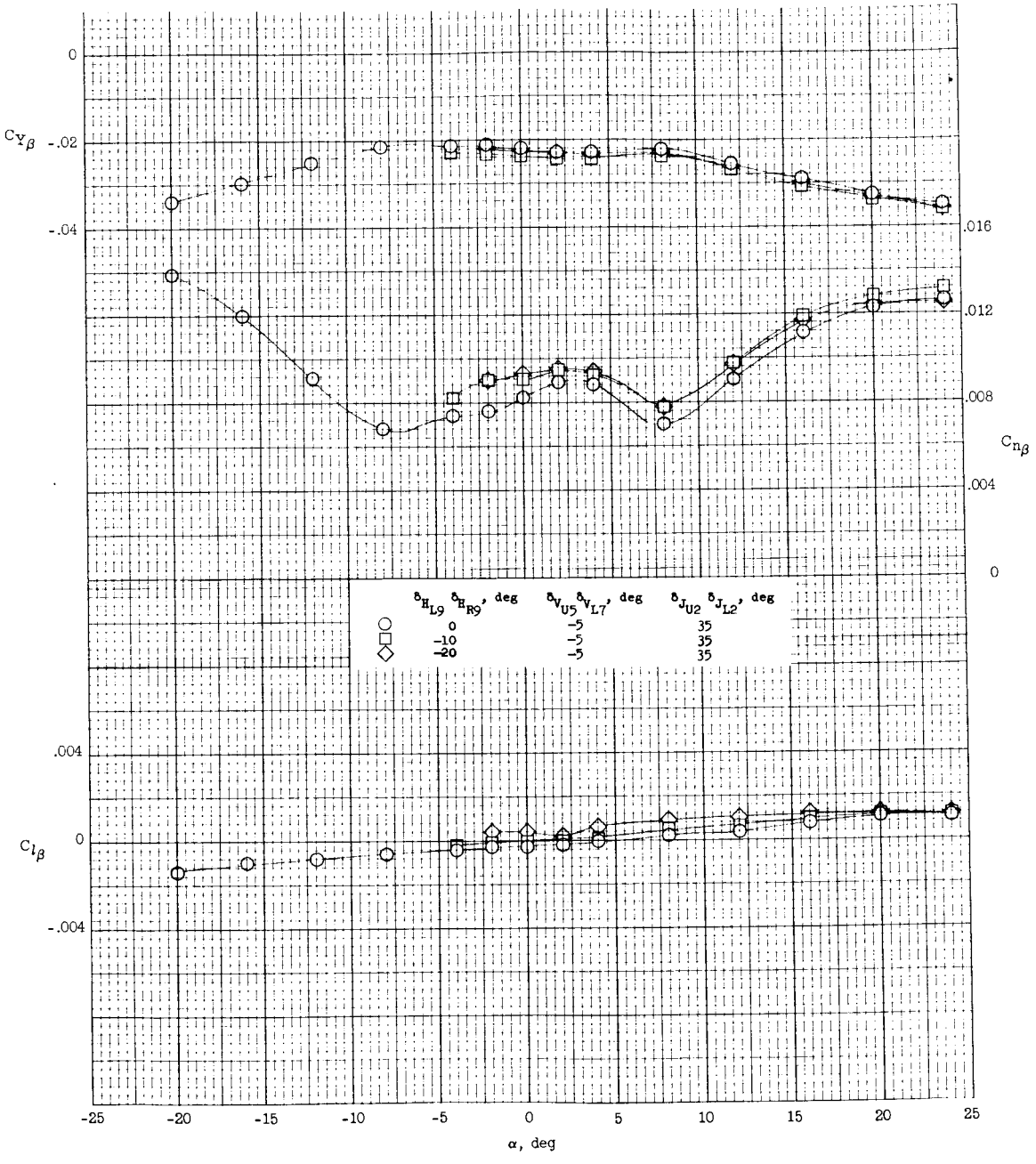

Figure 33.- Effect of horizontal-tail deflection on the lateral and directional stability characteristics of configuration 3 with vertical-tail and speed-brake deflections. M = 6.83; R = 640,000.

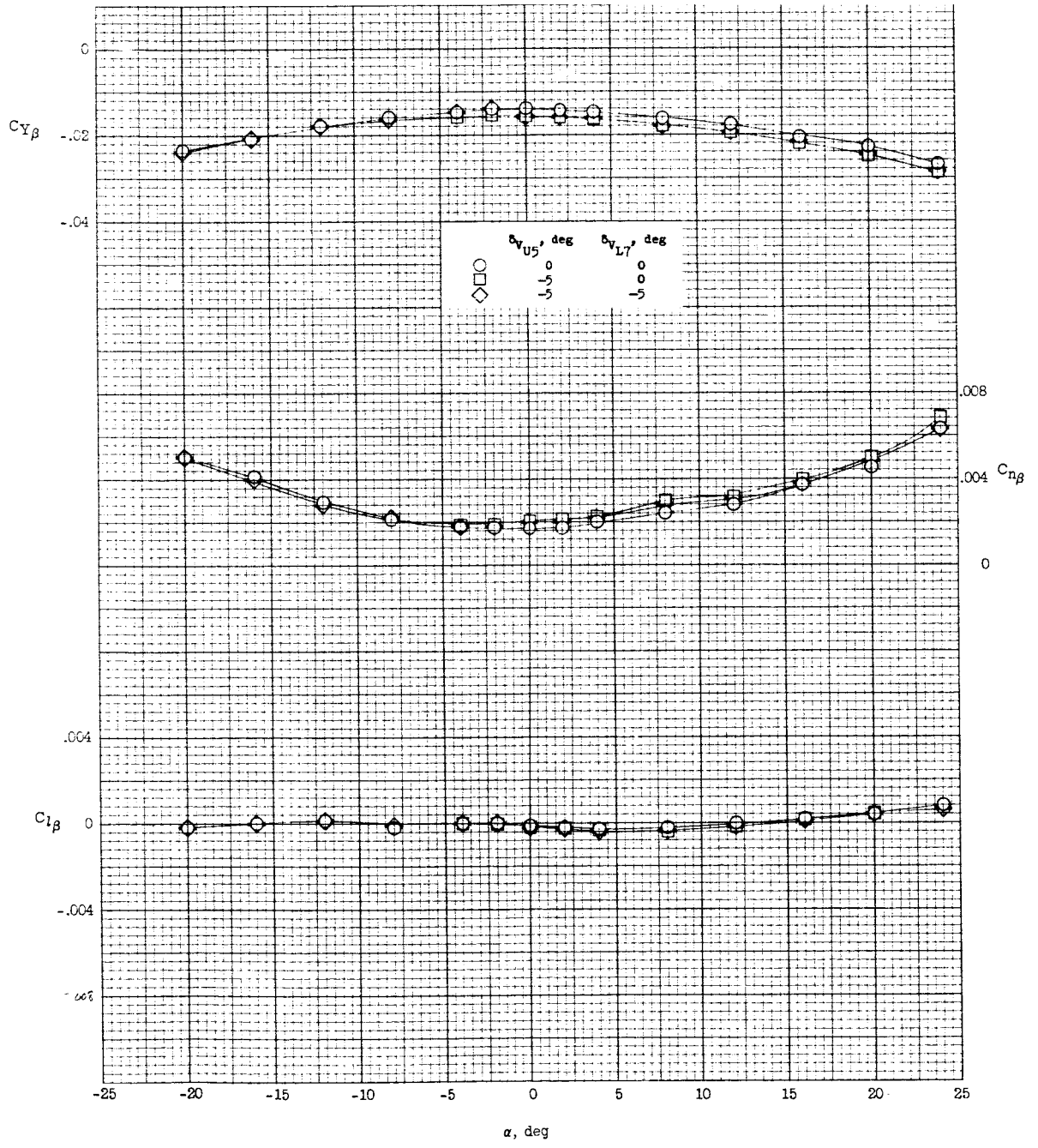

Figure 34.- Effect of upper vertical-tail deflection on the lateral and directional stability characteristics of configuration 3. M = 6.83; R = 640,000.

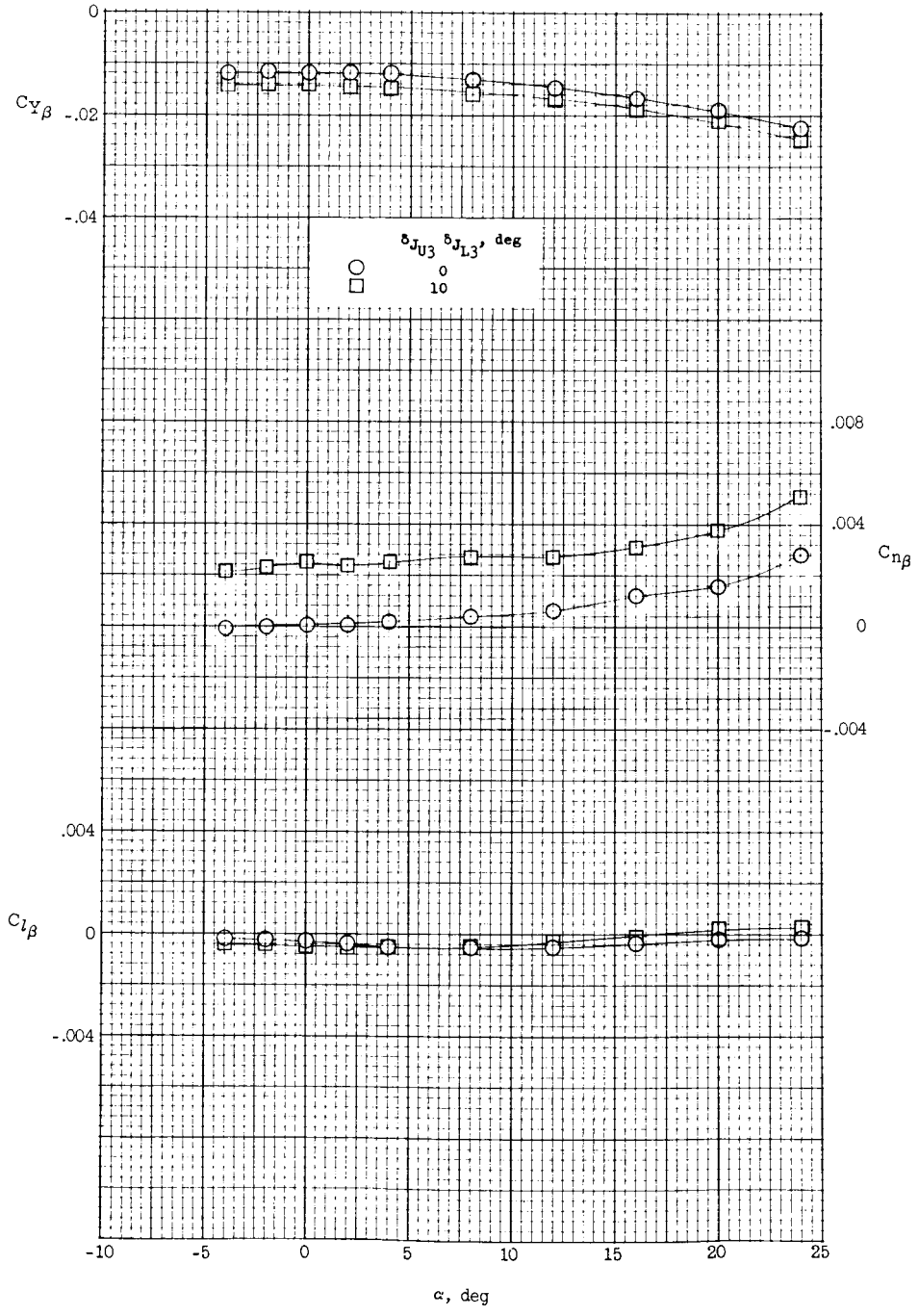

Figure 35.- Effect of speed-brake deflection on the lateral and directional stability characteristics of modified configuration 3, $B_2W_2X_4H_3V_{U8}V_{L9}J_{U3}J_{L3}$. M = 6.83; R = 640,000.

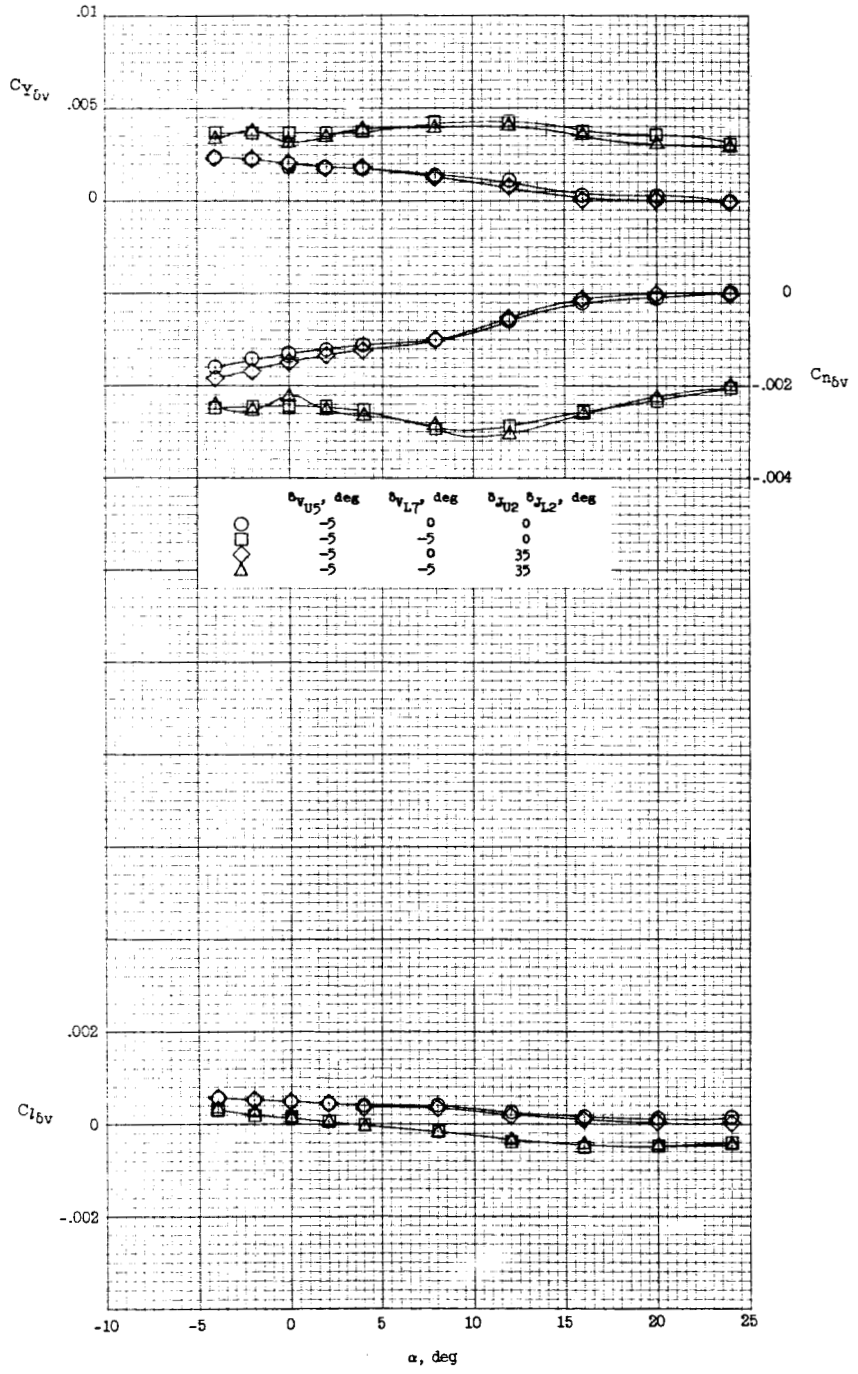

Figure 36.- Directional control characteristics of configuration 3 for various vertical-tail and speed-brake deflections. M = 6.83; R = 640,000.

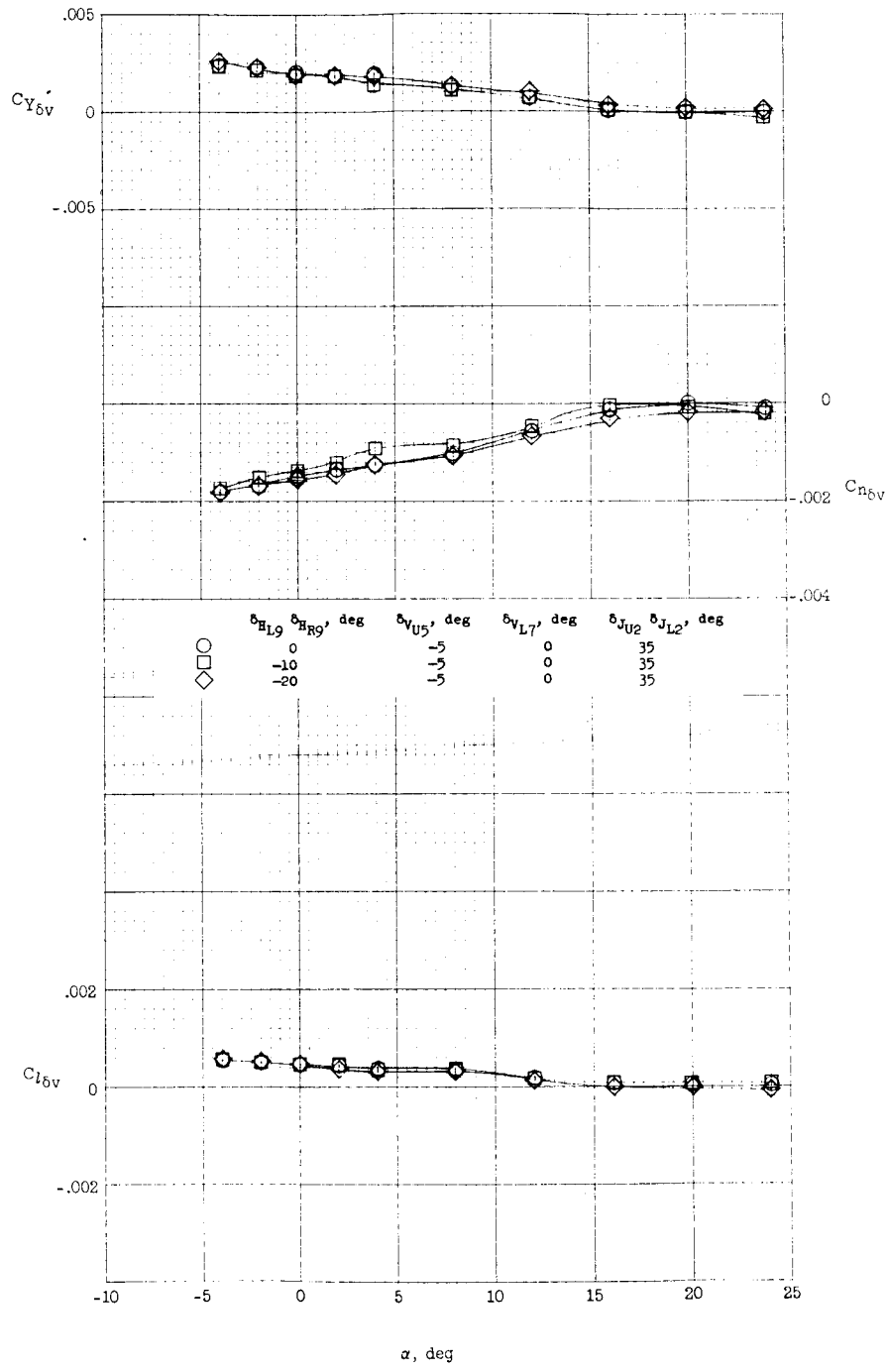

Figure 37.- Effect of horizontal-tail deflection on the directional control characteristics of configuration 3 with upper vertical-tail and speed-brake deflections. M = 6.83; R = 640,000.

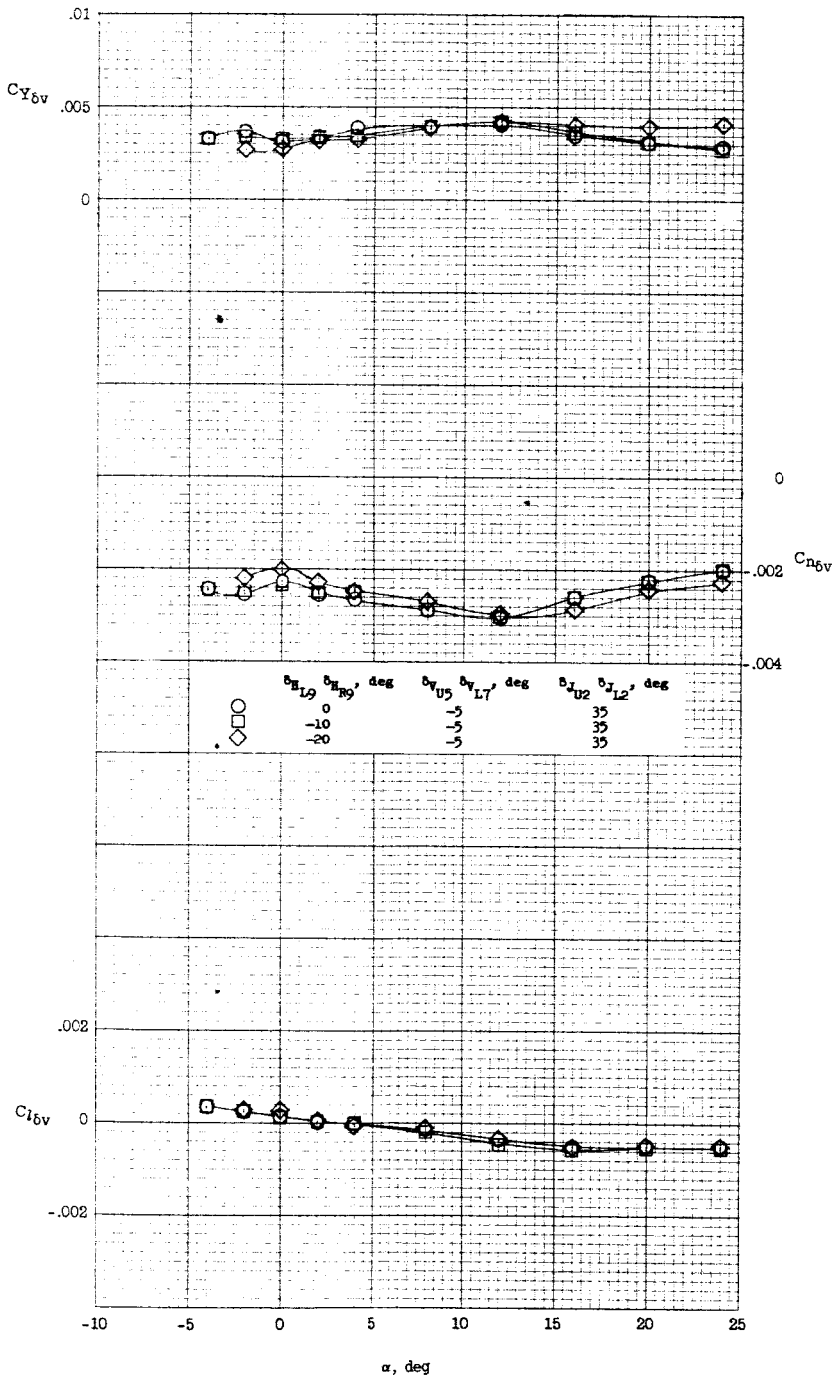

Figure 38.- Effect of horizontal-tail deflection on the directional control characteristics of configuration 3 with vertical-tail and speed-brake deflections. M = 6.83; R = 640,000.

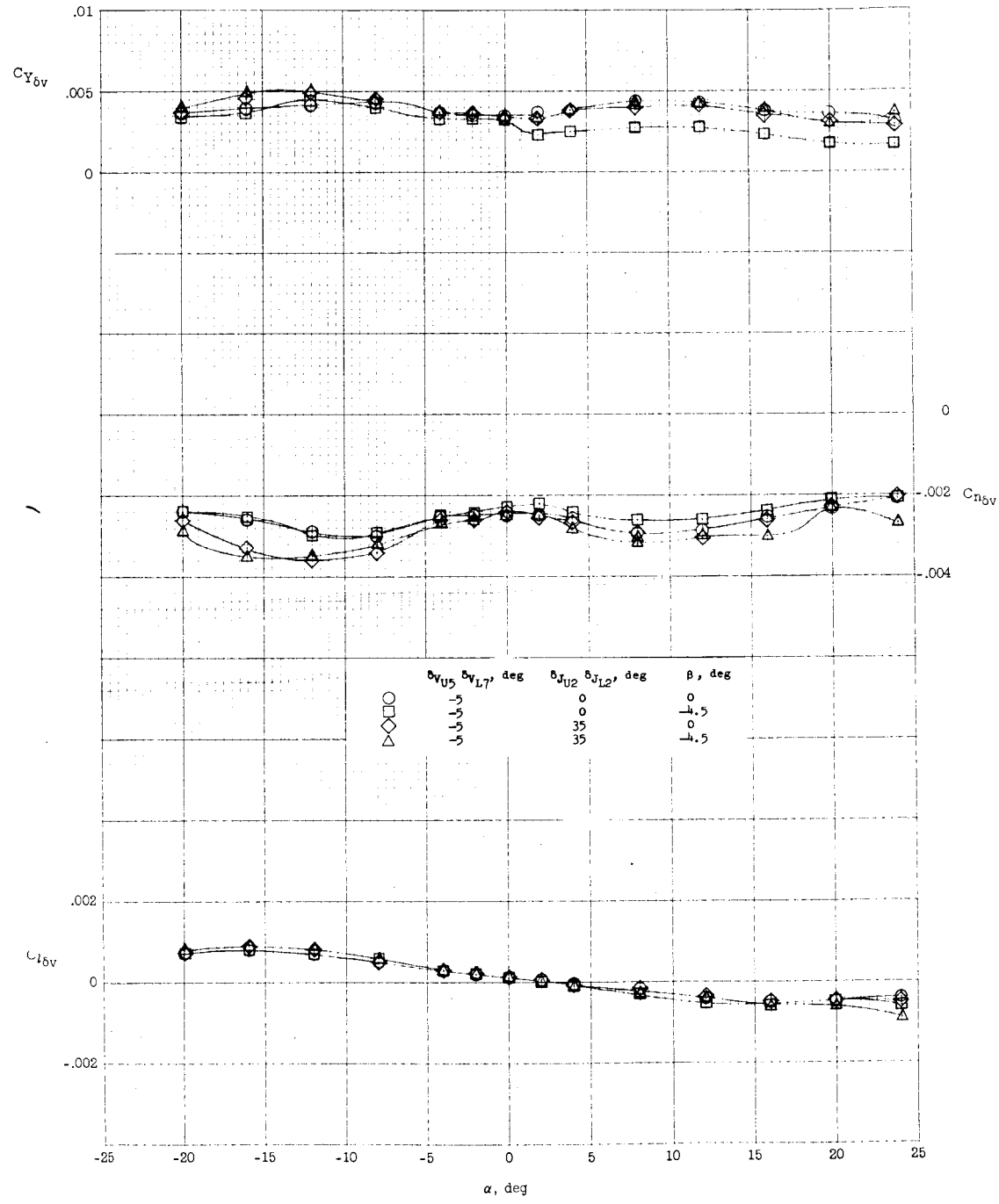

Figure 39.- Effect of -4.5° sideslip and speed-brake deflection on the directional control characteristics of configuration 3. M = 6.83; R = 640,000.

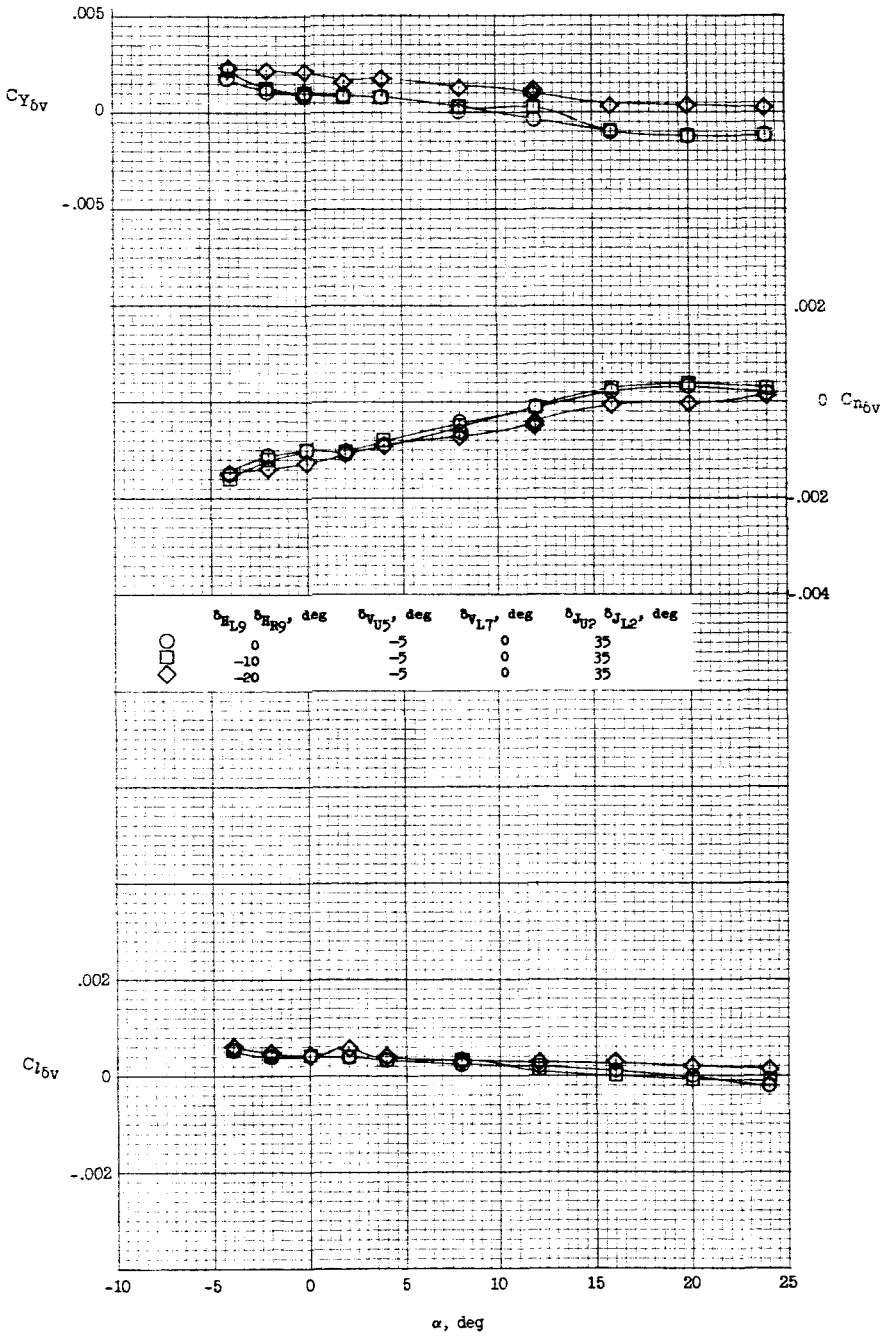

Figure 40.- Effect of horizontal-tail deflection on the directional control characteristics of configuration 3 at -4.5° sideslip with upper vertical-tail and speed-brake deflections. M = 6.83; R = 640,000.

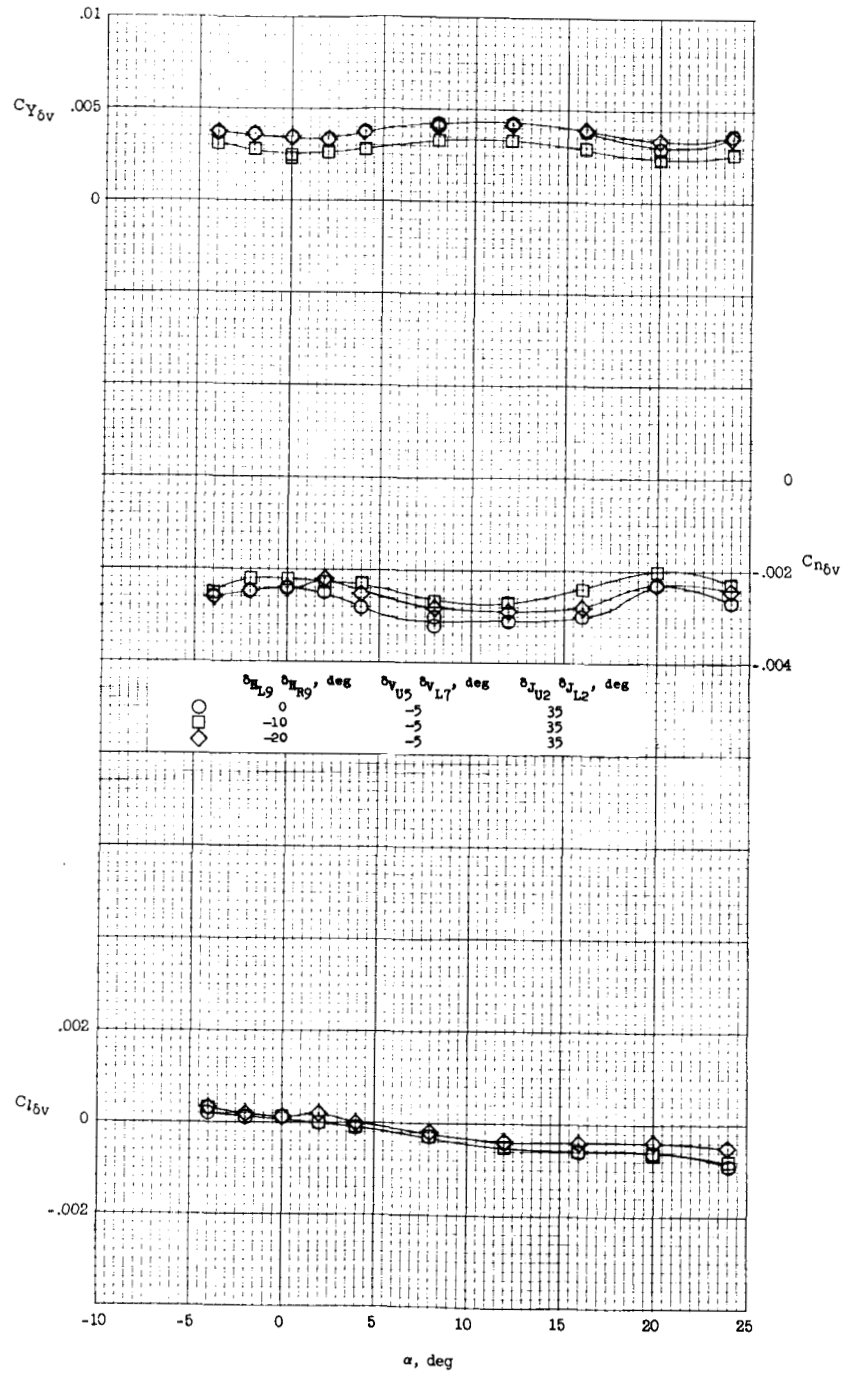

Figure 41.- Effect of horizontal-tail deflection on the directional control characteristics of configuration 3 at -4.5° sideslip with vertical-tail and speed-brake deflections. M = 6.83; R = 640,000.

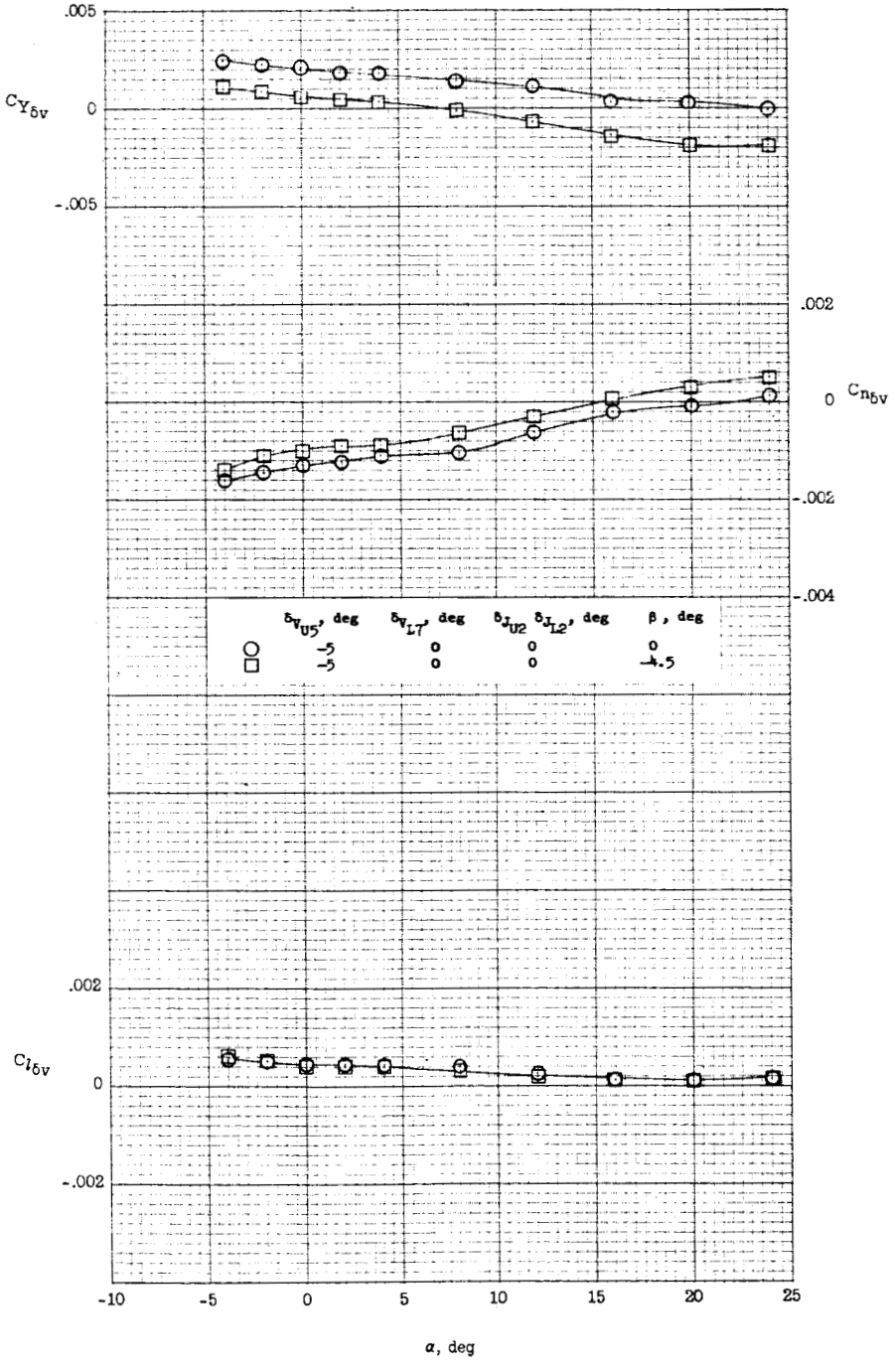

Figure 42.- Effect of -4.5° sideslip on the directional control characteristics of configuration 3 with upper vertical-tail deflection. M = 6.83; R = 640,000.

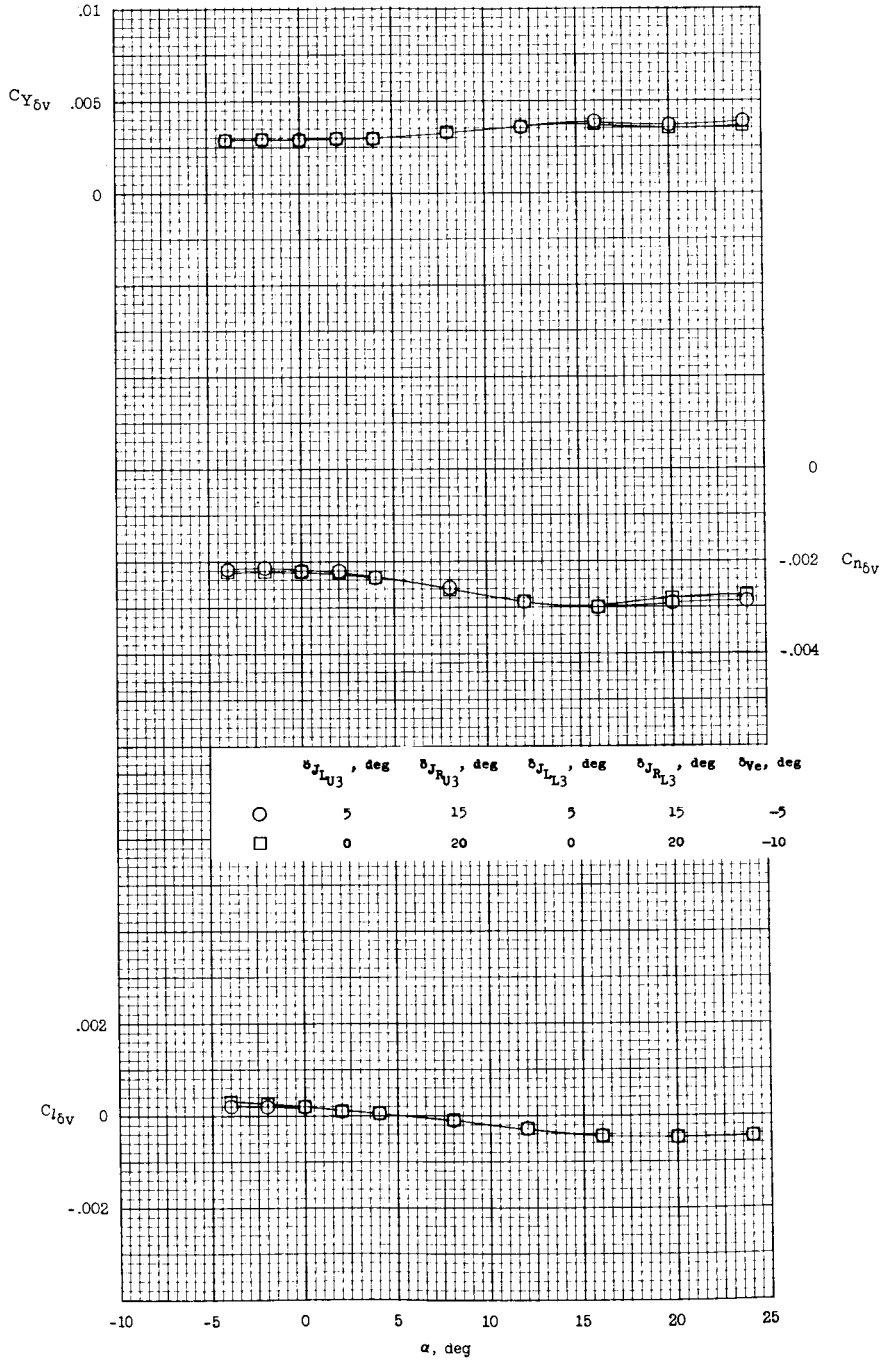

Figure 43.- Directional control characteristics of modified configuration 3, $B_2W_2X_4H_3V_{U8}V_{L9}J_{U3}J_{L3}$, for various differential speed-brake deflections. M = 6.83; R = 640,000.

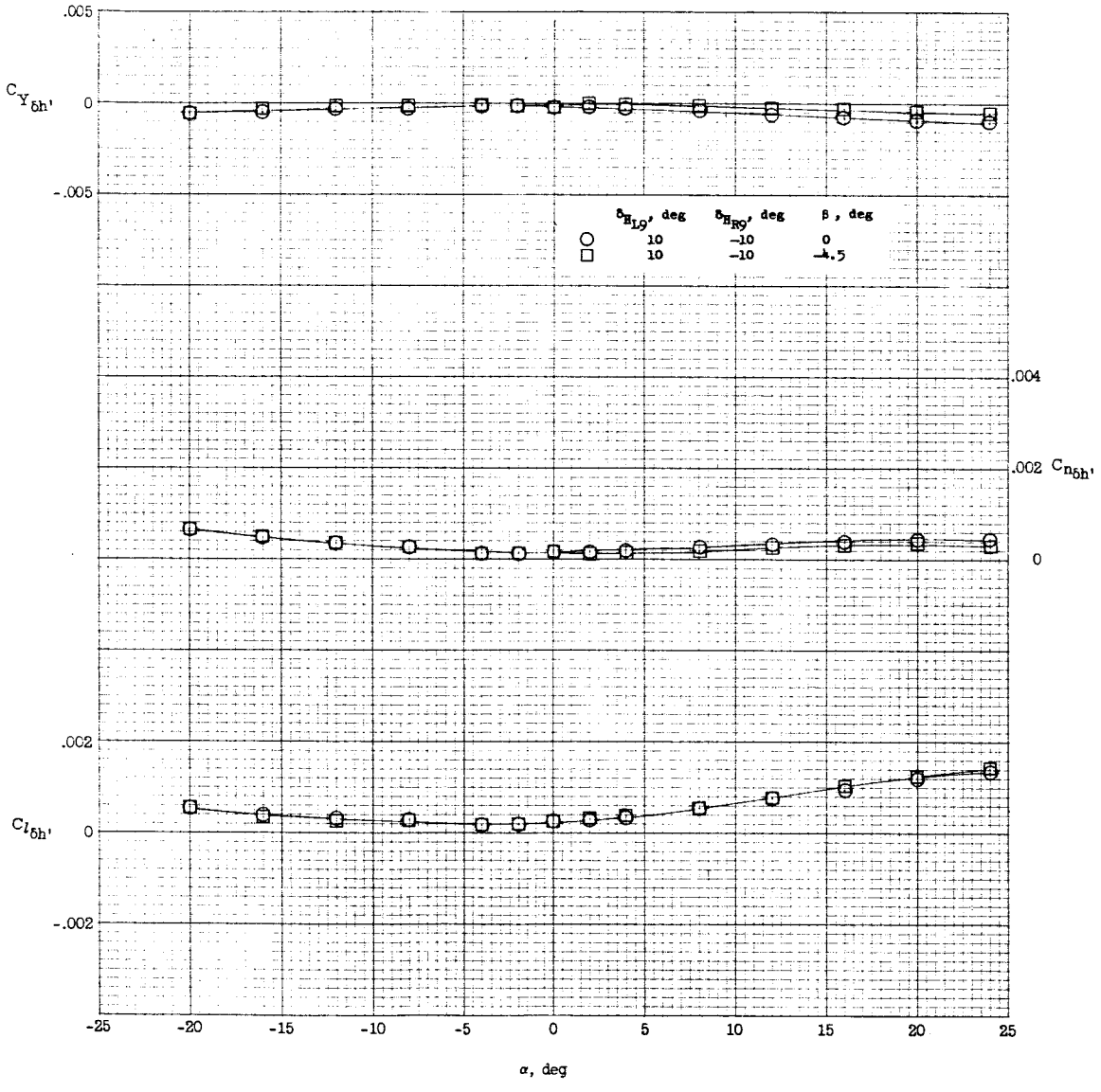

Figure 44.- Effect of -4.5° sideslip on the lateral control characteristics of configuration 3. M = 6.83; R = 640,000.

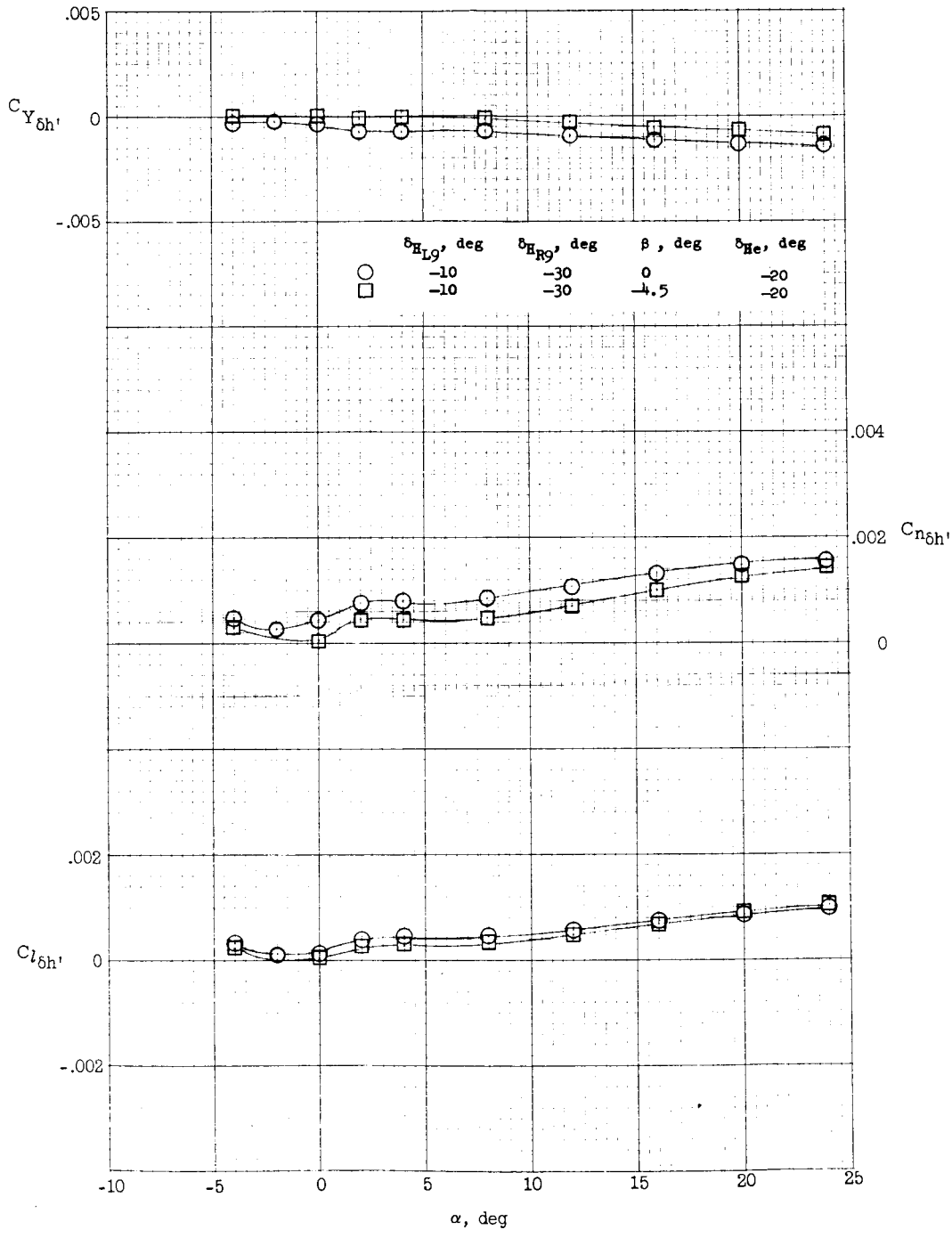

Figure 45.- Effect of -4.5° sideslip on the lateral control characteristics of configuration 3 with an equivalent horizontal-tail deflection. M = 6.83; R = 640,000.

L-739

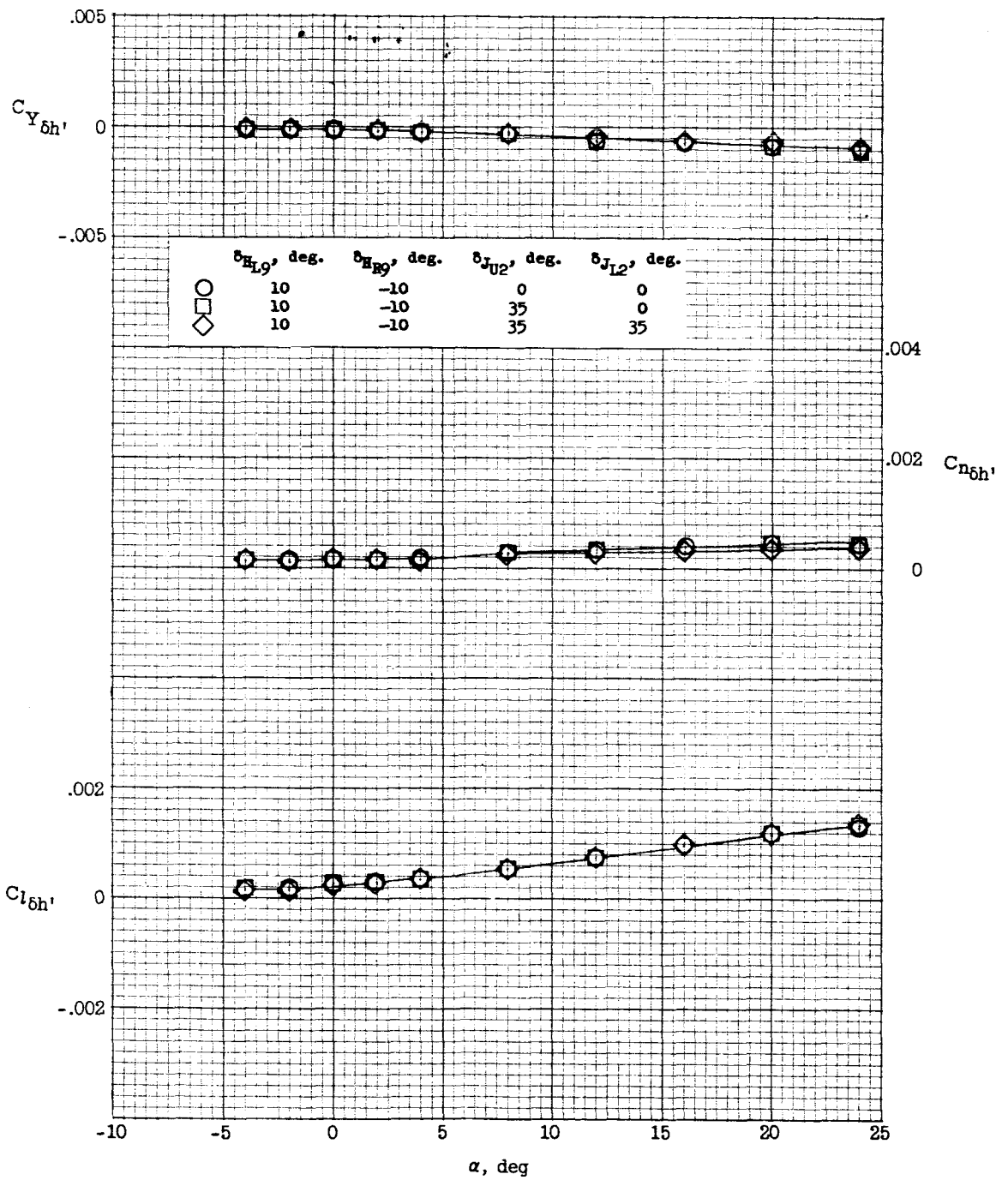

Figure 46.- Effect of speed-brake deflection on the lateral control characteristics of configuration 3. M = 6.83; R = 640,000; β = 0°.

L-739

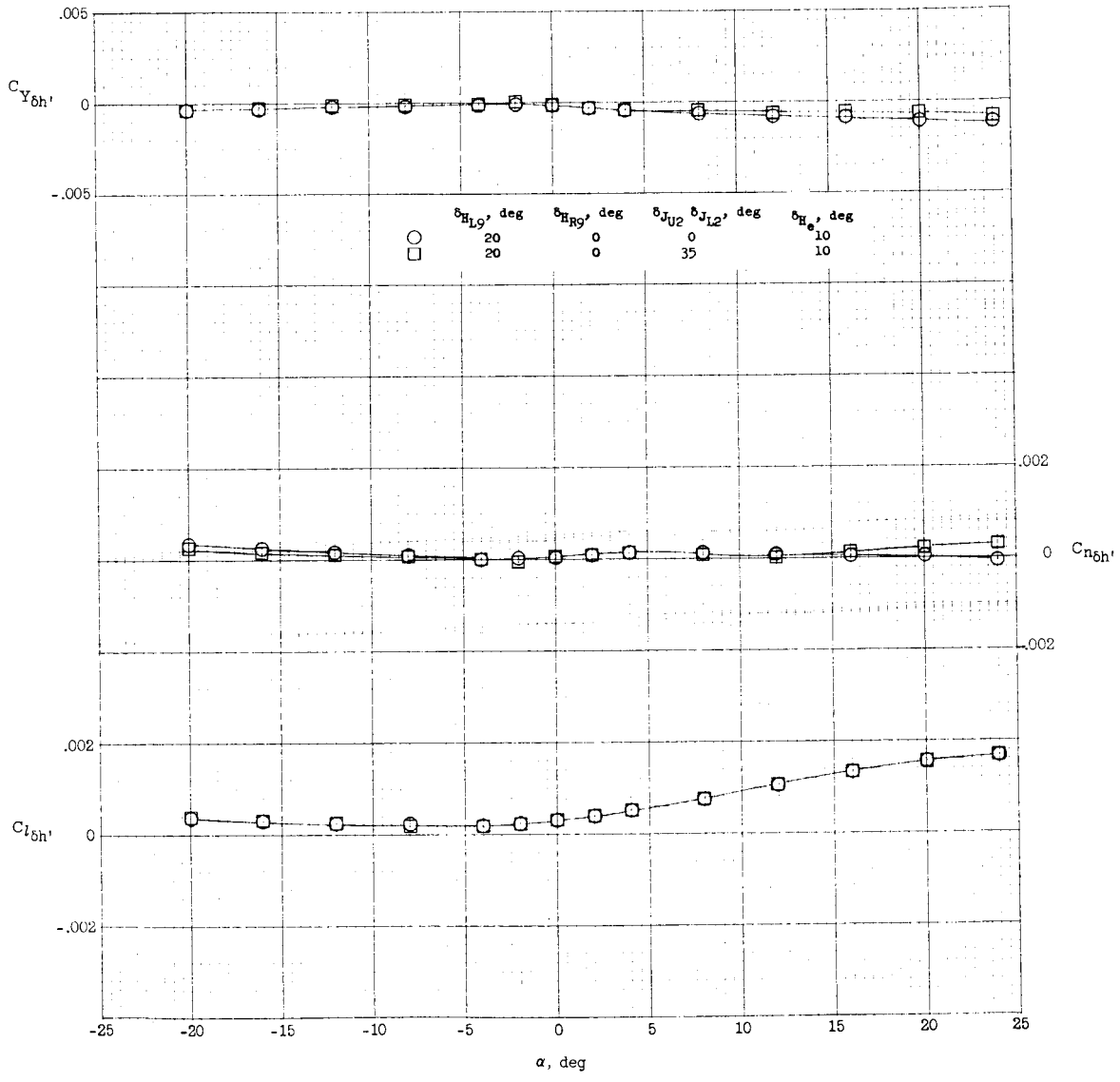

Figure 47.- Effect of speed-brake deflection on the lateral control characteristics of configuration 3 with an equivalent horizontal-tail deflection. M = 6.83; R = 640,000; β = 0°.

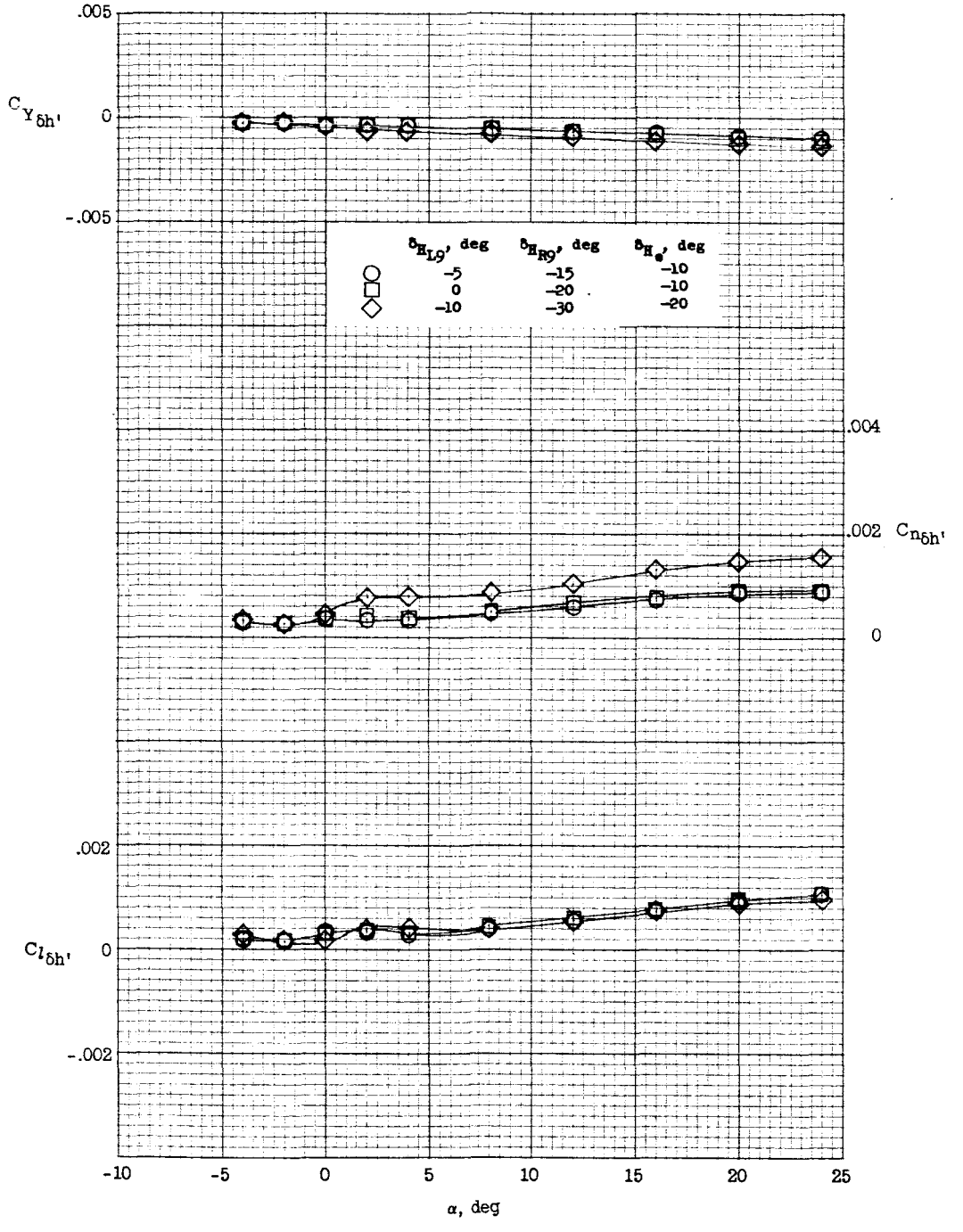

Figure 48.- Effect of equivalent horizontal-tail deflection on the lateral control characteristics of configuration 3. M = 6.83; R = 640,000; $\beta = 0^{\circ}$.